GENERATION OF FAST NETURON SPECTRA USING AN ADAPTIVE GAUSS-KRONROD QUADRATURE ALGORITHM

By

BRIAN SCOTT TRIPLETT

A DISSERTATION PRESENTED TO THE GRADUATE SCHOOL
OF THE UNIVERSITY OF FLORIDA IN PARTIAL FULFILLMENT
OF THE REQUIREMENTS FOR THE DEGREE OF
DOCTOR OF PHILOSOPHY

UNIVERSITY OF FLORIDA

2011

To the Creator, who orders the Universe according to His purpose and enables our attempts to understand and describe that order

ACKNOWLEDGMENTS

I would first like to acknowledge Dr. Samim Anghaie for his support and encouragement throughout my time at University of Florida. Without his guidance and support I would not be where I am today.

I would also like to thank Dr. Eric Loewen for his constant encouragement and not allowing me to slow down or quit.

Brett Dooies and Andrew Caldwell were always available for discussing ideas and giving input into the content of this dissertation. I would like to acknowledge Brett for peer-checking my work and assisting in the development of the error quantification procedure used to analyze the results.

Finally, I would like to acknowledge Kristen Triplett who provided support in the form of plot generation consulting and computer programming advice.

TABLE OF CONTENTS

LIST OF TABLES

LIST OF FIGURES

LIST OF ABBREVIATIONS

ACE	A Compact ENDF
ASCII	American Standard Code for Information Interchange
BONAMI	Bondarenko AMPX Interpolator
BWR	Boiling water reactor
CENTRM	Continuous Energy Transport Module
cm	Centimeter
COM	Center-of-mass
CRAWDAD	Code to Read And Write Data for Discretized solution
ENDF	Evaluated nuclear data file
eV	Electronvolt
GEMINEWTRN	Group and energy-pointwise methodology implemented in NEWT for resonance neutronics
GKQ	Gauss-Kronrod Quadrature
GLQ	Gauss-Legendre Quadrature
GQ	Gauss Quadrature
JEFF	Joint Evaluated Fission and Fusion File
JENDL	Japanese Evaluated Nuclear Data Library
K	Kelvin
keV	Kilo-electronvolt
LHS	Left hand side
LWR	Light water reactor
MCNP	Monte Carlo n-particle
MeV	Mega-electronvolt
MG	Multigroup

MOX	Mixed oxide
MWD/MTHM	Megawatt-days per metric ton of heavy metal
ORIGEN-S	Oak Ridge Isotope Generation
ORNL	Oak Ridge National Laboratory
PENDF	Pointwise evaluated nuclear data file
PMC	Produce Multigroup Cross sections
PWFSG	Pointwise Fast Spectrum Generator
PW	Pointwise
PWR	Pressurized water reactor
RHS	Right hand side
s	Second
SCALE	Standardized Computer Analysis for Licensing Evaluation
SFR	Sodium fast reactor
TRU	Transuranic
wt%	Weight percent
UNF	Used nuclear fuel

Abstract of Dissertation Presented to the Graduate School
of the University of Florida in Partial Fulfillment of the
Requirements for the Degree of Doctor of Philosophy

GENERATION OF FAST NETURON SPECTRA USING AN ADAPTIVE GAUSS-KRONROD QUADRATURE ALGORITHM

By

Brian Triplett

May 2011

Chair: DuWayne Schubring
Major: Nuclear Engineering Sciences

A lattice physics calculation is often the first step in analyzing a nuclear reactor. This calculation condenses regions of the reactor into average parameters (i.e., group constants) that can be used in coarser full-core, time-dependent calculations. This work presents a high-fidelity deterministic method for calculating the neutron energy spectrum in an infinite medium. The spectrum resulting from this calculation can be used to generate accurate group constants. This method includes a numerical algorithm based on Gauss-Kronrod Quadrature to determine the neutron transfer source to a given energy while controlling numerical error. This algorithm was implemented in a pointwise transport solver program called Pointwise Fast Spectrum Generator (PWFSG). PWFSG was benchmarked against the Monte Carlo program MCNP and another pointwise spectrum generation program, CENTRM, for a set of fast reactor infinite medium example cases. PWFSG showed good agreement with MCNP, yielding coefficients of determination above 98% for all example cases. In addition, PWFSG had 6 to 8 times lower flux estimation error than CENTRM in the cases examined. With run-times comparable to CENTRM, PWFSG represents a robust set of methods for generation of fast neutron spectra with increased accuracy without increased computational cost.

CHAPTER 1
INTRODUCTION

The Importance of Lattice Physics

A complete description of the neutron population in the reactor is necessary to accurately model a nuclear reactor. The neutron population determines the distribution of the nuclear reactions in the reactor. These reactions govern the distribution of power, the utilization of fuel, and the safety margins in a nuclear system.

It is impractical to completely model the neutron population within a nuclear reactor as a function of time, space, direction, fuel exposure, temperature, etc.; therefore, a coarser calculation must be performed. The coarser calculation typically discretizes one or more of the aforementioned variables. This process requires system parameters that have been properly averaged over one or more of the neutron population's governing variables (e.g., space, energy). This averaging process is referred to as a lattice calculation or lattice physics because it involves performing high-fidelity calculations on a small unit of a nuclear reactor, such as a single fuel pin or assembly. The average parameters resulting from a lattice physics calculation are then used for core-wide calculations in a broader time and space domain. Lattice physics computer programs include LANCER02 used by GE Hitachi Nuclear Energy,[1] CASMO from Studsvik,[2] and CENTRM/PMC from Oak Ridge National Laboratory (ORNL).[3]

Since a lattice physics calculation is often the first step in reactor analysis, errors in lattice physics can propagate into further core-wide calculations. This can lead to misprediction of important reactor parameters such as neutron balance and reactor power distribution. A great effort has been made over the past few decades to improve multidimensional transport methods for core-wide solutions; however, much less progress has been made on the lattice physics

methods that inform these transport methods. Recent efforts at ORNL have sought to increase the fidelity of lattice physics methods beyond the current state-of-the-art.[4]

The present work focuses on improving lattice physics calculations for fast neutron spectrum reactors (i.e., reactors where neutrons remain at high energies and do not thermalize). A new approach to calculating the neutron transfer source based on Gauss-Kronrod Quadrature was implemented in a pointwise solution to the Neutron Slowing-Down Equation. This approach provided excellent agreement with high-fidelity Monte Carlo methods and resulted in a factor of 6 to 8 reduction in spectrum estimation error over the current fast spectrum generation methods for the cases studied.

The following sections will provide the background of neutron transport as it relates to lattice physics. Chapter 2 will provide an overview of the common lattice physics methods, also known as group constant generation methods. Chapter 3 will introduce the new methods developed for this work. Chapter 4 will discuss the implementation of these improved methods into a computer program called Pointwise Fast Spectrum Generator (PWFSG). Chapter 5 will include comparison of these improved methods against high-fidelity Monte Carlo methods and other lattice physics programs in a set of example cases. These example cases include a U-238 infinite medium, a sodium fast reactor (SFR) fuel cell, and a SFR fuel cell with recycled, transuranic-bearing fuel. Finally, Chapter 6 will include conclusions and recommendations for future work.

Nuclear Cross Sections

Overview

The distribution of neutrons inside a reactor core is the underlying driver for many of the behaviors observed at a macroscopic scale. A complete description of this population requires complete knowledge of the every neutrons' position, energy (i.e., speed), and direction as a

function of time. Such comprehensive knowledge of the neutron population is impractical to obtain; therefore, a number of assumptions are usually made about one or more of these independent variables to efficiently arrive at a solution.

Although the underlying behavior of a reactor is governed by the neutron distribution, the final reactor performance ultimately depends on the rate of the reactions occurring inside of the reactor core. A reaction rate is a product of the neutron flux and the probability of a specific interaction occurring. It is possible to have a large number of neutrons with a specific position, energy, and direction that are not reacting with the medium and not impacting reactor behavior.

The neutron angular flux is given in Eq. (1-1) where n is the neutron distribution as a function of position, $\vec{r}$; energy, E; direction, $\hat{\Omega}$; time, t; and the neutron speed, v.[5,6]

$$\psi\left(\vec{r},E,\hat{\Omega},t\right)=v\left(E\right)n\left(\vec{r},E,\hat{\Omega},t\right) \tag{1-1}$$

Figure 1-1 gives a sketch of the neutron flux in space and angle. At fast reactor energies (i.e., between a few eV and 20 MeV), the nuclear reaction rates are independent of the incident neutron direction. This makes the directionally-independent scalar flux an important quantity in reactor calculations. The definition of scalar flux is given in Eq. (1-2).

$$\phi\left(\vec{r},E,t\right)=\int_{4\pi} d\Omega\,\psi\left(\vec{r},E,\hat{\Omega},t\right) \tag{1-2}$$

The differential solid angle, $d\Omega$, in Eq. (1-2) is expanded in Eq. (1-3) where ω is the azimuthal angle with respect to the x-axis and θ is the polar angle with respect to the z-axis (see Fig. 1-1).

$$d\Omega=d\omega\,\sin\left(\theta\right)d\theta \tag{1-3}$$

The differential polar angle is commonly condensed into the parameter, μ.

$$d\mu=\sin\theta d\theta \tag{1-4}$$

$$d\Omega=d\omega\,d\mu \tag{1-5}$$

The reaction rate for a specific reaction is a product of the scalar flux, the atomic number density, and the reaction's microscopic cross section. This microscopic cross section is the effective area presented by a nucleus to a neutron for a given reaction. The microscopic cross section is often given in barns (1 b = 10^{-24} cm^2). The relationship for reaction rate, R_x, is shown for nuclear reaction x in Eq. (1-6) where $N(\vec{r},t)$ is the atomic number density at position $\vec{r}$ and time t and $\tilde{\sigma}_x(E)$ is the microscopic cross section for reaction x at energy, E.[6]

$$R_x(\vec{r},E,t) = N(\vec{r},t)\tilde{\sigma}_x(E)\phi(\vec{r},E,t) \tag{1-6}$$

The product of the microscopic cross section and number density can be combined into a single parameter known as the macroscopic cross section as shown in Eq. (1-7). The units of macroscopic cross section are area per volume (i.e., inverse length).

$$\sigma_x(\vec{r},E,t) = N(\vec{r},t)\tilde{\sigma}_x(E) \tag{1-7}$$

The use of the macroscopic cross section leads to the definition of the reaction rate given in Eq. (1-8).

$$R_x(\vec{r},E,t) = \sigma_x(\vec{r},E,t)\phi(\vec{r},E,t) \tag{1-8}$$

Cross sections are estimated by a combination of experimentation and modeling. In most cases, the cross section is not a smooth function of energy that is easily described by analytical functions. An example total cross section (i.e., sum of all reactions) for U-238 is given in Fig. 1-2. Below 4 eV and above 20 keV the cross section is relatively smooth; however, sharp peaks in the cross section occur between these energies. These cross section resonances occur at locations where the additional binding energy added to the nucleus by the neutron plus the neutron kinetic energy corresponds to an excitation level in the resulting compound nucleus (i.e., the combination of the nucleus plus the captured neutron, U-239). This causes the probability of neutron interaction at these resonance energies to significantly increase.

At higher energies, these resonances become more closely spaced eventually reaching a continuum. This behavior does not imply an absence of resonances but simply that the resonances are no longer resolvable. Hence, this region is termed the unresolved resonance region. For the U-238 total cross section in Fig. 1-2, this region is between 20 keV and 149 keV.

The cross section can also exhibit complicated behavior at much lower (<0.01 eV) or much higher (>20 MeV) energies. These energies are extremely rare in fission reactor analysis and are not considered in this work.

While not shown explicitly, the reaction rate of Eq. (1-8) is also a function of temperature. This temperature dependence is introduced by the Doppler-broadening phenomenon[7] that causes the cross section resonances to broaden and flatten at higher temperatures due to random atomic thermal motion. Cross section data are typically presented unbroadened, at a temperature of 0 K. Prior to use, the cross section data must be broadened to the appropriate temperature.

Cross section data are collected from experiments and models into libraries for use in nuclear physics calculations. These libraries are promulgated by the laboratories and government organizations that produced them. Examples of cross section libraries include the ENDF/B series from the United States,[8] the JEFF library from the European Union,[9] and the JENDL library from Japan.[10] These libraries may focus on different isotopes and applications, but share many original experimental evaluations. These libraries follow the standard ENDF-6 format[11] that allows processing programs to manipulate any set of library data, regardless of the source.

Cross Section Usage in Reactor Calculations

To determine the reaction rates in a reactor system, the flux (i.e., neutron population) and cross sections (i.e., interaction probabilities) must be known. As the cross sections are known via experiment, the flux, with respect to all of its independent variables, is the parameter of

interest. The equation for describing neutron behavior in a medium is the neutron transport equation. This equation describes the neutron balance over differential position, energy, and angle.

The neutron transport equation is given in Eq. (1-9).[5]

$$\frac{1}{v(E)}\frac{\partial \psi}{\partial t} = -\hat{\Omega}\bullet\nabla\psi - \sigma_t\left(\vec{r},E,t\right)\psi\left(\vec{r},E,\hat{\Omega},t\right) + \int_0^\infty dE'\left[\int_{4\pi} d\Omega'\,\sigma_s\left(\vec{r},E'\to E,\hat{\Omega}'\to\hat{\Omega},t\right)\psi\left(\vec{r},E',\hat{\Omega}',t\right)\right] + S\left(\vec{r},E,\hat{\Omega},t\right) \tag{1-9}$$

The negative terms on the right hand side (RHS) represent loss by streaming to another location in space (1st term) and loss by absorption and scatter out of the current phase space (2nd term). The two positive terms represent transfer into the phase space of interest from other phase spaces (3rd term) and neutron sources within the current phase space (4th term). This source term can be a fixed neutron source or sources due to reactions such as fission or (n, xn).

The cross section in the 3rd term is not a cross section in the sense described in the previous section but a differential cross section. In this case the cross section is a double-differential scattering cross section in energy and solid angle, with units of inverse length, energy, and angle (e.g., 1/cm-eV-sr). This cross section describes the probability per unit length of neutron transfer from a specific energy E' to a new energy E and from a direction $\hat{\Omega}'$ to a new direction $\hat{\Omega}$ following a scattering event. When integrated over all possible resulting energies and angles, this parameter reduces to the scattering cross section at E'.

Direct solution of the neutron transport equation in its full form is not possible analytically; however, this is not necessary for most reactor applications. A number of simplifications can be applied to the neutron transport equation to arrive at a form that is able to be implemented in a computer program. The neutron transport equation is often solved at a steady-state conditions (i.e., $\partial / \partial t = 0$) as in Eq. (1-10).

$$\hat{\Omega}\bullet\nabla\psi+\sigma_t\left(\vec{r},E\right)\psi\left(\vec{r},E,\hat{\Omega}\right)= \int_0^\infty dE'\int_{4\pi}d\Omega'\,\sigma_s\left(\vec{r},E'\to E,\hat{\Omega}'\to\hat{\Omega}\right)\psi\left(\vec{r},E',\hat{\Omega}'\right)+S\left(\vec{r},E,\hat{\Omega}\right) \tag{1-10}$$

Discretization of space, energy, and angle is often performed as well. In the case of Diffusion Theory, the angular dependence is removed completely through use of a diffusion coefficient applied to the streaming term.[12] Diffusion theory is applicable when the angular dependence of the neutron flux in the system is weak. This condition is met in the interior of many nuclear reactors. In regions of strong angular dependence (e.g., near reactor boundaries, areas of strong absorption), the diffusion assumption yields inaccurate results. Diffusion theory has found wide application in many core simulation programs such as DIF3D,[13] AETNA,[14] and SIMULATE.[15]

Asymptotic Flux Solution in Energy

A description of the asymptotic form of the neutron flux in energy will aid in determining the expected form of the neutron energy behavior in a simplified case. The knowledge of this asymptotic solution will inform future solutions and can form a first estimate of the flux profile with respect to the energy variable.

The first step in reducing the steady-state neutron transport equation to its asymptotic form is assuming the neutrons are present in an infinite medium. This removes any spatial dependence of the neutron flux and eliminates the streaming term (i.e., $\nabla=0$).[16]

$$\sigma_t\left(E\right)\psi\left(E,\hat{\Omega}\right)=\int_0^\infty dE'\int_{4\pi}d\Omega'\,\sigma_s\left(E'\to E,\hat{\Omega}'\to\hat{\Omega}\right)\psi\left(E',\hat{\Omega}'\right)+S\left(E,\hat{\Omega}\right) \tag{1-11}$$

Equation (1-11) can be integrated over $d\Omega$ to yield Eq. (1-12).

$$\sigma_t\left(E\right)\int_{4\pi}d\Omega\psi\left(E,\hat{\Omega}\right)= \int_0^\infty dE'\int_{4\pi}d\Omega'\psi\left(E',\hat{\Omega}'\right)\left[\int_{4\pi}d\Omega\;\sigma_s\left(E'\to E,\hat{\Omega}'\to\hat{\Omega}\right)\right]+\int_{4\pi}d\Omega\,S\left(E,\hat{\Omega}\right) \tag{1-12}$$

The next step is removing the angular dependence by integration over $d\Omega$. The differential scattering cross section depends on the change in angle and not the specific incoming and outgoing neutron angles.[12] This alters the scattering term to the form shown in Eq. (1-13).

$$\int_{4\pi} d\Omega\, \sigma_s\left(E' \to E, \hat{\Omega}' \to \hat{\Omega}\right) = \int_{2\pi} d\omega \int_{-1}^{+1} d\mu_0 \sigma_s\left(E' \to E, \mu_0\right) \tag{1-13}$$

The cosine of the scattering angle, μ_0, is given by the following relationship.

$$\mu_0 = \hat{\Omega} \bullet \hat{\Omega}' = \cos\left(\theta_0\right) \tag{1-14}$$

The angular dependence of the double-differential scattering cross section can now be removed because of the integration over all possible cosines from -1 to +1. This yields a single-differential scattering cross section in energy.

$$2\pi \int_{-1}^{+1} d\mu_0\, \sigma_s\left(E' \to E, \mu_0\right) = \sigma_s\left(E' \to E\right) \tag{1-15}$$

Substitution of Eq. (1-15) into Eq. (1-12) gives the infinite medium transport equation.

$$\sigma_t\left(E\right)\phi\left(E\right) = \int_0^{\infty} dE' \sigma_s\left(E' \to E\right)\phi\left(E'\right) + S\left(E\right) \tag{1-16}$$

The neutron transport equation has now been simplified to an integral equation in terms of energy only. If neutrons only lose energy in collisions, as is the case above thermal energies, the lower limit of integration of the scattering term is restricted to the current energy. This leads to the Neutron Slowing-Down Equation of Eq. (1-17).[17]

$$\sigma_t\left(E\right)\phi\left(E\right) = \int_E^{\infty} dE' \sigma_s\left(E' \to E\right)\phi\left(E'\right) + S\left(E\right) \tag{1-17}$$

In treating neutron slowing-down, the flux is often given in terms of the independent variable of lethargy. Lethargy is a measure of neutron slow-down relative to a reference energy. As the neutron slows down its lethargy increases, as is defined in Eq. (1-18). Differential lethargy is defined in Eq. (1-19).

$$u = \ln\left(\frac{E_o}{E}\right) \tag{1-18}$$

$$du = -\frac{1}{E}dE \tag{1-19}$$

The parameter E_0 is a specified reference energy, which is typically a source energy or maximum reachable energy in the model. The neutron flux function in energy can be given in terms of lethargy, u, as in Eq. (1-20).

$$\phi(u)\,du = -\phi(E)\,dE \tag{1-20}$$

$$\phi(u) = E\phi(E) \tag{1-21}$$

The solution to the slowing-down equation with isotropic scattering and no absorption in the center-of-mass frame of reference takes the form given in Eq. (1-22).[12]

$$\phi(E) = \frac{C}{E} \tag{1-22}$$

The parameter C is a constant representing the source strength or a normalization factor. If Eq. (1-22) is given with lethargy as the independent variable, then Eq. (1-22) reduces to the following form.

$$\phi(u) = C \tag{1-23}$$

This constant flux in lethargy is the asymptotic form of the flux which can serve as the starting point for more complicated spectrum calculations discussed in Chapter 2.

Group Constants

Spatial and energy dependence are often treated in a discrete fashion in the neutron transport equation. Without discretization of the neutron transport equation, the time and computational resources required to arrive at a solution would be impractical for engineering design and analysis. Discretization allows for a reactor system to be described by a few spatial nodes or zones and energy to be defined by a few groups. The trade-off of this approach is that the flux dependence within the node, zone, or group is lost in the final solution.

Reactor spatial dependence will often be discretized by homogenizing material properties over a volume and calculating an average flux in this volume. This volume is often a repeating structure such as a fuel pin or fuel assembly. Care must be taken to preserve any important flux variation in energy or space within this volume if it will affect the final system solution.

A similar discretization procedure is performed for energy by calculating the average flux in an energy group. These groups are sections of the neutron energy spectrum with similar properties. For example, in LWR analysis it is common to have an energy group below a 1 eV assigned to the thermal group, neutrons in the resonance energy range (e.g., 1 eV to 100 keV) assigned to a slowing-down group and neutrons above 100 keV assigned to a fast group.[14] Since the energy dependence of the flux within the group is lost during discretization, corresponding average cross sections in energy must be developed for each group to be used with the energy-averaged flux. These average cross sections are known as group constants.

The averaging of group constants is not as simple as weighting the cross section value in space and energy. Instead, the flux at the specific energy and point in space must be used to weight a cross section at a given location and energy to preserve reaction rates.

The flux weighted averaging of cross sections is complicated by self-shielding, which is where a large cross section depresses the flux at that specific energy and location. The energy self-shielding effect is often the result of strong resonances in the cross section. As the neutron population approaches the resonance energy, the number of neutrons available for interaction decreases due to neutron absorption or transfer away from the resonance energy. Therefore, the sharp resonance peak shields itself from the neutron interaction at the resonance energy. The result is a lower overall reaction rate at the resonance energy than if the neutron population

remained unshielded. Figure 1-3 is a sketch of how the flux is depressed in the vicinity of a resonance.

The self-shielding effect can also have spatial dependence, such as in a heterogeneous zone with both a resonant absorber and non-resonant material. The non-resonant material would be shielded from the resonant neutron energy because of the resonant absorber. Any spatial homogenization of this zone requires consideration of this effect to product accurate group constants. This effect is of particular importance in LWRs, where neutrons are born in fuel material, slow-down in moderator material, and then return to fuel material for reabsorption.

A number of methods have been developed to account for spatial self-shielding in lattice physics, also called cell calculations.[18,19,20] These methods are not discussed in Chapter 2. This work focuses on application to fast spectrum systems, where the energy self-shielding is of primary importance, and on a computer program developed for infinite medium calculations.

The standard method for deterministically modeling reactor systems is shown in Fig. 1-4. The energy self-shielding calculation is typically performed first on a unit cell of the reactor. A simplified geometric model, such as one-dimension or infinite medium, is applied to the unit cell. During this step, the continuous cross section data is processed into to a set of fine group constants, typically including tens, hundreds, or possibly thousands of energy groups. This work focuses on the process of generating the weighting spectrum for fine group constant generation. A method is presented in Chapter 3 for using continuous nuclear data to generate a pointwise flux solution for use in group constant generation.

The next step in reactor modeling is applying the fine group constants to a detailed cell calculation. This cell flux is then used to generate a few broad group constants for use in the full-core simulation. This cell calculation can be repeated for different operating conditions

(e.g., temperature, void, composition) resulting in a set of cell-averaged group constants as a function of energy and operating conditions. The result is a set of coarse group constants (e.g., fewer than 10) at a specific operating condition for each cell.

The final coarse group constants generated from the cell calculation are then applied to a full-core reactor simulation with the appropriate average values used for each unit cell and energy group.

The entire exercise of group constant generation would be trivial if the flux were known continuously as a function of space, energy, angle, and time. If the flux were known in perfect detail, the cross sections could be averaged with zero bias. However, as knowledge of the flux profile is the goal of solving the neutron transport equation, it will not be known beforehand. Even if the flux were known completely in a reactor system, any perturbation (e.g., temperature change, control rod insertion, flow or power change) could alter the flux profile and invalidate the current set of group constants. Therefore, the difficulty of creating group constants arises from the requirement of the flux to be known for all potential operating conditions before the flux is actually known. Chapter 2 describes some of the common approaches to handling the problem of group constant generation for both thermal and fast spectrum systems.

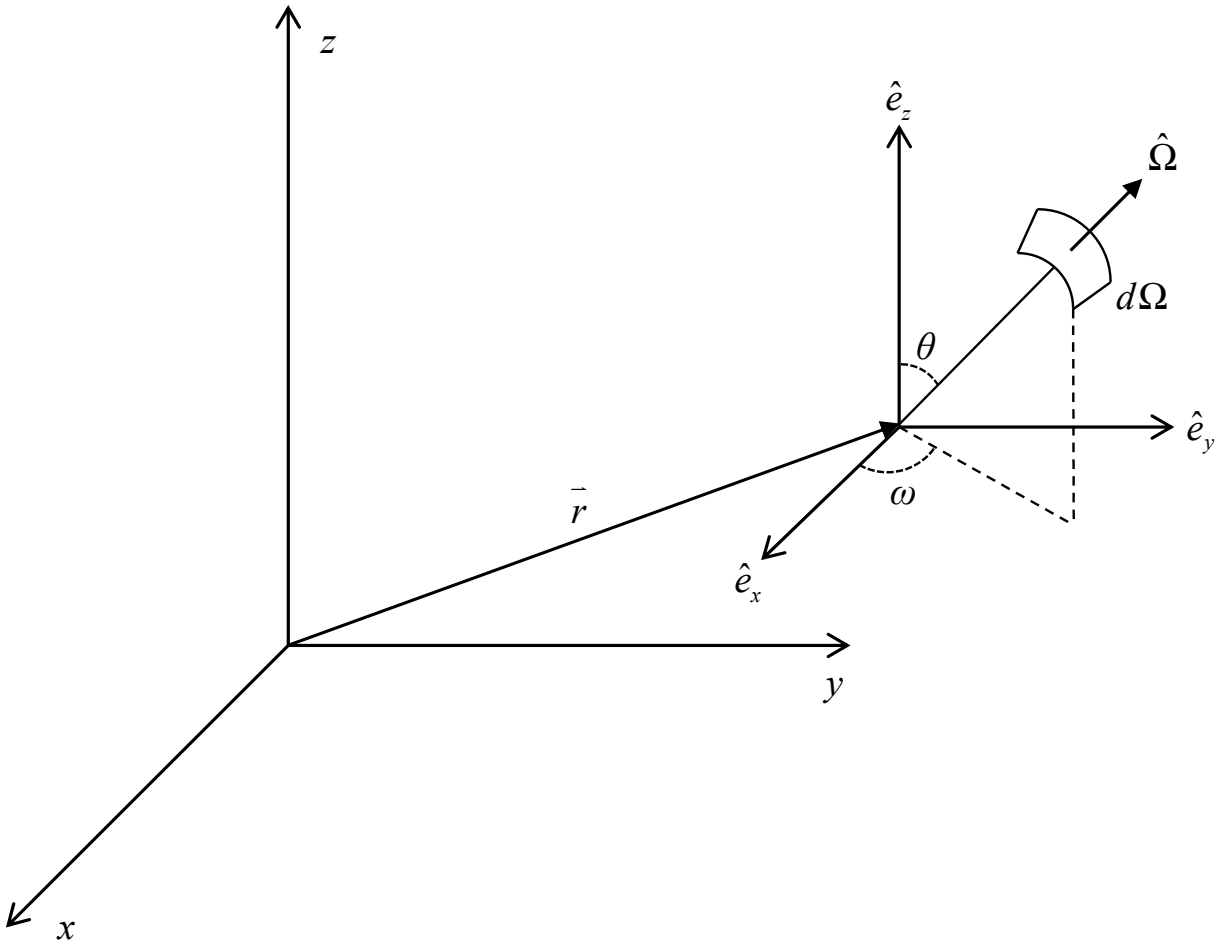

Figure 1-1. Diagram of neutron flux in space and angle. Diagram based on Figure 4-2 of Duderstadt and Hamilton.[5]

.

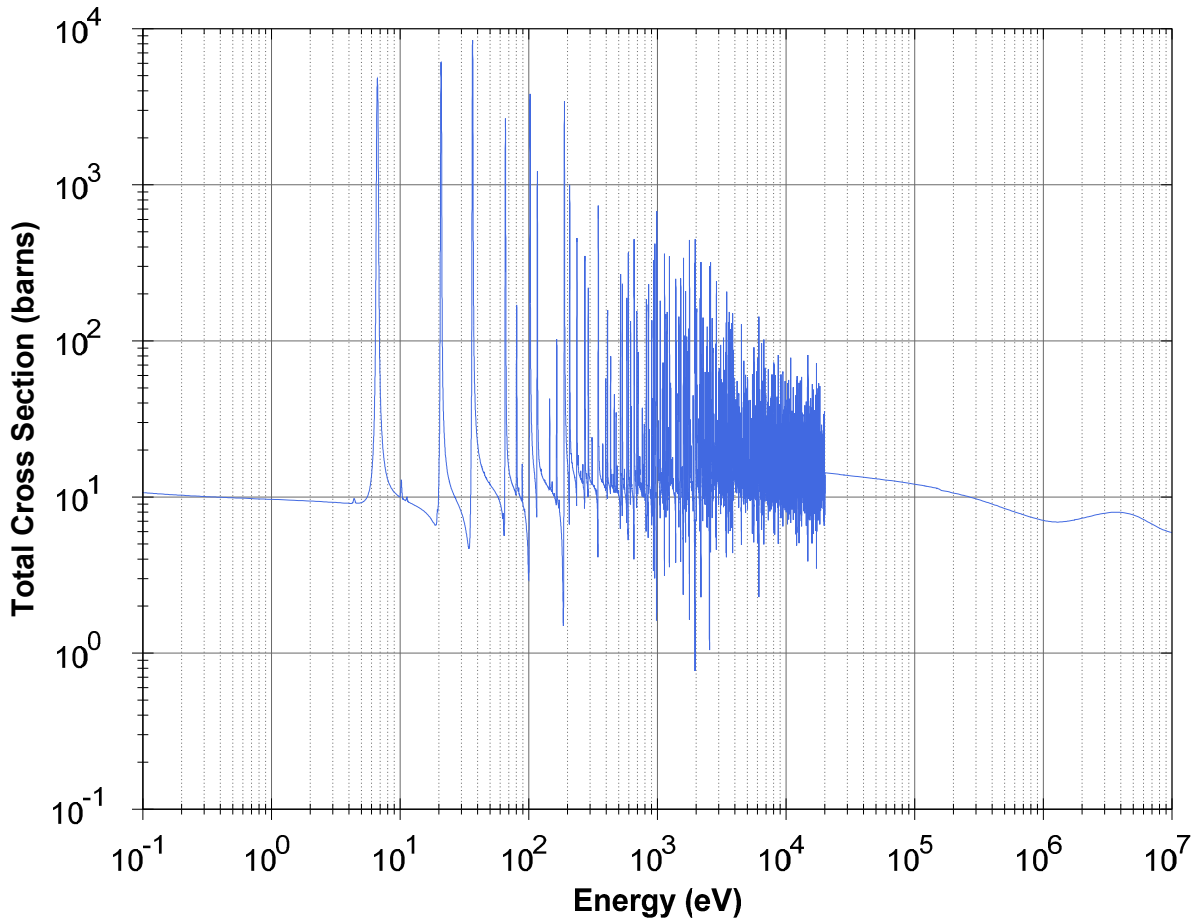

Figure 1-2. Example cross section in nuclear analysis. Example plot is total cross section of U-238.

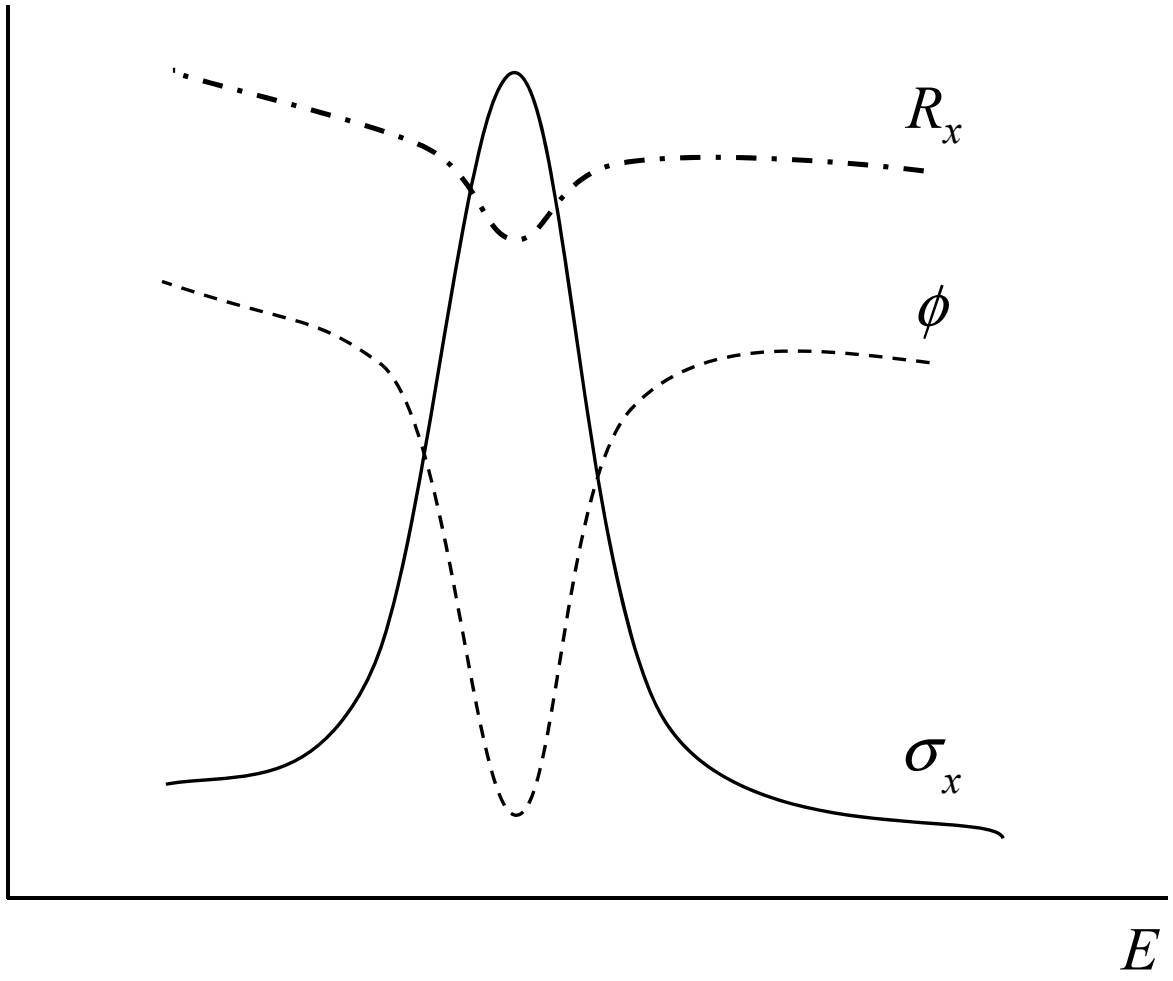

Figure 1-3. The flux self-shielding effect. The sharp resonance of the cross section, σ_x shields the neutron flux, ϕ, by removing neutrons from near resonance energies. The resulting reaction rate, R_x, is less than it would be if the flux had remained unshielded.[5]

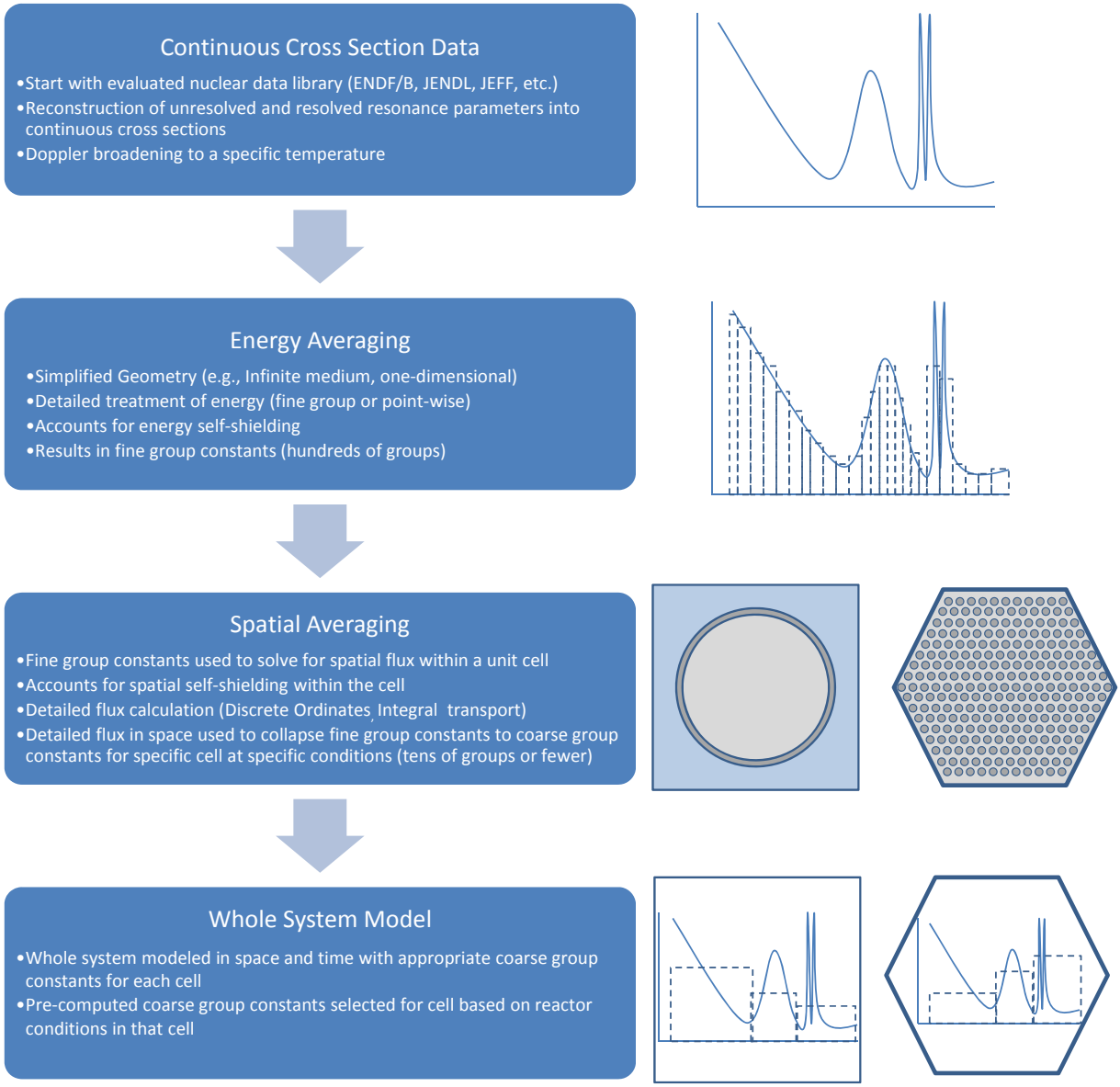

Figure 1-4. Group constant generation process

CHAPTER 2
CURRENT LATTICE PHYSICS/GROUP CONSTANT GENERATION METHODS

Introduction to Group Constants

The average value of a function over an interval is calculated as shown in Eqs. (2-1) and (2-2) where $x(t)$ is the function to be averaged over an independent variable t and $w(t)$ is the weighting function for averaging.

$$\int_a^b dt\, x(t)\, w(t) = \bar{x} \int_a^b dt\, w(t) \tag{2-1}$$

$$\bar{x} = \frac{\int_a^b dt\, x(t)\, w(t)}{\int_a^b dt\, w(t)} \tag{2-2}$$

In the simple case of determining the mean value of a function, the weighting function of Eq. (2-2) is equal to one. In the case of group constant generation where the reaction rates must be preserved, the weighting function is the scalar flux.

$$\bar{\sigma}_x(\vec{r}) = \frac{\int_{E_a}^{E_b} dE\, \sigma_x(\vec{r}, E)\, \phi(\vec{r}, E)}{\int_{E_a}^{E_b} dE\, \phi(\vec{r}, E)} \tag{2-3}$$

The difficulty arising from solution of Eq. (2-3) is the requirement that flux is known as a function of energy at a specific location in space. The most straightforward approach to solving Eq. (2-3) is to assume an approximate energy dependence of the flux. This would require experiential basis of the reactor system in question. This method would also assume that the net errors associated with this approach would be acceptable. The next section describes some of the common weighting spectrum methods.

Weighting Spectrum Methods

Bondarenko Method

In the original work on group constants, I. I. Bondarenko[21] proposed flux spectrum of the form of Eq. (2-4) where $\phi_0(u)$ is a smoothed flux spectrum without perturbation given in terms of lethargy.

$$\phi(u) \sim \frac{\phi_0(u)}{\sigma_t(u)} \tag{2-4}$$

Bondarenko proposed using the asymptotic flux solution as described in Eq. (1-23) where $\phi_0(u)$ is assumed to be constant. This reduces Eq. (2-3) to the form of Eq. (2-5).

$$\bar{\sigma}_x = \frac{\int_{u_a}^{u_b} du \frac{\sigma_x(u)}{\sigma_t(u)}}{\int_{u_a}^{u_b} du \frac{1}{\sigma_t(u)}} \tag{2-5}$$

Variations of Eq. (2-5) are made for the transport and elastic cross section but this basic form is the basis of the group constant generation method proposed by Bondarenko.

While the Bondarenko method is valid for a wide range of energies, the assumption of asymptotic flux is invalid near neutron sources, where neutrons have not yet reached asymptotic behavior. It is also invalid at energies where neutrons have thermalized with the medium. In the group constant set presented by Bondarenko, the asymptotic flux spectrum was used for all groups lower than 2.5 MeV. For the highest energy groups an analytic expression representing the neutron fission spectrum was used.[21]

The group constant method of Bondarenko is an example of how to apply knowledge of the system through different forms of the flux spectrum. For light water reactors (LWRs), the unperturbed flux profile is often a combination of a fission energy distribution at high energies,

the asymptotic form at slowing-down energies, and a Maxwellian distribution at thermal energies.

A noted weakness of a straightforward application of Eq. (2-5) is that it considers a medium containing only a single resonance absorber. As is often the case of nuclear reactors, the medium in question could be a mixture of different resonant materials (e.g., fuel isotopes) with non-resonant materials (e.g., structure and coolant isotopes). Bondarenko proposed a correction to Eq. (2-4) by including a background cross section, σ_0.

$$\phi(u) = \frac{\phi_0(u)}{\sigma_t(u) + \sigma_0} \tag{2-6}$$

The σ_0 term represents the constant background section from non-resonant isotopes. Spatial effects (leakage) can also be accounted for through σ_0.[7]

Inclusion of the background cross section dilutes the effect of the resonance on the flux. As σ_0 goes to infinity, the flux perturbation goes to zero. This condition is known as infinite dilution. If this condition, coupled with the asymptotic form, is substituted into Eq. (2-3) the group constant is simply the mean value of the cross section over the interval. This can be interpreted as no self-shielding taking place.

$$\bar{\sigma}_x = \frac{\int_{u_a}^{u_b} du\, \sigma_x(u)}{u_b - u_a} \tag{2-7}$$

Recall from Eq. (2-4) that the slowing-down form assumes that the total neutron interaction rate, $\sigma_t(u)\phi(u)$, is relatively constant. This condition is true if a collision within a resonant material removes the neutron from the resonance either by absorption or by scatter out of the resonance. This condition is given in Eq. (2-8) where Γ is the practical width of the resonance and ξ is the average fractional energy loss per scatter in the absorber.

$$\Gamma \ll \xi E \tag{2-8}$$

The Bondarenko method is based upon this Narrow Resonance Approximation. If collisions occur inside a resonance and the neutron fails to leave the resonance, then the condition of Eq. (2-8) no longer holds.

The constraint of a narrow resonance is well met if the scattering band (i.e., range of resultant energies) is wide compared to the resonance width. A plot of the scattering band width for various atomic weight isotopes is given in Fig. 2-1. At high energies, the large scattering band and narrower resonances (recall Fig. 1-1) lead to the satisfaction of Eq. (2-8) and validity of the Narrow Resonance Approximation.

At lower energies, the scattering band becomes logarithmically smaller and the resonances widen. These factors create difficulties for the Narrow Resonance Approach. At these energies the Wide or Intermediate Resonance Approximations[7,12] are more appropriate.

The Wide Resonance Approximation starts with the same fundamental equations as the Narrow Resonance method but assumes that a neutron does not leave a resonance upon collision. This condition is also expressed by the assumption that resonant isotope is infinitely absorbing (i.e., always absorbs neutrons which interact in the resonance rather than transfer them). Therefore this approximation is also called the Wide Resonance Infinite Absorber Approximation. The Wide Resonance Approximation arrives at the flux spectrum of Eq. (2-9).[7]

$$\phi(u) = \frac{\phi_0(u)}{\sigma_a(u) + \sigma_0} \tag{2-9}$$

The only difference between Eq. (2-6) and Eq. (2-9) is the use of the absorption cross section of the resonant isotope in the denominator rather than the total cross section.

The Intermediate Resonance Approximation is a combination of the Narrow and Wide Resonant approximations. The narrow and wide resonance expressions are combined and

weighted with the parameters λ and $(1-\lambda)$, respectively.[7] This approximation can be used for energies where neither the assumptions of the narrow or wide resonance approximations are valid.

The Bondarenko method based on the Narrow Resonance Approximation has been a standard approach for generation of group constants for three decades. The GROUPR module of the NJOY computer program is commonly used to produce group constants with the Narrow Resonance approach.[22] The fundamental formula used in GROUPR is given in Eq. (2-10), where *i* is the isotope index, ℓ is the Legendre component of the angular flux ($\ell = 0$ for scalar flux), and $C(E)$ is an input weighting spectrum.

$$\phi_\ell^i(E) = \frac{C(E)}{\left[\sigma_t^i(E) + \sigma_0^i\right]^{\ell+1}} \tag{2-10}$$

In the GROUPR module, $C(E)$ and σ_0 are input from the user resulting in cross sections at a set of temperatures and σ_0 values. A similar methodology is employed in the BONAMI module[23] of the SCALE computer package.[24]

The strength of the Narrow Resonance approach is its simplicity and ability to generate reusable group constants. A library of group constants can be generated as a function of temperature and background cross section. Examples of such group constant libraries include the VITAMIN-B6 library[25] processed by NJOY into the AMPX format used by SCALE. These group constant libraries are pseudo problem-independent because they have been processed with variable temperatures and background cross sections but a fixed weighting spectrum. These group constant libraries and are often the starting point for the generation of problem-specific libraries. For example, the 199 group VITAMIN-B6 library was collapsed with a specific

pressurized water reactor (PWR) and boiling water reactor (BWR) flux spectrum to create the 47 group BUGLE-96 library for pressure vessel shielding calculations.[26]

The Bondarenko method is often used in conjunction with an f-factor approach. In this approach a set of group constants are generated at zero temperature (no Doppler broadening) and infinite dilution conditions. This zero-temperature, infinite dilute set are scaled by an f-factor.

$$\sigma(T,\sigma_0) = f(T,\sigma_0)\sigma(0,\infty) \tag{2-11}$$

In this scenario, a table of f-factors is generated for scaling of the zero-temperature, infinite dilute group constants. The LANCER02 lattice physics generates f-factors via NJOY from a set of infinitely dilute cross sections at 0 K and cross sections at other values of temperature and background cross section. During LANCER02 execution, a logarithmic interpolation is performed on the background cross section and a quadratic interpolation is performed on the square root of the fuel temperature. This allows the LANCER02 program to obtain group constants for a specific amount of moderation and reactor temperature conditions without the need for recalculation of the group constants.[1]

The weakness of the Bondarenko method is the assumption of narrow, widely-spaced resonances. Resonance overlap, either within or between resonant materials, will introduce error because the flux will not be shielded as $1/\sigma_t$. Areas of particular concern are wide resonances at lower energies of fuel materials (e.g., U-235, Pu-239) and the closely-spaced, overlapping resonance region of fuel materials. The former issue can be treated by direct flux calculation in the thermal region (as in GROUPR) or by a wide or intermediate resonance approximations. The latter issue is of great importance in fast reactor analysis and often leads to the need to solve the flux with a higher degree of energy resolution.

Subgroup Method

The Subgroup method has found use in LWR lattice physics applications such as CASMO,[2] APOLLO2,[27] and HELIOS.[28] In newer lattice physics programs it has replaced the Bondarenko method because of its ability to create accurate group constants without resorting to direct solution of the transport equation. The Subgroup method offers improved accuracy over the Bondarenko method with similar computational requirements.

The Subgroup method, also known as the Multiband method or Probability Table method, was originally proposed as a method of self-shielding by Levitt[29] and Nikolaev[30] then advanced in the works of Cullen in the 1970s.[31] The Subgroup method has been further refined in the works of Hérbert[32] and incorporated into many modern lattice physics programs such as APOLLO2.[32,33]

The Subgroup method is based upon subdivision of the total cross section into subgroups, also called bands, within an energy group. A probability density function is developed for the total cross section within the group. Figure 2-2 demonstrates the translation from a cross section as a function of energy to a probability density function versus cross section value. The translation of a cross section versus lethargy or energy to a probability table is performed by taking a Riemann integral of the cross section and replacing it with an equivalent Lebesgue integral[34] as in Eq. (2-12).

$$\frac{1}{\Delta u_g}\int_{u_{g-1}}^{u_g} du\, f\left[\sigma(u)\right] = \int_0^{\max(\sigma)} d\sigma\, \Pi(\sigma) f(\sigma) \tag{2-12}$$

The LHS of Eq. (2-12) is the common definition of a cross section perturbed flux profile as in the Bondarenko approach. The RHS of Eq. (2-12) contains the probability density function of σ where $\Pi(\sigma)d\sigma$ is the probability that the cross section value with lie between σ and

$\sigma + d\sigma$. This probability density function is then represented by a finite, weighted set of Dirac distributions at discrete values of the cross section, $\delta(\sigma - \sigma_k)$.

$$\Pi(\sigma) = \sum_{k=1}^{K} \delta(\sigma - \sigma_k) w_k \tag{2-13}$$

Substituting Eq. (2-13) into Eq. (2-12) yields the relationship of Eq. (2-14) that forms the basis for Subgroup programs.

$$\frac{1}{\Delta u_g} \int_{u_{g-1}}^{u_g} du\, f\left[\sigma(u)\right] = \sum_{k=1}^{K} w_k f(\sigma_k) \tag{2-14}$$

The weights and σ_k values in Eq. (2-14) can be determined by a number of methods.[29,30,31]

The Subgroup method is an improvement of the Bondarenko method for resonance self-shielding. Instead of adding a finer group structure, the Subgroup method adds a dimension of variation on the total cross section via probability tables. Some of the works of Cullen demonstrate that a 175 group, 2 band calculation (350 equations) can yield reaction rates with equal or less error than a 2020 group calculation for U-235 critical spheres.[7] This improved efficiency has made the Subgroup method a popular choice for many LWR lattice applications.

One drawback of the Subgroup approach is the lack of resonance interference treatment. A common example of this interference effect can be observed in LWRs between the 20.9 eV resonance of U-238 and the 20.45 eV resonance of Pu-240. When resonances of multiple materials (e.g., a mixture of actinides in a fuel assembly) interfere with each other, the assumed shape function may be invalidated. Any calculation where the flux within a region of the problem is assumed to follow a prescribed shape dependent on the total cross section can be limited by this problem.

Direct Solution Methods

Fine Group Method

The fine group approach involves the solution of the discretized neutron transport equation with energy groups selected at energy (or lethargy) widths fine enough that the intra-group flux will be slowly varying (i.e., a linear variation or constant). The flux is then solved for directly, typically in simplified infinite medium or one-dimensional geometry. The resulting flux energy spectrum is then used as the weighting spectrum for group constant generation via Eq. (2-3).

The multigroup (MG) form of the transport equation is obtained by integrating the transport equation over discrete energy ranges. The MG form of the steady-state, angularly-independent neutron transport equation is shown in Eq. (2-15) for the energy range E_g to E_{g-1}.

$$\int_{E_g}^{E_{g-1}} dE\, \hat{\Omega}\bullet\nabla\psi + \int_{E_g}^{E_{g-1}} dE\, \sigma_t\left(\vec{r},E\right)\psi\left(\vec{r},E,\hat{\Omega}\right) = \int_{E_g}^{E_{g-1}} dE \int_{-1}^{+1} d\mu_0 \int_0^{\infty} dE'\sigma_s\left(\vec{r},E'\to E,\mu_0\right)\psi\left(\vec{r},E',\hat{\Omega}'\right) + \int_{E_g}^{E_{g-1}} dE\, S\left(\vec{r},E,\hat{\Omega}\right) \tag{2-15}$$

To simplify Eq. (2-15), group flux, group constants, and group source are defined in Eqs. (2-16), (2-17), and (2-18), respectively.

$$\psi_g\left(\vec{r},\hat{\Omega}\right) = \int_{E_g}^{E_{g-1}} dE\,\psi\left(\vec{r},E,\hat{\Omega}\right) \tag{2-16}$$

$$\sigma_{x,g}\left(\vec{r}\right) = \frac{\int_{E_g}^{E_{g-1}} dE\,\sigma_x\left(\vec{r},E\right)\psi\left(\vec{r},E,\hat{\Omega}\right)}{\int_{E_g}^{E_{g-1}} dE\,\psi\left(\vec{r},E,\hat{\Omega}\right)} \tag{2-17}$$

$$S_g\left(\vec{r},\hat{\Omega}\right) = \int_{E_g}^{E_{g-1}} dE\, S\left(\vec{r},E,\hat{\Omega}\right) \tag{2-18}$$

With the definitions above, Eq. (2-15) can be reduced to Eq. (2-19).

$$\hat{\Omega}\bullet\nabla\psi_g + \sigma_{t,g}\left(\vec{r}\right)\psi_g\left(\vec{r},\hat{\Omega}\right) = \int_{E_g}^{E_{g-1}} dE \int_{-1}^{+1} d\mu_0 \int_0^{\infty} dE'\sigma_s\left(\vec{r},E'\to E,\mu_0\right)\psi\left(\vec{r},E',\hat{\Omega}'\right) + S_g\left(\vec{r},\hat{\Omega}\right) \tag{2-19}$$

To accommodate the scattering term of Eq. (2-19), the total energy range considered is broken into G subintervals (i.e., energy groups) as shown in Eq. (2-20). A group to group transfer cross section is then defined in Eq. (2-21).

$$\hat{\Omega}\bullet\nabla\psi_g + \sigma_{t,g}\left(\vec{r}\right)\psi_g\left(\vec{r},\hat{\Omega}\right) = \sum_{g'=1}^{G}\int_{E_g}^{E_{g-1}} dE \int_{-1}^{+1} d\mu_0 \int_{E_{g'}}^{E_{g'-1}} dE'\sigma_s\left(\vec{r},E'\rightarrow E,\mu_0\right)\psi\left(\vec{r},E',\hat{\Omega}'\right) + S_g\left(\vec{r}\right) \tag{2-20}$$

$$\sigma_{s,g'\rightarrow g}\left(\vec{r},\mu_0\right) = \frac{\int_{E_g}^{E_{g-1}} dE \int_{E_{g'}}^{E_{g'-1}} dE'\,\sigma_s\left(\vec{r},E'\rightarrow E,\mu_0\right)\psi\left(\vec{r},E',\hat{\Omega}'\right)}{\int_{E_{g'}}^{E_{g'-1}} dE'\,\psi\left(\vec{r},E',\hat{\Omega}'\right)} \tag{2-21}$$

Equation (2-20) can now be reduced to the final MG form of the transport equation shown in Eq. (2-22).

$$\hat{\Omega}\bullet\nabla\psi_g + \sigma_{t,g}\left(\vec{r}\right)\psi_g\left(\vec{r},\hat{\Omega}\right) = \sum_{g'=1}^{G}\int_{-1}^{+1} d\mu_0\,\sigma_{s,g'\rightarrow g}\left(\vec{r},\mu_0\right)\psi_{g'}\left(\vec{r},\hat{\Omega}\right) + S_g\left(\vec{r},\hat{\Omega}\right) \tag{2-22}$$

The group fluxes in Eq. (2-22) are coupled via the scattering transfer term. This can become problematic as finer group structures are employed because the probability of transfer from every group to every other group must be calculated. In the worst, case this would require G^2 calculations.

Approximations can be made to Eq. (2-22) to reduce the computational burden of group-to-group scatter. A common approximation in fast neutron systems is to assume neutrons only down-scatter. This allows the scattering term of Eq. (2-22) to be summed from the current group to the highest energy group, ignoring all lower energy groups. Another approximation is to space groups such that scatter will only occur to the next lowest group. This approximation is of great utility in coarse-group, whole-core simulations because there is a fixed input to the lower groups and no summation loop required.

Group constants must still be determined for application of the MG methods (see Eqs. (2-17) and (2-21)). The difference with the fine group approach is that the impact of the assumed weighting spectrum is minimized because the energy group size is relatively fine. With the fine-group approach, the Bondarenko method can be used to develop initial group constants for the MG solution. These group constants can then be updated with the resulting flux from the fine group solution if desired.

In the fine group approach the spatial dependence is often treated with a course approximation. Infinite medium calculations are common when spatial dependence is of secondary importance, a zero-dimensional correction can be used to account for the leakage effect on the energy spectrum. In this zero-dimensional approach the spatial dependence of the flux approximated via a geometric buckling factor, $\vec{B}$.

$$\psi\left(\vec{r},E,\hat{\Omega}\right)=\psi\left(E,\hat{\Omega}\right)e^{i\vec{B}\bullet\vec{r}} \tag{2-23}$$

The lumped buckling parameter describes the loss of neutrons by leakage and can be given on a group-wise basis if necessary.

The zero-dimensional transport equation can be derived by substitution of Eq. (2-23) into the neutron transport equation.

$$\left[\sigma_t\left(E\right)+i\vec{B}\bullet\hat{\Omega}\right]\psi\left(E,\hat{\Omega}\right)=\int_E^\infty dE\int_{-1}^{+1}d\mu_0\,\sigma_s\left(E'\rightarrow E,\mu_0\right)\psi\left(E',\hat{\Omega}'\right)+S\left(E,\hat{\Omega}\right) \tag{2-24}$$

If the angular component of the flux and scattering cross section are expanded into spherical harmonics the following relationship is obtained for planar geometry.[35]

$$\left[\Sigma_t\left(E\right)+iB\mu\right]\psi\left(E,\mu\right)=\int_E^\infty dE\sum_{\ell=0}^{\infty}\frac{\left(2\ell+1\right)}{2}\Sigma_{s\ell}\left(E'\rightarrow E\right)\phi_\ell\left(E\right)P_\ell\left(\mu\right)+S_\ell\left(E\right) \tag{2-25}$$

The zero-dimensional transport equation can be simplified through the recursion relationship for Legendre Polynomials given by Eq. (2-26) and the application of the orthogonality property of Legendre Polynomials.

$$(\ell+1)P_{\ell+1}(x)-(2\ell+1)xP_{\ell}(x)+\ell P_{\ell}(x)=0 \tag{2-26}$$

Use of these Legendre Polynomial properties results in Eq. (2-27) where ℓ is the Legendre order of the flux or differential cross section.

$$\frac{\ell+1}{2\ell+1}iB\phi_{\ell+1}(E)+\frac{\ell}{2\ell+1}iB\phi_{\ell-1}(E)+\sigma_t(E)\phi_{\ell}(E)= \int_E^{\infty}dE'\sigma_{s\ell}(E'\rightarrow E)\phi_{\ell}(E')+S_{\ell}(E) \tag{2-27}$$

The fast reactor group constant program MC^2 solves Eq. (2-27) using a number of transport methods including ultra and hyper fine MG.[35]

Pointwise Method

Another direct approach to developing problem dependent group constants is a pointwise (PW) method. In this approach, the flux is solved at a set of energy points that are spaced such that the flux variation between points can be assumed linear. The resulting PW flux is then a linear-interpolatable function in energy. At resonance energies this continuous energy, PW solution can be useful as it represents one of the highest fidelity methods currently available. This PW method was first introduced by Williams[36] and has been implemented in the CENTRM module[37] of the SCALE analysis package from Oak Ridge National Laboratory.[24]

The CENTRM method combines a classic MG approach with a PW flux solution. CENTRM applies a high-fidelity, PW solution where the flux has strong energy dependence (e.g., resonance energies) and a traditional MG solution where the flux is slowly varying (e.g., high energies).

Figure 2-3 shows the regions of solution for CENTRM. In the MG regions the group constants can be self-shielded by the Bondarenko method; the MG fluxes solved by the aforementioned MG solution methods. In the PW range the transport equation is written as Eq. (2-28) where *n* is the energy point where the flux will be balanced.

$$\begin{aligned}\hat{\Omega}\bullet\nabla\psi_n\left(\vec{r},\hat{\Omega}\right)+\sigma_{t,n}\left(\vec{r}\right)\psi_n\left(\vec{r},\hat{\Omega}\right)\\ =\int_{-1}^{+1}d\mu_0\int_E^{\infty}dE'\,\sigma_s\left(\vec{r},E'\rightarrow E,\mu_0\right)\psi\left(\vec{r},E',\hat{\Omega}'\right)+S_n\left(\vec{r},\hat{\Omega}\right)\end{aligned} \tag{2-28}$$

Note that the form of the equation in Eq. (2-28) is very similar to the MG form of Eq. (2-22) with the exception of the cross section definitions and the scattering source.[36] The CENTRM program uses the same subroutines to solve the transport equation in the PW region as it does in the MG region.

CENTRM uses sub-moment expansion[38] to separate the final energy dependence, *E*, out of the transfer source integrand of Eq. (2-28) and into a series of sub-moments. The removal of the final energy dependence from the integrand allows for a continuous summation of the transfer source over initial energy, *E′*, as the calculation progresses from high energy to low energy. This avoids the recomputing of the transfer source at each energy point and, therefore, makes the PW solution method in CENTRM more efficient.

The primary difference between the PW and MG solutions is the definition of the resulting flux. The PW formula of Eq. (2-28) describes neutron balance at a specific energy, while the MG form describes neutron balance over an energy interval. The units of flux in the PW solution are 1/eV-cm^2-s and the MG solution flux has the normal scalar flux units of 1/cm^2-s. Conversion between the two quantities can be performed by dividing the MG flux by ΔE or Δu. This assumes the PW flux is an accurate representation of the average flux over the entire interval.

The PW method does not conserve reaction rates over an energy interval. By using a PW solution, the overall particle balance on an energy interval is not maintained. However, for the

purposes of obtaining a weighting spectrum, a PW solution is typically acceptable because the overall flux shape is of primary importance and not the actual reaction rates occurring in the system. This effect is further mitigated by using a larger number of energy points. CENTRM uses enough points to assume linear flux dependence between the energy points. A typical PW solution for CENTRM includes 10,000 to 70,000 points, depending on the isotopes present.[37]

The inclusion of spatial dependence in a PW solution is dependent on the degree of fidelity desired. CENTRM contains options ranging from infinite medium to one-dimensional geometry. Often in lattice physics methods for LWRs, the flux spectrum variation in a unit cell, particularly a large unit cell like a fuel assembly, can be significant enough to warrant inclusion of detailed spatial treatment. The PW solution can be solved in two- or three-dimensional space using the Discrete Ordinates (i.e., S_N) method or the Method of Characteristics.[6]

An example of spatial and PW coupling is the GEMINEWTRN module of SCALE.[4] GEMINENTRN couples a two-dimensional Discrete Ordinates method with the CENTRM PW flux module. This can yield highly accurate results for highly heterogeneous fuel designs such as mixed oxide (MOX)-bearing BWR lattices.

The strength of the fine group or PW approach is its high degree of fidelity. The neutron transport equation is solved directly for the material and temperature of interest instead of using an assumed weighting spectrum perturbed by a function of the cross section or other factors. The drawback of this approach is that the resulting group constants are not reusable, because the detail of the system has been captured in the higher accuracy group constants. Application of these group constants to temperatures and compositions different from the original basis would introduce error. There is no straightforward means of scaling the group constants to a different application with the fine-group approach.

The PW solution method represents one of the highest accuracy methods for calculating the neutron energy spectrum. The work presented here is based on the work of the PW solution method, particularly the methods employed in the CENTRM computer package.

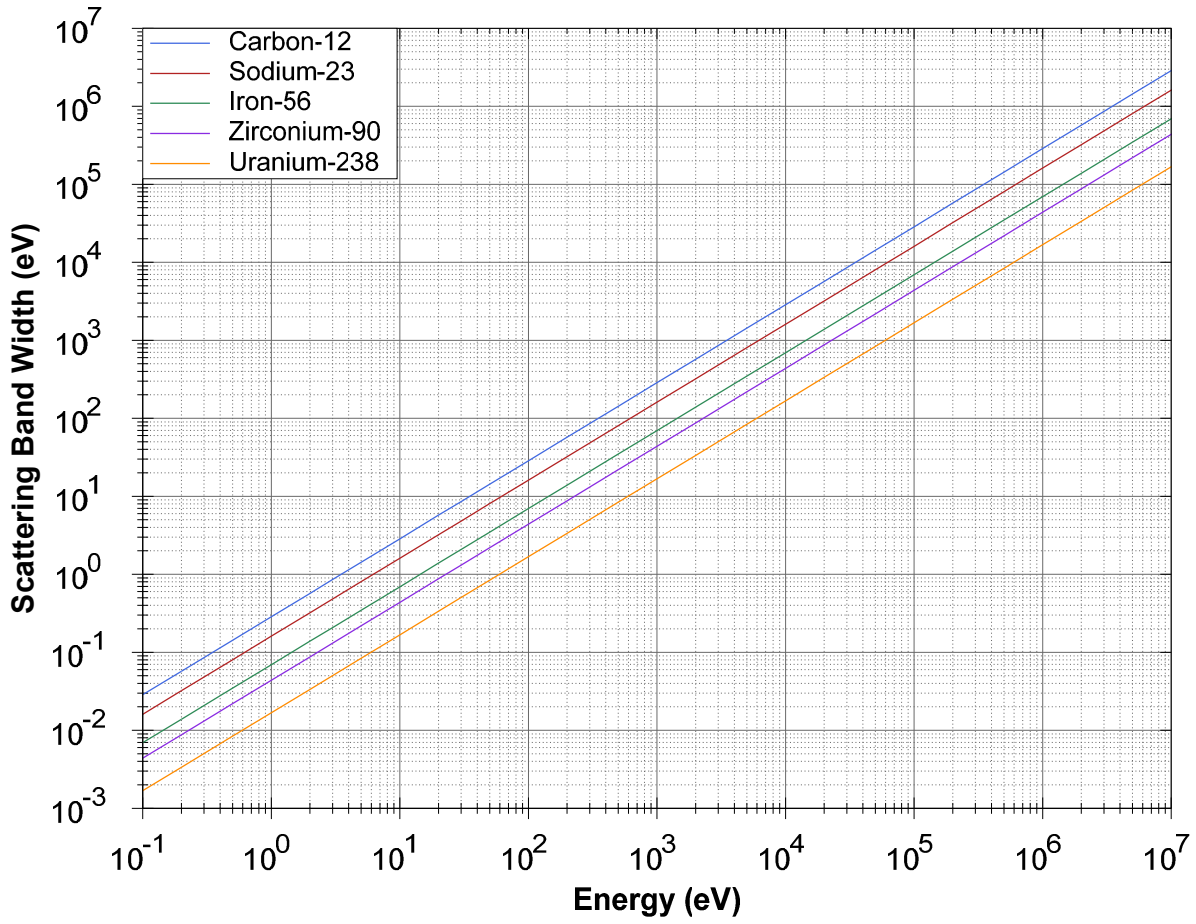

Figure 2-1. Scattering band width for various isotopes

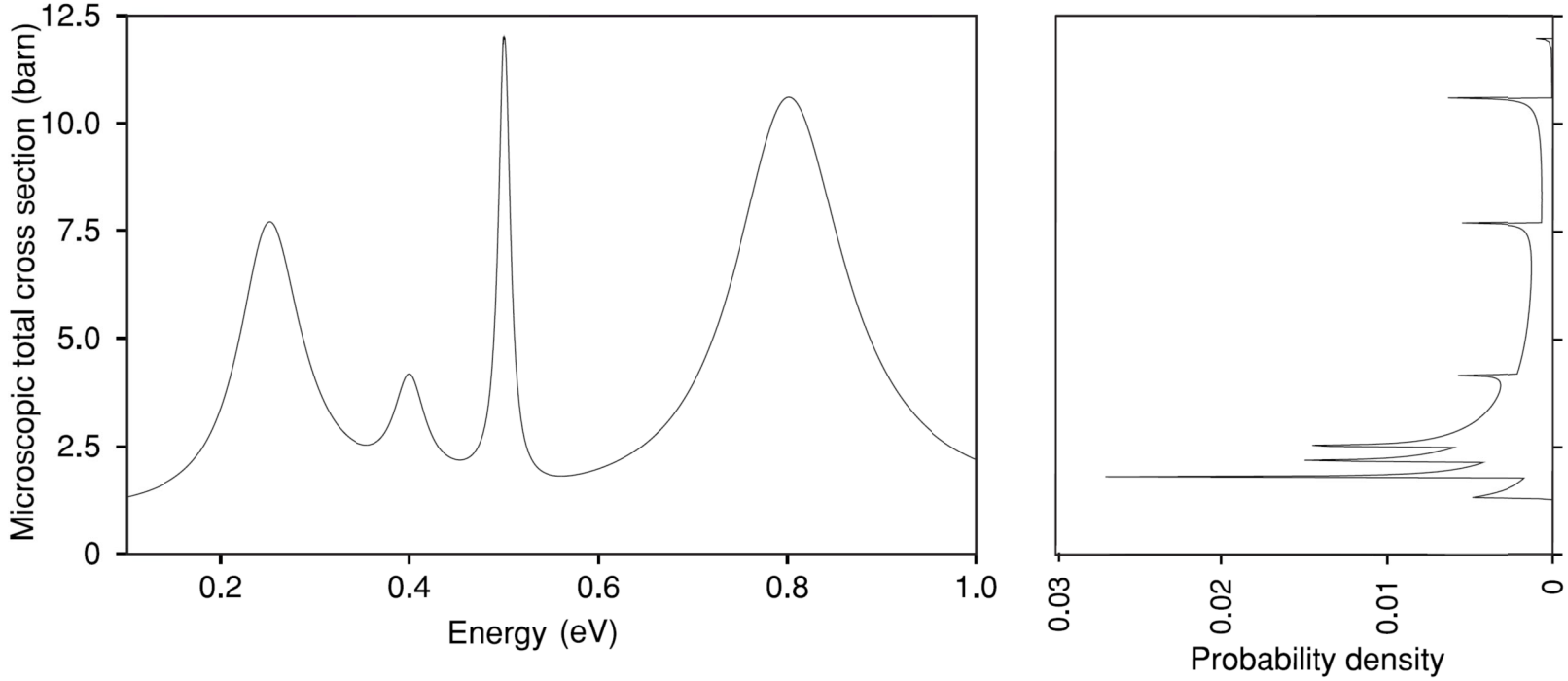

Figure 2-2. Representation of the total cross section probability density function for the Subgroup method. Total cross section versus energy is shown on the left and the probability density versus cross section value is shown rotated on the right. Example plot from Figure 1 of Hébert and Coste.[34]

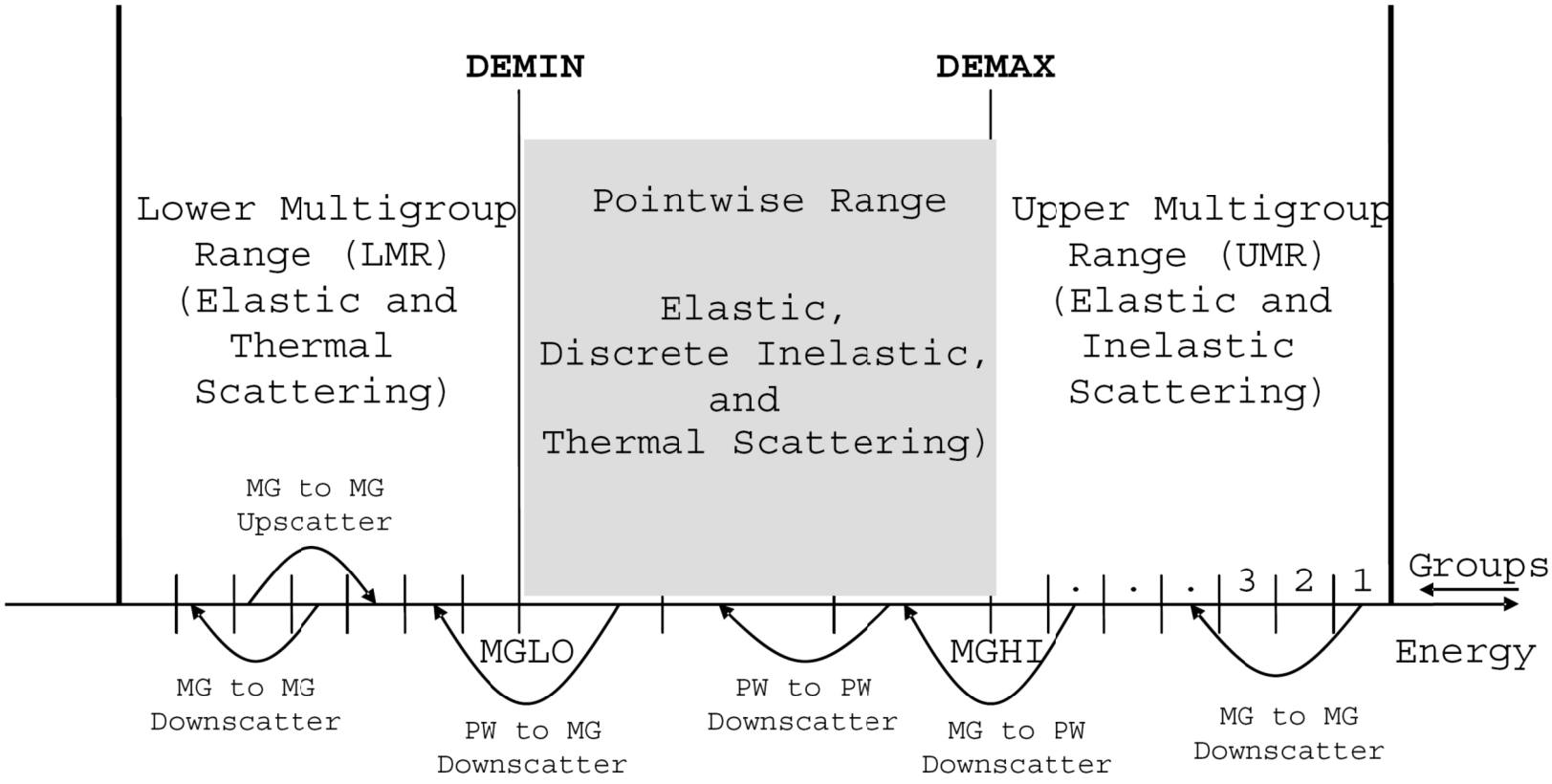

Figure 2-3. Regions of solution for the CENTRM program. Diagram from Figure F18.1.1 of Williams, Asgari, and Hollenbach.[37]

CHAPTER 3
POINTWISE FLUX SPECTRA GENERATION WITH ADAPTIVE QUADRATURE

Neutron Energy Transfer Mechanisms

The generation of accurate group constants is highly dependent on adequately describing the energy dependence of the neutron flux. Collisions with nuclei in a system transfer neutrons from source energies to lower energies. In a thermal reactor, such as a light water reactor (LWR), these neutrons slow down until they thermalize (reach energies comparable with the thermal motion of the reactor medium). In a fast reactor, the neutrons are usually absorbed or leak from the system before thermalizing and thus remain in the slowing-down mode for their entire lifetime.

The primary mode of neutron energy transfer within a nuclear reactor is scattering. Neutron scattering occurs when neutrons collide with the nucleus of an atom and impart some of their kinetic energy to the nucleus. If the nucleus is left in an excited state after the collision, the kinetic energy of the reaction is not conserved and this reaction is inelastic. In this scenario, the nucleus de-excites via some subsequent nuclear decay mechanism such as gamma ray emission. Otherwise, the scattering reaction is a two-body collision where kinetic energy is conserved and is considered elastic.

As the scattering energy transfer mechanism is important to describing the neutron energy dependence and, by extension, determining the group constants, it is important to briefly describe the relationships that govern energy transfer in scattering reactions.

Scattering Kinematics

Figure 3-1a diagrams the neutron-nucleus interaction before and after a scattering event. A neutron with mass, m, and velocity, v_0, strikes a nucleus, assumed to be at rest, scatters into a new angle, θ_0, and imparts some of its kinetic energy to the nucleus. This assumption of the

nucleus at rest is valid when the neutron energy is well above *kT,* where *k* is Boltzmann's constant of 8.617×10^{-5} eV/K and *T* is the temperature of the medium in K.

The conservation of energy before and after collision is given in Eq. (3-1) where *Q* is the excitation energy of the nucleus if the reaction is inelastic. For an elastic collision, *Q* is equal to zero.

$$\frac{1}{2}mv_0'^2 = \frac{1}{2}mv_o^2 + \frac{1}{2}MV_0^2 - Q \tag{3-1}$$

The conservation of momentum before and after collision is given in the *x* and *y* direction by Eqs. (3-2) and (3-3), respectively.

$$mv_0' = mv_0 \cos(\theta_0) + MV_0 \cos(\varphi_0) \tag{3-2}$$

$$0 = mv_0 \sin(\theta_0) + MV_0 \sin(\varphi_0) \tag{3-3}$$

This system of coordinates is referred to as the laboratory system. To facilitate a full description of this scattering event, the system will be cast into a new frame of reference. In this new frame of reference, the entire system is moving at the same velocity as the center-of-mass of the neutron-nucleus pair. Therefore this system is referred to as the center-of-mass (COM) system. A diagram of the COM system is shown in Fig. 3-1b.

Solution of the neutron energy and momentum equations in the COM system enables solution of the scattering angle in the laboratory system. The details of this procedure can be found in Ref. 12. Following this procedure and converting velocity to kinetic energy provides the following relationship for scattering angle in the laboratory system.

$$\cos(\theta_0) = \left(\frac{A+1}{2} - \frac{QA}{2E}\right)\sqrt{\frac{E}{E'}} - \frac{A-1}{2}\sqrt{\frac{E'}{E}} \tag{3-4}$$

The variable E' is used to denote initial energy and E to denote final energy. This convention is used to maintain consistency with the differential scattering cross section in the neutron transport equation.

The cosine of the scattering angle on the left hand side (LHS) of Eq. (3-4) is commonly condensed into a single parameter, μ_0. The formulation for the scattering energy transfer in the lab system is then given by Eq. (3-5).

$$\mu_0\left(E,E'\right)=\alpha_1\sqrt{\frac{E}{E'}}-\alpha_2\sqrt{\frac{E'}{E}} \tag{3-5}$$

The parameters α_1 and α_2 are defined in Eqs. (3-6) and (3-7), respectively.

$$\alpha_1=\frac{A+1}{2}-\frac{QA}{2E} \tag{3-6}$$

$$\alpha_2=\frac{A-1}{2} \tag{3-7}$$

The above scattering angle formulation is used in many nuclear simulation programs such as CENTRM.[37]

It can also be useful to describe the energy transfer in terms of the COM scattering angle. The energy-angle relationship in the COM system can be developed using the velocity vectors as shown in Fig. 3-1c and the Law of Cosines. The result of this procedure is the following energy-angle relationship in the COM system.

$$\mu_c\left(E,E'\right)=\frac{1}{2}\left[\frac{\frac{E}{E'}\left(A+1\right)^2-1}{\gamma\left(E'\right)}-\gamma\left(E'\right)\right] \tag{3-8}$$

$$\gamma\left(E'\right)=A\sqrt{1+\frac{A+1}{A}\frac{Q}{E'}} \tag{3-9}$$

Again the convention is used where E' is the initial neutron energy before scatter and E is the final energy after scatter.

Scattering Kernel

The neutron scattering kernel describes the probability of neutron energy transfer between two energies. The scattering kernel appears in the neutron transport equation as a double-differential cross section, $\sigma_s(E' \to E, \mu_0) dE\, d\mu_0$. This parameter gives the probability that a neutron will scatter from an energy, E', to a new energy interval dE about E with a change of direction within $d\mu_0$ about μ_0.

The value of $d\mu_0$ varies between -1 (full backscatter) to +1 (glancing collision). This allows the angular dependence of the scattering kernel to be represented by an infinite series of Legendre Polynomials. Legendre Polynomials exist in the domain of [-1, +1] and can be expanded to the necessary order to describe the angular dependence of the scattering kernel. Application of these Legendre Polynomials to the double-differential scattering cross section yields the relationship in Eq. (3-10), where $P_{\ell'}(\mu_0)$ is a Legendre Polynomial of order ℓ' and $\sigma_{s\ell'}(E' \to E)$ is the associated polynomial coefficient.

$$\sigma_s\left(E' \to E, \mu_0\right) = \sum_{\ell'=0}^{\infty} \frac{\left(2\ell'+1\right)}{2} \sigma_{s\ell'}\left(E' \to E\right) P_{\ell'}\left(\mu_0\right) \tag{3-10}$$

Both sides of Eq. (3-10) can be multiplied by another Legendre Polynomial of order ℓ and integrated over the entire range of μ_0, resulting in Eq. (3-11).

$$\int_{-1}^{+1} d\mu_0 \sigma_s\left(E' \to E, \mu_0\right) P_\ell\left(\mu_0\right) = \int_{-1}^{+1} d\mu_0 \sum_{\ell'=0}^{\infty} \frac{\left(2\ell'+1\right)}{2} \sigma_{s\ell'}\left(E' \to E\right) P_{\ell'}\left(\mu_0\right) P_\ell\left(\mu_0\right) \tag{3-11}$$

Legendre Polynomials are orthogonal functions. As such, Legendre Polynomials with the normalization of $(2m+1)/2$ have the property of Eq. (3-12) where δ_{mn} is the Kronecker delta function given in Eq. (3-13).

$$\int_{-1}^{+1} dx\, P_m(x) P_n(x) = \frac{2\delta_{mn}}{2m+1} \tag{3-12}$$

$$\delta_{mn} = \begin{cases} 1 & \text{if } m = n \\ 0 & \text{if } m \neq n \end{cases} \tag{3-13}$$

Using the orthogonality property of Legendre Polynomials, Eq. (3-11) reduces to Eq. (3-14).

$$\int_{-1}^{+1} d\mu_0 \sigma_s(E' \to E, \mu_0) P_\ell(\mu_0) = \sigma_{s\ell}(E' \to E) \tag{3-14}$$

To determine the right hand side (RHS) of Eq. (3-14), another form of the scattering kernel is necessary. The scattering kernel is separated into components and expressions are developed for each.[39]

$$\sigma_s(E' \to E, \mu_0)\, dE d\mu_0 = \sigma_s(E')\, p_0(E', \mu_0)\, d\mu_0\, g(\mu_0, E' \to E)\, dE \tag{3-15}$$

The variable $\sigma_s(E')$ is the total probability of scattering at E', while $p_0(E', \mu_0)$ is the probability that, if scattered at E', the neutron will scatter within the angle $d\mu_0$ about μ_0. Finally, $g(\mu_0, E' \to E)$ is the probability that, once a neutron scatters through μ_0, the resulting energy will be within dE about E.

In both elastic and discrete inelastic scattering, the energy transfer is directly related to angle. These relationships are given via Eq. (3-5) in the lab system or Eq. (3-8) in the COM system. This leads to the expression for $g(\mu_0, E' \to E)$ given in Eq. (3-16) where the RHS is the Dirac delta function defined in Eq. (3-17).

$$g(\mu_0, E' \to E)\, dE = \delta\left[\mu_0 - \mu_0(E, E')\right] d\mu_0 \tag{3-16}$$

$$\int_{-\infty}^{\infty} dx\, f(x)\, \delta(x - x_0) = f(x_0) \tag{3-17}$$

The usage of the Dirac delta function restricts the energy probability density function to the specific energy resulting from the scatter. An alternate form of the scattering kernel is now given in Eq. (3-18).

$$\sigma_s\left(E'\to E,\mu_0\right)=\sigma_s\left(E'\right)p_0\left(E',\mu_0\right)\delta\left[\mu_0-\mu_0\left(E,E'\right)\right]\frac{d\mu_0}{dE} \tag{3-18}$$

The form of the scattering kernel in Eq. (3-18) can be inserted into Eq. (3-14) yielding Eq. (3-19).

$$\sigma_{s\ell}\left(E'\to E\right)=\int_{-1}^{+1}d\mu_0\sigma_s\left(E'\right)p_0\left(E',\mu_0\right)\delta\left[\mu_0-\mu_0\left(E,E'\right)\right]\frac{d\mu_0}{dE}P_\ell\left(\mu_0\right) \tag{3-19}$$

The Dirac delta function property in Eq. (3-17) can be used to reduce Eq. (3-19) to Eq. (3-20).

$$\sigma_{s\ell}\left(E'\to E\right)=\sigma_s\left(E'\right)p_0\left[E',\mu_0\left(E,E'\right)\right]\frac{d\mu_0\left(E,E'\right)}{dE}P_\ell\left[\mu_0\left(E,E'\right)\right] \tag{3-20}$$

The result in Eq. (3-20) may be substituted back into Eq. (3-10) to yield an expression for the coefficient ℓ of the scattering kernel, where μ_0 is the specific scattering angle in the given coordinate system that results from an energy transfer of E' to E.

$$\sigma_s\left(E'\to E,\mu_0\right)=\sum_{\ell'=0}^{\infty}\frac{2\ell'+1}{2}\sigma_s\left(E'\right)p_0\left(E',\mu_0\right)\frac{d\mu_0}{dE}P_\ell\left(\mu_0\right)P_{\ell'}\left(\mu_0\right) \tag{3-21}$$

The primary focus of a slowing-down calculation is the scalar neutron flux energy dependence; therefore, the angular dependence of Eq. (3-21) can be removed via integration. Equation (3-22) is obtained by integrating Eq. (3-21) over angle and using the property of Legendre Polynomials given in Eq. (3-12).

$$\sigma_s\left(E'\to E\right)=\sigma_s\left(E'\right)p_0\left(E',\mu_0\right)\frac{d\mu_0}{dE} \tag{3-22}$$

The Jacobian in Eq. (3-22) accounts for the change in variable from a per unit energy to a per unit cosine basis. The Jacobian can be determined by taking the derivative of Eq. (3-5). This derivative is given for the laboratory system in Eq. (3-23).

$$\frac{d\mu_0}{dE}=\frac{1}{4}\left(EE'\right)^{-1/2}\left[A+1+\frac{QA+\left(A-1\right)E'}{E}\right] \tag{3-23}$$

If a probability density function is directly supplied via experiment or model, all terms of Eq. (3-22) are known and the scattering kernel is fully described. In some ENDF evaluations the function $p_0(E',\mu_0)$ is given as a tabulated function of probability versus cosine at a number of energies for a given isotope and reaction.[11]

Often the ENDF representation of the probability density function is an expansion of Legendre Polynomials. The probability density function in this form would be given by a Legendre Polynomial expansion with $N+1$ terms as in Eq. (3-24) where the ENDF libraries supply the Legendre coefficients, $a_n(E')$.[11]

$$\sigma_s\left(E' \to E\right) = \sigma_s\left(E'\right)\left[\sum_{n=0}^{N} \frac{2n+1}{2} a_n\left(E'\right) P_n\left(\mu_0\right)\right] \frac{d\mu_0}{dE} \tag{3-24}$$

Elastic scattering is often isotropic, or nearly isotropic, in the COM frame of reference. The closer the scattering is to isotropic, the fewer terms required in the expansion in Eq. (3-24). For the latest ENDF/B library release, ENDF/B-VII.0, all elastic scattering is represented entirely in the COM system.

A transition from the lab representation of Eqs. (3-22) and (3-24) to the COM system is performed by a change of variables for the probability density function of Eq. (3-22).

$$p_c\left(E',\mu_c\right) d\mu_c = p_0\left(E',\mu_0\right) d\mu_0 \tag{3-25}$$

Substitution of Eq. (3-25) into Eq. (3-22) yields the following result.

$$\sigma_s\left(E' \to E\right) = \sigma_s\left(E'\right) p_c\left(E',\mu_c\right) \frac{d\mu_c}{dE} \tag{3-26}$$

The form of Eq. (3-26) is the same as the lab representation of Eq. (3-22). The probability density function is altered to a COM system representation and the Jacobian is that of COM angle to energy. This Jacobian can be determined by taking the derivative of Eq. (3-8), yielding Eq. (3-27).

$$\frac{d\mu_c}{dE} = \frac{1}{2}\left[\frac{(A+1)^2}{E'\gamma(E')}\right] \tag{3-27}$$

As with the lab system, it is common to represent the probability density function of Eq. (3-26) in the ENDF libraries as a finite series of Legendre Polynomials as demonstrated in Eq. (3-28), where the coefficients, $a_n(E')$, are provided in the data libraries in the COM system.

$$\sigma_s(E' \to E) = \sigma_s(E')\left[\sum_{n=0}^{N}\frac{2n+1}{2}a_n(E')P(\mu_c)\right]\frac{d\mu_c}{dE} \tag{3-28}$$

Equations (3-22), (3-24), (3-26), and (3-28) represent all the possible angular descriptions of scattering energy transfer in the lab and COM frames of reference present in File 4 of the current ENDF-6 standard.[11] These equations are used to describe the slowing-down of neutrons within a reactor system via elastic and inelastic scatter.

Uncorrelated Energy-Angle Distributions

In elastic scatter, the neutron scattering angle has a unique value for a given incoming and outgoing energy. The same is true with discrete inelastic scatter (i.e., a scatter that leaves the nucleus at a specific excitation energy). For other reactions, this correspondence does not exist and a full description of both the angular distribution, $p_0(E', \mu_0)d\mu_0$, and resulting energy distribution, $g(\mu_0, E' \to E)dE$, are required.

Two important examples of uncorrelated reactions are continuum inelastic and (n,xn) reactions. Continuum inelastic scatter occurs at energies where the discrete nuclear excitation levels of an isotope reach a continuum and are no longer resolvable. A (n,xn) reaction occurs when a neutron strikes a nucleus, freeing x-1 additional bound neutrons, which results in x neutrons from the scatter event.

The ENDF-6 standard[11] combines the energy and angle dependence into one distribution as described in Eq. (3-29), where $m(E)$ is the multiplicity of the reaction at E. The multiplicity is the number of neutrons that result from the reaction (e.g., 2 for (n,2n), ν for fission).

$$\sigma(\mu, E, E') = \sigma(E')\, m(E')\, f(\mu, E, E') \tag{3-29}$$

This differential cross section would be given in units of barns per unit cosine.

The ENDF-6 standard includes a number of ways for describing the energy-angle distribution following a reaction for different types of incident and resultant particles. These data are included in File 6 of an ENDF library for a given isotope. Below are two of the most common representations for neutron-nucleus reactions.

Legendre coefficients representation

The first common representation for energy-angle distributions of neutrons in the ENDF-6 standard[11] is via Legendre Polynomials.

$$f(\mu, E, E') = \sum_{\ell=0}^{NA} \frac{2\ell+1}{2} f_\ell(E, E')\, P_\ell(\mu) \tag{3-30}$$

In this representation the angular component of the distribution is represented by an expansion of Legendre Polynomials, where the $f_\ell(E, E')$ terms are the Legendre coefficients given for NA number of terms in the ENDF data files. The value of NA is dependent on the angular distribution at a given energy. If the angular distribution is complicated, more polynomial terms are necessary to describe the resulting angular distribution.

If only the total neutron energy transfer is desired, both sides of Eq. (3-30) can be multiplied by another Legendre Polynomial and integrated over angle.

$$f_\ell(E, E') = \int_{-1}^{+1} d\mu\; f_\ell(\mu, E, E')\, P_\ell(\mu) \tag{3-31}$$

The zero-order Legendre Polynomial coefficient, $f_0(E,E')$, is the total probability of scattering from E' to E. The $f_0(E,E')$ values would be equivalent to the energy distribution data given in File 5 of the ENDF data.

When determining only the probability of energy transfer from one energy to another, a full description of the resulting angular distribution is not necessary. Therefore the value of $f_0(E,E')$ is sufficient for determining the probability of transfer from E' to E.

Kalbach-Mann Systematics representation

Another means of describing an energy-angle distribution is through Kalbach-Mann Systematics.[40,41] Kalbach and Mann proposed a generalized means of representing the energy-angle distribution of an incident particle on a nucleus with the function shown in Eq. (3-32) where the parameters $f_0(E,E')$, $a(E,E')$, and $r(E,E')$ are stored in the ENDF data.

$$f(\mu,E,E') = \frac{a(E,E')\,f_0(E,E')}{2\sinh\left(a(E,E')\right)}\left[\cosh\left(a(E,E')\mu\right) + r(E,E')\sinh\left(a(E,E')\mu\right)\right] \quad (3\text{-}32)$$

As with the Legendre representation, the energy transfer probability is desired, rather than the angular distribution. If Eq. (3-32) is integrated over all possible values of μ, Eq. (3-32) reduces to $f_0(E,E')$. This parameter can be obtained from the ENDF tapes.

Quadrature Integration of the Transfer Source

One of the difficulties of representing the flux with a fine group structure is characterizing the group to group transfer cross sections. To obtain the flux in a specific group, the contribution from all other possible groups must be calculated. This requirement makes a fine group approach increasingly computationally expensive as the number of groups and reaction types is increased. Methods such as sub-moment expansion[38] in CENTRM or the RABANL[35] module in MC^2 have been developed to mitigate the issue of transfer source calculation. This work presents and alternate form of accounting for the transfer source via a numerical approximation.

The transfer source term is represented by the integral of Eq. (3-22) or Eq. (3-26) over all possible neutron energies. Because the transfer source is given as a definite integral of continuous functions, numerical integration is used to obtain the value of the scattering source at a given energy. One possible technique for numerically integrating a function is the Gauss Quadrature (GQ) method.[42] This section gives a brief overview of the GQ method and its refinements from the general form to application to the neutron transfer source given in the neutron transport equation.

Overview of Gauss Quadrature Integration

Given a general function, $f(x)$, to be integrated over an independent variable *x,* the integrand may be expressed by Eq. (3-33).

$$I = \int_a^b dx\, f(x) \tag{3-33}$$

The GQ method seeks to numerically obtain an accurate estimate of the integral by selecting the optimum points (i.e., nodes) and evaluating the weighted sum of the function values at these points.

The Gauss Quadrature Theorem states that "[the nodes] of the *n*-point Gaussian quadrature formula are precisely the roots of the orthogonal polynomial for the same interval and weighting function."[43] This condition is stated in Eq. (3-34) where $P_n(x)$ is the function to be integrated represented in polynomial form, $P_m(x)$ is a polynomial which is orthogonal to the function on the interval [*a*,*b*], and $w(x)$ is a weighting function.[44]

$$\int_a^b dx\, P_n(x) P_m(x) w(x) = \delta_{nm} \tag{3-34}$$

If the condition of Eq. (3-34) is met, then Eq. (3-35) is true according to the Gaussian Quadrature Theorem.

$$I = \sum_{i=1}^{n} w_i f(x_i) \tag{3-35}$$

The values of x_i are the roots of the orthogonal polynomial and the values of w_i are determined by assuming the function can be represented by a polynomial of order $2n-1$ and solving for the undetermined coefficients. An example of this procedure for a 2nd order GQ estimate using Legendre Polynomials is given in Ref. 42.

The utility of this numerical approximation is that it allows accurate estimation of complicated functions via a minimum number of function evaluations. Other numerical integration schemes such as the Trapezoid Rule or Simpson's Rule[45] typically require a greater number of function evaluations to obtain the same accuracy.

Limitations of Gauss Quadrature Integration

One potential drawback of GQ is the irregular spacing of the nodes in the interval of $[a,b]$. This makes implementation of GQ for evenly spaced tabular data less straightforward. If the data are given in tabular form, interpolation must also be performed.

For a GQ estimate using n nodes (i.e., of order n), the GQ method can exactly estimate a function of order $2n-1$. If a function requires a very high order polynomial to be represented accurately, the benefit of the GQ method is diminished because more function evaluations would be required. In some exceptional cases, the trapezoid rule with fine enough spacing is less expensive than the GQ method for the same accuracy.[42]

The GQ method also requires integration over a finite interval. The GQ method cannot be applied to functions with singularities or integrals with infinite or semi-infinite bounds.

Gauss-Legendre Quadrature

The GQ method relies on the appropriate selection of weights and nodes. These values are tied to the choice of orthogonal polynomial in Eq. (3-34). The use of Legendre Polynomials with

$w(x)=1$ is a common polynomial selection. Legendre Polynomials are orthogonal on the interval [-1,+1] and follow simple recursion relationships that facilitate implementation in a computer program.

In an order *n* Gauss-Legendre Quadrature (GLQ) approach, the nodes are determined from the roots of the order *n* Legendre Polynomial. The corresponding weights can be determined by the properties of Legendre Polynomials at a given order by the method described by Hildebrand.[46] Using this method, the weight for order *n* and node x_i can be calculated via Eq. (3-36).

$$w_i = \frac{2\left(1-x_i^2\right)}{\left(n+1\right)^2\left[P_{n+1}\left(x_i\right)\right]^2} \tag{3-36}$$

The nodes and weights do not change based on the function to be integrated. Therefore, the node-weight pairs for a given GLQ order can be stored in a computer program without need for recalculation during each execution. The GLQ nodes and weights for orders 2 thru 6 are given in Table 3-1.

Adjustment of Integration Limits

For GLQ integration to be practical, the restriction of integration only over the interval [-1,+1] must be removed by a change in variable such that the new variable is equal to -1 at the lower limit of *a* and +1 at the upper limit of *b* as shown in Eq. (3-37).

$$\int_a^b dx\, f\left(x\right) = \int_{-1}^{+1} dt\, f\left(t\right) \tag{3-37}$$

The substitution variable and differential is defined in Eqs. (3-38) and (3-39), respectively.

$$t = \frac{b-a}{2}x + \frac{b+a}{2} \tag{3-38}$$

$$dt = \frac{b-a}{2}dx \tag{3-39}$$

The GLQ formulation can now be applied to the definite integration of any function that satisfies the aforementioned restrictions by changing the independent variable and adjusting the value of *dx*.

Gauss-Kronrod Error Estimation

Since the GLQ method is accurate to order $2n-1$, any integral estimate of a function of greater than order $2n-1$ will retain some numerical error. One way to estimate this error is to compare a higher-order estimate to current estimate. Necessary adjustments can then be made to step size, number of points, etc. to reduce numerical error to acceptable levels.

Kronrod[47] proposed a method for estimating the error in Gauss-Legendre Quadrature, known as Gauss-Kronrod Quadrature (GKQ), also known as Gauss-Legendre-Kronrod Quadrature. Kronrod started with an order *n* Gauss Estimate as given in Eq. (3-40) and inserted $n+1$ additional nodes to obtain the higher-order Kronrod estimate of Eq. (3-41).

$$G_n = \sum_{i=1}^{n} w_i f\left(x_i\right) \tag{3-40}$$

$$K_{2n+1} = \sum_{i=1}^{n} a_i f\left(x_i\right) + \sum_{j=1}^{n+1} b_j f\left(y_j\right) \tag{3-41}$$

Kronrod determined the additional weights, b_j, and nodes, y_j, which would yield an estimate that is order $3n+1$ accurate by inserting $n+1$ additional nodes. The low-order, high-order estimate used in a GKQ estimate is known as a Gauss-Kronrod pair. The (G_7, K_{15}) pair, a common set used for GKQ, is given in Table 3-2.

The GKQ method reuses the nodes from the GLQ estimate. This makes the GKQ more efficient than comparing a high-order and low-order GLQ estimate, where the nodes cannot be reused due to the irregular spacing. For a GKQ estimate, a total of $2n+1$ function evaluations would yield a $3n+1$ order integral estimate and an error estimate. The same number of function

evaluations with GLQ integration would yield the more accurate $4n+1$ order integral estimate but without any error estimate.

The error estimate from GKQ can be used to create adaptive algorithms, which reduce error below a limiting value. An error estimate is necessary for the numerical algorithm to adapt to the input functions and maintain error below acceptable levels.

Neutron Transfer Source Calculation Using Gauss-Kronrod Quadrature

The Neutron Slowing-Down Equation in an infinite medium is given in Eq. (3-42).

$$\sigma_t(E)\phi(E) = \int_E^\infty dE' \sigma_s(E' \to E)\phi(E') + S(E) \tag{3-42}$$

The scattering source term on the RHS of Eq. (3-42) is the candidate for a GKQ integration treatment.

While scattering is typically the largest contribution to energy transfer, the scattering source term can be generalized into a transfer kernel for any reaction causing an energy transfer. A general form of Eq. (3-42) is given in Eq. (3-43) where the transfer source is generalized to any reaction, *x*, with a multiplicity of *m*.

$$\sigma_t(E)\phi(E) = \sum_{\text{all}\,x} \int_0^\infty dE' m(E') \sigma_x(E' \to E)\phi(E') + S(E) \tag{3-43}$$

All non-flux terms in Eq. (3-42) can be determined from ENDF data based on given data and scattering kinematics. These data can be in the lab or COM frame of reference and given as Legendre expansion coefficients, as tabulated probability density functions, or in Kalbach-Mann Systematics.[40,41] The transfer kernel in this general form can include many types of energy transfer reactions, including elastic scattering, inelastic scattering, or (n,xn).

At the highest possible energy in the system, there is no transfer contribution from higher energies. Therefore the initial value of the flux can be determined from Eq. (3-44).

$$\phi\left(E_{\max}\right)=\frac{S\left(E_{\max}\right)}{\sigma_t\left(E_{\max}\right)} \tag{3-44}$$

From this point the calculation can sweep down to lower energies using the higher energy flux values in the transfer source.

An exception to this general slowing-down treatment is fission. Fission reactions occurring at low energies yield neutrons at higher energies. Typically, the implementation of a source and eigenvalue iteration procedure is necessary to describe the system. Therefore, the source term in Eq. (3-43) is left as a general source term that can be either a fixed source, fission source, or a combination of both.

Bounds of Integration for Neutron Transfer

The appropriate bounds of integration must be determined to calculate an accurate transfer source for a given reaction. These bounds can be input based on the kinematics of the reaction or the input ENDF data. For all slowing-down reactions, the bounds of integration will be from the present energy, at a minimum, to the highest possible energy based on the reaction.

For the case of elastic scattering, the minimum energy occurs during a glancing collision with no energy transfer; therefore, the minimum energy would be the present neutron energy. In a glancing collision, the scattering cosine in both the laboratory and COM systems is +1. For the opposite case of maximum energy transfer (i.e., full backscatter), the scattering cosine is -1. For the case of elastic (i.e., $Q=0$) scattering, inserting a scattering cosine of -1 into Eqs. (3-5) or (3-8) yields the following result.

$$E_{\max}=\frac{E}{\alpha} \tag{3-45}$$

$$\alpha=\left(\frac{A-1}{A+1}\right)^2 \tag{3-46}$$

The case of inelastic scattering follows the same procedure. Again the minimum and maximum energies are obtained by substitution of -1 and +1 into the kinematic equations. In this case the result is Eqs. (3-47) and (3-48).

$$E_{\max} = \frac{E}{(A-1)^2}\left[A^2+1+2A\sqrt{1-\frac{Q(A-1)}{AE}}\right]-\frac{QA}{(A-1)} \tag{3-47}$$

$$E_{\min} = \frac{E}{(A-1)^2}\left[A^2+1-2A\sqrt{1-\frac{Q(A-1)}{AE}}\right]-\frac{QA}{(A-1)} \tag{3-48}$$

For reactions where the kinematics are not easily described (e.g., continuum inelastic and (n,xn)) the available ENDF data must be used to determine the bounds of integration. In these cases, the ENDF evaluations typically include a secondary energy distribution that is either tabulated, given as parameters of a Legendre expansion, or as Kalbach-Mann parameters. The minimum and maximum energies are then determined by the interpolated secondary energy distribution at a given incident neutron energy.

Numerical Form of the Neutron Slowing-Down Equation

With the bounds of integration determined and using the GKQ method for treating the transfer source, the Neutron Slowing-Down Equation at a given energy E is expressed in Eq. (3-49).

$$\phi(E) = \frac{1}{\sigma_t(E)}\left[\sum_{\text{all}\,x}\left(\frac{E_{\max,x}-E_{\min,x}}{2}\sum_{i=1}^{n}a_i f_x(E_i',E)+\sum_{j=1}^{n+1}b_j f_x(E_j',E)\right)+S(E)\right] \tag{3-49}$$

The i nodes and a_i weights correspond to the Gauss-Legendre estimate and the j nodes and b_j weights to the higher-order Kronrod estimate. The function evaluated by GKQ at i or j for reaction x is given in Eq. (3-50) with $g_x(E_i',E)$ being the transfer function from E_i' to E determined either from scattering kinematics or directly from the given ENDF data.

$$f_x(E_i',E) = m_x(E_i')\sigma_x(E_i')g_x(E_i',E)\phi(E_i') \tag{3-50}$$

The E_i' nodes are determined via Eq. (3-51), where x_i are the corresponding nodes in the range of [-1,+1] given by the selected Gauss-Kronrod pair.

$$E_i' = \frac{E_{\max} - E_{\min}}{2} x_i + \frac{E_{\max} + E_{\min}}{2} \tag{3-51}$$

With the exception of the flux, the values in Eqs. (3-49) and (3-50) are all known. No numerical approximations other than those discussed in the GKQ approach have been used to this point. While a number of important assumptions were made to arrive at this slowing-down equation, this form is intended to describe the energy behavior in a reactor system for the purposes of generating group constants and not for a full description of neutron behavior in energy, space, and time.

The GKQ form of the slowing-down equation can be solved on a given pointwise (PW) mesh of energy points such that the resulting flux points are linearly interpolatable to within a specified numerical error. Assuming no error is introduced by the reduction of the neutron transport equation to the slowing-down form, the following are the major sources of error in the resulting PW flux.

1. Error in the input nuclear data parameters. While potentially substantial, this error cannot be controlled by solution of the slowing-down equation. Error can also arise from interpolation of parameters such as cross sections, transfer probabilities, and multiplicity.
2. Error from the GKQ integration technique. This error is controllable via adjustments in the bounds of integration or order of the GKQ estimate.
3. Error from the linearization of the PW flux. This error can be controlled by applying the appropriate energy mesh. This mesh is often best informed by the underlying nuclear data, which are also linearly interpolatable to within a given error.
4. Any error resulting from numerical limitations of a computer. This could include floating-point precision error or truncation.

The methods developed in this chapter have particular applicability to fast spectrum systems where the flux at each energy is a function of only higher energy fluxes. Chapter 4

describes the implementation of this PW spectrum generation methodology into a computer program. The algorithms used to control error in the transfer source, determine the energy mesh, process the ENDF data, etc. will be described for the implementation of these methods.

Table 3-1. Nodes and weights for Gauss-Legendre Quadrature of order 2 to 6. Values from Table 22.1 of Chapra and Canale.[42]

Order	Nodes	Weights
2	±0.577350269	1.0000000
3	±0.774596669	0.5555556
	0.000000000	0.8888889
4	±0.861136312	0.3478548
	±0.339981044	0.6521452
5	±0.906179846	0.2369269
	±0.538469310	0.4786287
	0.000000000	0.5688889
6	±0.932469514	0.1713245
	±0.661209386	0.3607616
	±0.238619186	0.4679139

Table 3-2. Nodes and weights for the (G_7, K_{15}) Gauss-Kronrod pair. Values from Table 5.3 of Kahaner, Moler, and Nash.[48]

Set	Nodes	Weights
7-point Gauss	±0.9491079123	0.1294849662
	±0.7415311856	0.2797053915
	±0.4058451514	0.3818300505
	0.0000000000	0.4179591837
15-Point Kronrod	±0.9915453711	0.0229353220
	±0.9491079123	0.0630920926
	±0.8648644234	0.1047900103
	±0.7415311856	0.1690047266
	±0.5860672355	0.1903505781
	±0.4058451514	0.2044329401
	0.0000000000	0.2094821411

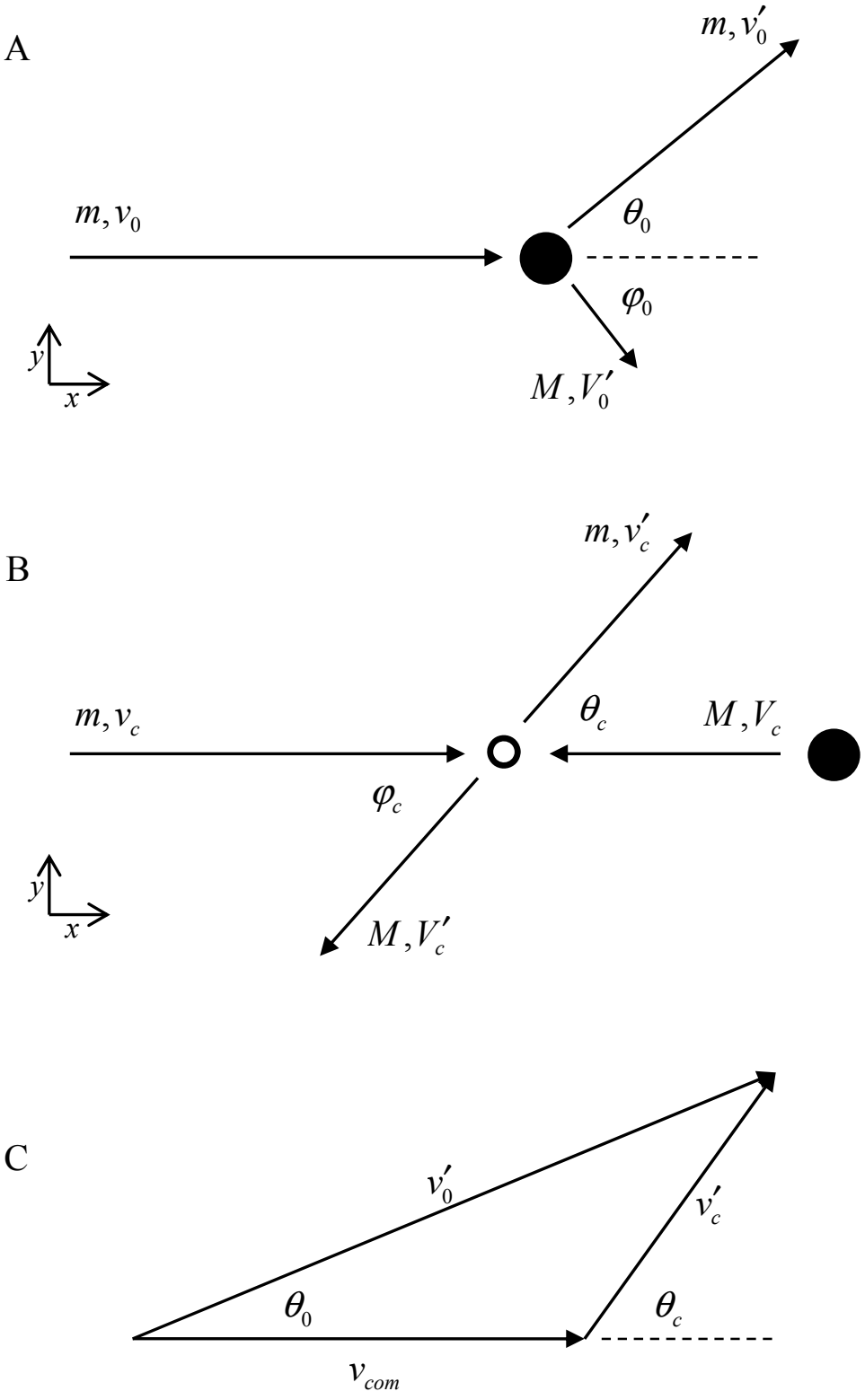

Figure 3-1. Scattering kinematic vectors. A) In the laboratory system. B) In the center-of-mass system. C) A vector diagram of resultant velocities and center-of-mass velocity.

CHAPTER 4
IMPLEMENTATION OF ADAPTIVE QUADRATURE METHODS

The methods developed in the previous chapter have been implemented in a computer program called Pointwise Fast Spectrum Generator (PWFSG). This program is intended to demonstrate an adaptive GKQ integration transfer kernel treatment.

PWFSG solves the Neutron Slowing-Down Equation in an infinite medium. The flux obtained by PWFSG is pointwise (PW) and linearly interpolatable. A high-level diagram of the inputs and outputs of PWFSG is shown in Fig. 4-1.

ENDF Input Data

Nuclear data, including cross sections and energy-angular distributions, are collected and distributed by a number of institutions as Evaluated Nuclear Data Files (ENDF). PWFSG draws fundamental nuclear data from these ENDF "tapes" which are ASCII text files that follow the ENDF-6 format.[11]

The ENDF-6 format specifies several types of 80 character lines of text, known as "cards," that are structured to facilitate reading by FORTRAN programs. The last 14 characters of each card are reserved for a four character material identifier (MAT), a two character file identifier (MF), a three character section identifier (MT), and a five character line number. These control characters are used by processing programs to determine their location in an ENDF tape. The first 66 non-control characters are the portion of the record that contains the nuclear data.

Most card types contain 6 entries of 11 character width followed by the control characters. The exception to this is the TEXT record, which contains one entry of 66 character width followed by the control characters. The mix of integer and floating point data on each card is dependent on the type of record. Control (CONT) records contain two floating point entries

followed by four integer entries. The two floating point entries typically contain data; the remaining integer data are typically control flags or a count of the number of entries that follow.

Tabulated data are represented in the ENDF-6 standard by the LIST, TAB1, and TAB2 record types. These are a series of multiple records which contain CONT records followed by floating point data. The CONT records provide control data about the following tabulated data. The tabulated data are then given as a simple list of values (LIST records), tabulated (x, y) data (TAB1 records), or a collection of LIST or TAB1 records at different values of an independent variable (TAB2 records).

Preprocessing with NJOY

In most instances, the ENDF-6 formatted data cannot be used directly in nuclear transport programs because the cross sections are given at one temperature (typically 0 K) and the resolved resonance energy region cross sections are given as resonance parameters. Therefore, the computer program NJOY[22] is commonly used to perform preprocessing of the ENDF data.

The first use of NJOY in PWFSG is processing the resonance data provided in the ENDF tapes. Isotopes that contain a large number of resonances (e.g., U-238) do not typically contain tabulated data for the entire resonance range. Instead the resonance data are stored as resonance parameters. These parameters can be in many forms such as Single or Multi-level Breit-Wigner, Reich-Moore, Alder-Alder, or Limited R-matrix.[11] The purpose of resonance parameters is to keep the ENDF files more compact. A resonance parameter representation limits the required energy resolution to represent rapidly varying cross sections around a resonance. Resonance parameters are widely used in the more recent ENDF evaluations, such as ENDF/B-VII.0, for medium and heavy mass isotopes that contain many resonances.[8]

If a nuclear transport program, such as PWFSG, needs a PW representation of the cross section, the resonance parameter data must be converted into tabulated, interpolatable cross sections. The resonances must also be broadened to the temperature of the material to account for Doppler Broadening.

PWFSG relies on NJOY to convert resonance parameters into Doppler-broadened, tabulated cross sections. The NJOY modules RECONR and BROADR are used to reconstruct and broaden the resonances, respectively. The output of these modules is a PENDF (pointwise ENDF) tape that follows the ENDF-6 standard and contains linearly-interpolatable cross section data generated by reconstructing and broadening the resonances.

The temperatures of the isotopes input into PWFSG are not required to be consistent. NJOY can process one material to a specific temperature and another material to a different temperature. The infinite medium calculation then uses the cross sections and number densities provided by NJOY to determine the reaction probabilities without the need to account for temperature effects. Therefore, a homogenous mixture of hot fuel could be mixed with cold coolant and simulated in PWFSG by providing the appropriate PENDF tapes.

ENDF Data Processing

Overview of EndfReader

A dynamic link library, EndfReader, was developed to facilitate the reading and interpolation of ENDF and PENDF data for PWFSG. The EndfReader library is based on accessing ENDF data using the standards provided in the ENDF-6 format specification.

The EndfReader library reads ENDF formatted records such as: TEXT, CONT, LIST, TAB1, and TAB2. It scans ENDF tapes and breaks them into materials, files, and section objects based on the MAT, MF, and MT tags, respectively. These components can then be accessed by a calling program such as PWFSG. The actual ENDF data are not processed at the time of the

scan; instead, they are sorted into a data structure for later access to eliminate computational cost in processing large ENDF sections not used by the calling program.

Due to the dynamic storage of ENDF records, the calling program is used to seek and rewind the ENDF tapes rather than EndfReader. A calling program will access a given section from a combination of MAT, MF, and MT number. It will then process the section's HEAD record and possibly the following CONT records to determine the number and type of records to follow. The calling program, based on the type of ENDF section being read, will make the appropriate calls to EndfReader instructing the types and number of records to process next. These method calls will cause EndfReader to seek forward in the ACSII formatted text contained in the ENDF section and create library objects representing records of type CONT, TAB1, etc. Therefore, the EndfReader class library provides a layer of abstraction that removes the need for the calling program to process CONT, TAB1, etc. records, while the calling program directs the reading of the records and interprets those records into physical quantities.

Interpolation within EndfReader

The library objects made available by EndfReader offer the ability to access ENDF data directly. There is also interpolation functionality for TAB and LIST records. TAB records, which contain tabulated two-dimensional (TAB1) or three-dimensional (TAB2) data, can be interpolated by their associated interpolation law.[11] LIST records, which contain lists of data at given independent variables (e.g., a list of Legendre coefficients at specific energies), can be interpolated to yield a new LIST record at an interpolated independent variable.

EndfReader supports the five one-dimensional interpolation laws used by ENDF:

1. Constant (histogram) interpolation
2. Linear-linear interpolation
3. Linear-log interpolation
4. Log-linear interpolation
5. Log-log interpolation

EndfReader interpolates dependent variables (e.g., cross section) using the appropriate interpolation law at a given independent variable (e.g., energy). These dependent variables can be a single value (e.g., cross section at an energy) or a set of values (e.g., Legendre Coefficients at an energy). This functionality allows EndfReader to present continuous data to the calling program.

Binary Search Algorithm for Interpolation

A PWFSG calculation spends a significant portion of its processing time on the interpolation of cross sections, transfer probabilities, etc. To improve the efficiency of this interpolation, a binary search algorithm[49] was implemented in EndfReader.

A binary search algorithm operates on sorted lists of data by comparing the middle of the list to the value sought. If the value sought is greater than the middle value of the list, then the lower half of the list is ignored and the middle becomes the new lower bound and vice versa. This process is performed recursively until the value sought is found. The binary search algorithm will converge logarithmically on the desired value leading to significant computational benefits when working with large sets of data.

A small modification was made to the EndfReader binary search algorithm. The continuous values sought by the calling PWFSG program are rarely the exact values tabulated in the ENDF data. Therefore, the EndfReader seeks the interval where the value lies rather than the exact value itself. Once the algorithm has found the desired interval, interpolation is performed on the ENDF data using the normal interpolation procedure.

Required Input

To perform the infinite medium slowing-down calculation, PWFSG requires continuous nuclear data (e.g., cross sections, transfer probabilities, etc.), the relative number densities of the

isotopes in the system, and the source distribution. Since the solution for an infinite medium, no geometrical information is required. A diagram of the PWFSG inputs is shown in Fig. 4-1.

The continuous nuclear data for PWFSG are provided through the EndfReader library. The source distribution and number densities must be specified in user input. When resonance parameters are used or the cross sections require broadening to a specific temperature, EndfReader requires a PENDF tape processed by NJOY in addition to the original ENDF tape.

Solution Algorithm

Figure 4-2 displays the solution algorithm used in PWFSG. PWFSG begins with ENDF and PENDF data and a given source distribution. The PWFSG solution procedure begins at the highest source energy and solves for the flux directly.

$$\phi\left(E_{\max}\right)=\frac{S\left(E_{\max}\right)}{\sigma_t\left(E_{\max}\right)} \tag{4-1}$$

The flux can be solved directly at $E_{\max}$ because no other flux values are needed (i.e., the transfer kernel is zero).

PWFSG assumes that the source is not coupled to the flux as in an eigenvalue calculation. PWFSG is only able to handle fixed source calculations, although the input source can be a fission spectrum. This same consideration is true for thermal scattering treatment.

Once the first flux point is determined, the flux solution algorithm progresses to lower energies. Each successive flux point is determined by the numerical form of the slowing-down equation with GKQ integration developed in the previous chapter. The form of the slowing-down equation used in PWFSG is shown in Eqs. (4-2), (4-3), and (4-4), where the subscript *k* refers to isotope, subscript *x* to reaction, and subscript *n* to energy point.

$$\phi\left(E_n\right)=\sum_{\text{all}\,k}\frac{1}{\sigma_{t,k}\left(E_n\right)}\left[\sum_{\text{all}\,x}\left(\frac{\Delta E_{x,k}}{2}\sum_{i=1}^{n}a_i f_{x,k}\left(E_i',E_n\right)+\sum_{j=1}^{n+1}b_j f_{x,k}\left(E_j',E_n\right)\right)+S\left(E_n\right)\right] \tag{4-2}$$

$$f_{x,k}\left(E_i',E_n\right)=m_{x,k}\left(E_i'\right)\sigma_{x,k}\left(E_i'\right)g_{x,k}\left(E_i',E_n\right)\phi\left(E_i'\right) \tag{4-3}$$

$$\Delta E_{x,k}=E_{\max,x,k}-E_{\min,x,k} \tag{4-4}$$

The total cross section at E_n is interpolated via EndfReader. To calculate the transfer source, EndfReader interpolates the transfer cross section, multiplicity, and transfer probability for each reaction included in the ENDF evaluation to the appropriate node given by the Gauss-Kronrod pair. PWFSG uses the nodes of the (G_7, K_{15}) pair given in Table 3-2 to determine the energies, E_i' or E_j', for these evaluations. The flux term given in Eq. (4-3) is determined by interpolation of the previously solved flux points.

Gauss-Kronrod Transfer Treatment

The GKQ method is used in Eq. (4-2) to calculate the transfer source. The function evaluations of Eq. (4-3) constitute the node values with a_i and b_j being the weighting coefficients.

For each reaction, the GKQ method is used to calculate the neutron transfer source to E_n. The GKQ method provides an error estimate for the integration of the transfer source. If the error is above a set tolerance, the integration range for the GKQ treatment is divided in half and treated as two separate regions. The intervals are continually subdivided until the integration error is below the given tolerance. This process is graphically depicted in Fig. 4-3.

Energy Mesh Determination

The energy mesh used for PWFSG is based on the total cross section of the system. First, a union of all the total cross section evaluation energies for every isotope in the system is generated. Following the creation of a union mesh, the total cross section at each point in the union mesh is calculated by summing the macroscopic cross sections.

After the creation of the union mesh, the mesh is thinned by removing any unnecessary points. During the mesh thinning process, an energy point is removed if the total cross section value at that point could be calculated via linear interpolation within a given error. This thinning can reduce the number of transport calculations significantly. The energy mesh of U-238 contains 129,402 points when processed with the RECONR and BROADR modules of NJOY to an error tolerance of 0.1%. The thinning process of PWFSG using an error tolerance of 0.1% yields an energy mesh of 43,247 points (67% reduction). If a less stringent tolerance of 1% is used the number of mesh points is reduced even further to 21,924 points (83% reduction). The result of the thinning process in CENTRM yields a similar reduction.[37] The choice of error tolerance is a balance of accuracy versus computational time and is left to the discretion of the user.

One exception to the thinning is determined by the following criterion.

$$\gamma\left(\Delta E_{\max}\right) \geq E_{n+1} - E_n \tag{4-5}$$

$$\Delta E_{\max} = E\left(\frac{1}{\alpha_{\max}} - 1\right) \tag{4-6}$$

Equation (4-6) gives the maximum possible energy change via an elastic scattering event. Elastic scattering reactions cause less energy change in the incident neutron than inelastic scatter and other reactions. The criterion of Eq. (4-5) states that the difference between the current energy point and the next energy point must be less than some fraction, γ, of the maximum possible energy loss by elastic scatter. This ensures that changes in the flux due to energy transfer are also included and not just those due to the total cross section.

While PWFSG thins energy mesh, it tests the criterion of Eq. (4-5). If the test fails, a new energy point is added at $\gamma(\Delta E_{\max})$. In the example of the U-238 mesh, a total of 7158 points are added to the mesh. These points are included in the aforementioned thinning results.

Parallelization of the Isotope Transfer Source Calculation

Each isotope in the summation term of Eq. (4-2) contributes separately to the overall transfer source. The summation of the neutron transfer from each individual isotope results in the total transfer to the present energy, E_n. Due to the number of interpolations and GKQ evaluations, this transfer probability calculation is typically the most computationally intensive portion of the PWFSG calculation.

In PWFSG, the transfer source summation term is broken into different process threads. For multi-core processing each core computes the transfer source for a given isotope. The threads rejoin to sum the total transfer source which is used for the flux calculation.

For cases where there are only a few isotopes, this parallelization does not yield any appreciable speedup. However, for cases with many isotopes, speedups of greater than 30% have been observed.

Flux Iteration Procedure

The GKQ procedure used during the PWFSG solution can require a flux at a point between E_n and E_{n+1}. Linear interpolation is normally used to obtain the flux for the GKQ procedure. In this case the flux is not known at E_n, so an interpolation cannot be performed between E_n and E_{n+1}.

A flux extrapolation and iteration procedure is used in PWFSG to predict fluxes between E_n and E_{n+1} (see Fig. 4-4). Prior to solving the flux at E_n, the flux at E_n is predicted by a quadratic extrapolation. A quadratic fit to the last three solution points is generated and the flux at E_n is

estimated via this quadratic fit. The actual flux at E_n is then solved using the normal PWFSG procedure given in Eqs. (4-2) and (4-3), with the result compared to the estimate. If the difference is below a given error, the solution procedure continues to the next point. If the error is not acceptable, the estimate is replaced with the value calculated via Eqs. (4-2) and (4-3). This process is repeated until the flux at E_n is converged.

Typically, only one or two nodes lie within the interval of E_n to E_{n+1}. These points are also the lowest weight points from the GKQ algorithm (see Table 3-2). Therefore, typically only one or two iterations are needed for convergence. When the solution is near the source energy, there are few higher energy flux values to draw from, so a greater than average number of iterations may be performed.

In addition to the extrapolation/iteration procedure, an additional check is performed to ensure convergence. In the event that the error starts to increase and the solution begins to diverge an extra energy point is inserted halfway between E_n and E_{n+1}. The solution procedure restarts with this new energy point as E_n.

Outputs

The output of PWFSG is a linearly-interpolatable PW flux. This flux represents a continuous function in energy and can therefore be used directly to produce group constants, according to Eq. (4-7) below.

$$\sigma_{x,g} = \frac{\int_{E_{g-1}}^{E_g} dE\, \sigma_x(E)\phi(E)}{\int_{E_{g-1}}^{E_g} dE\, \phi(E)} \tag{4-7}$$

An accurate flux energy spectrum will result in accurate energy dependence in the resulting group constants. PWFSG produces this flux spectrum with high accuracy in energy

using the GKQ integration procedure for the transfer source. PWFSG can then be coupled with another process to account for spatial effects as needed.

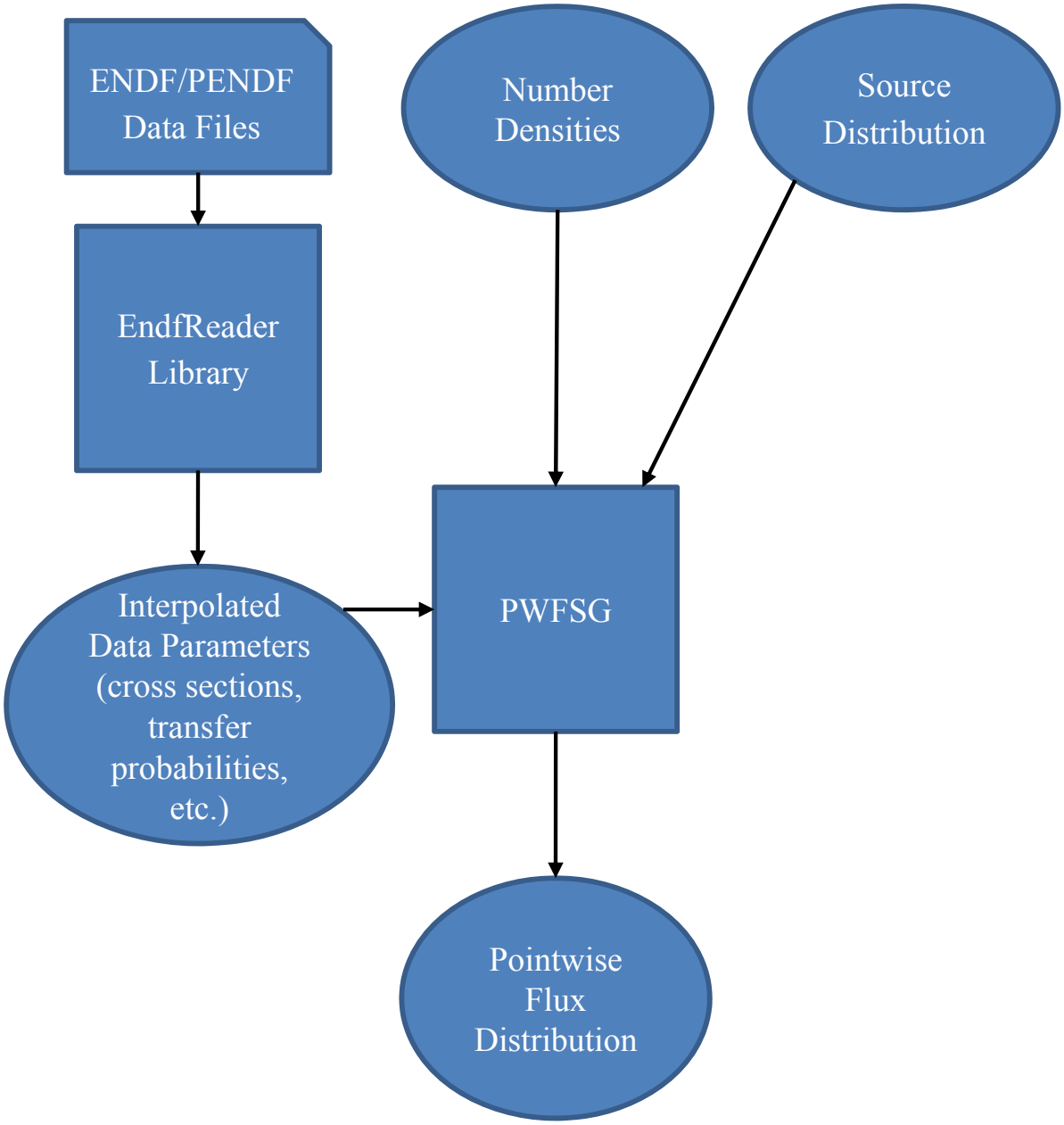

Figure 4-1. Overall program/data flow for PWFSG program

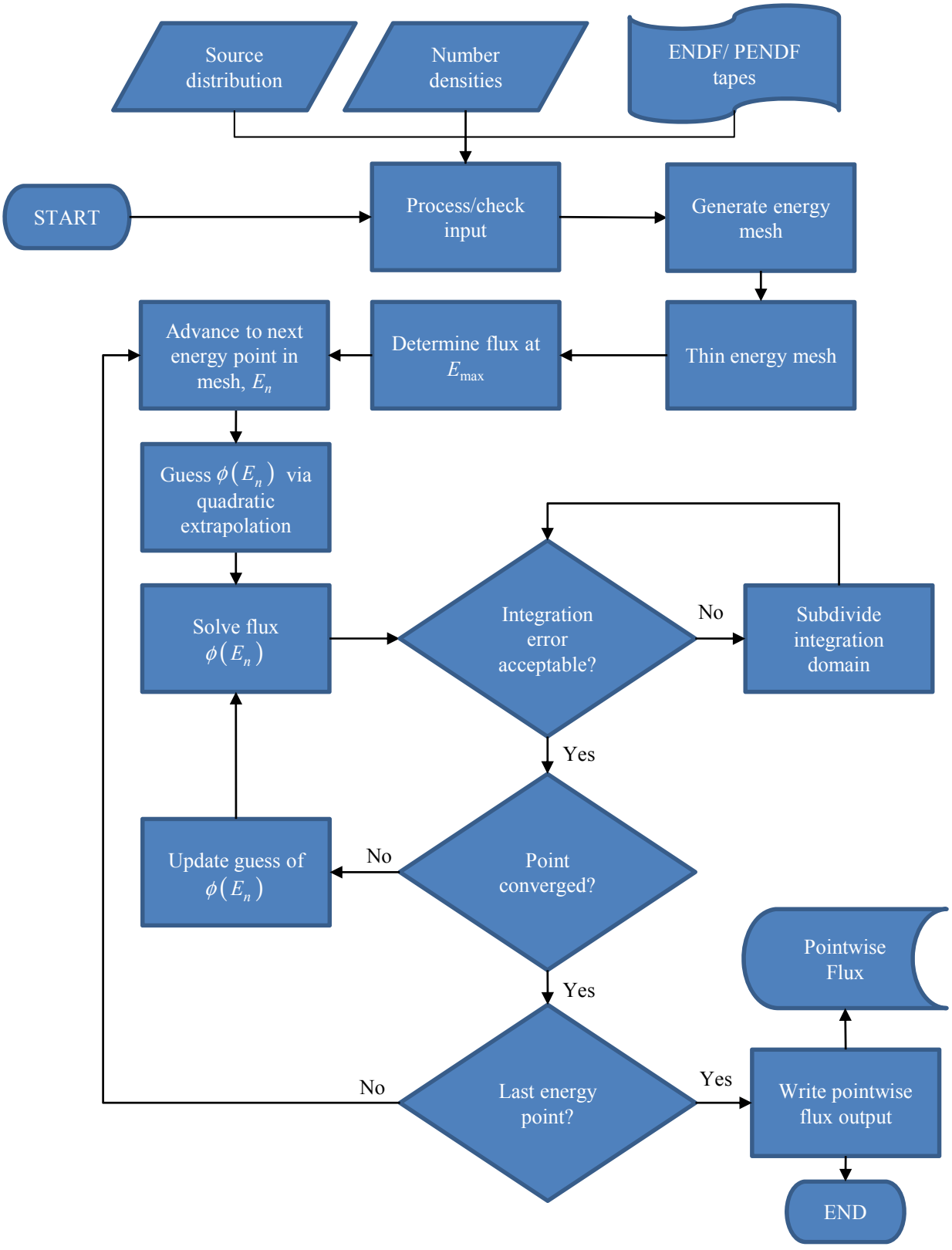

Figure 4-2. PWFSG solution algorithm

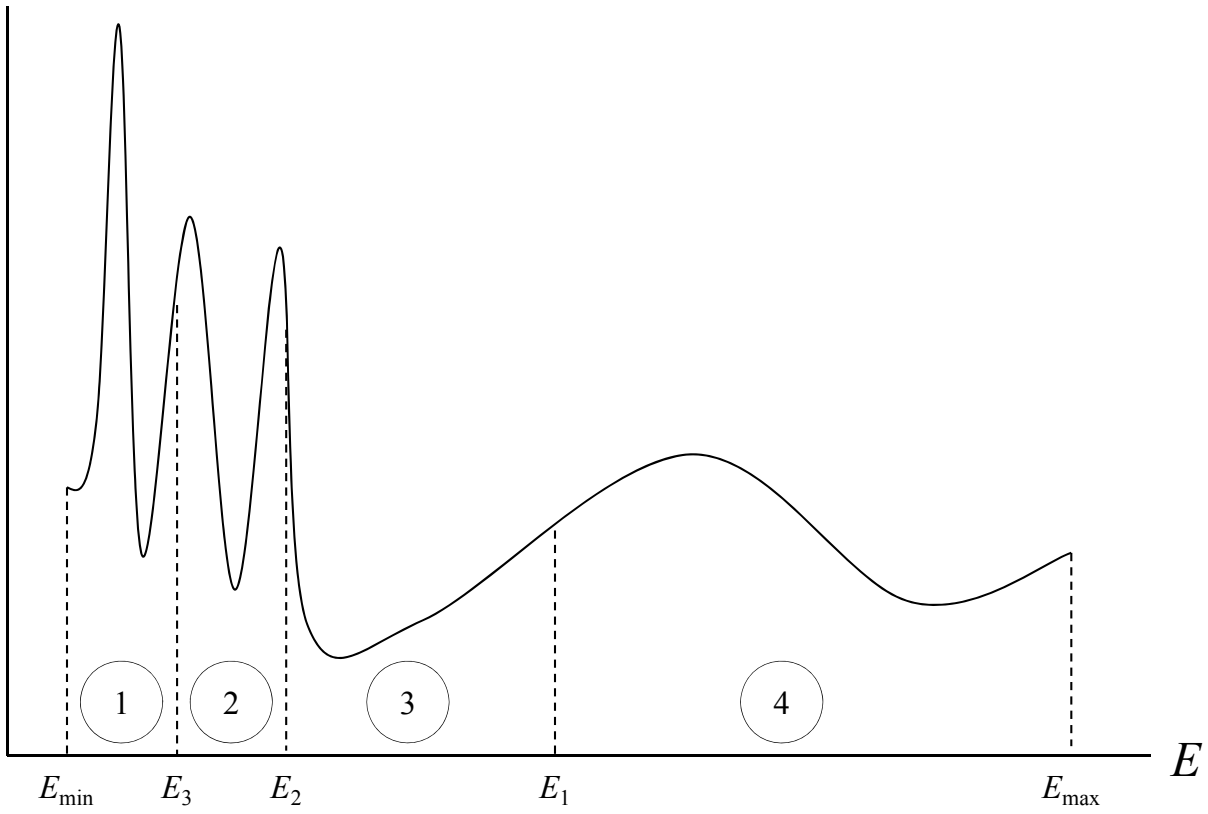

Figure 4-3. Example of how the GKQ algorithm breaks up integration bounds until error is acceptable. In this example, the GKQ algorithm would attempt integration between E_{min} and E_{max} first. When that error is unacceptable it would attempt integration from E_{min} to E_1 and E_1 to E_{max}, where E_1 is the halfway point between E_{min} and E_{max}. In this case, the error from the integration from E_1 to E_{max} (region 4) would be acceptable and subdivision would cease. The lower half would continue subdividing into regions 1, 2, and 3 until the integration error in all regions is acceptable.

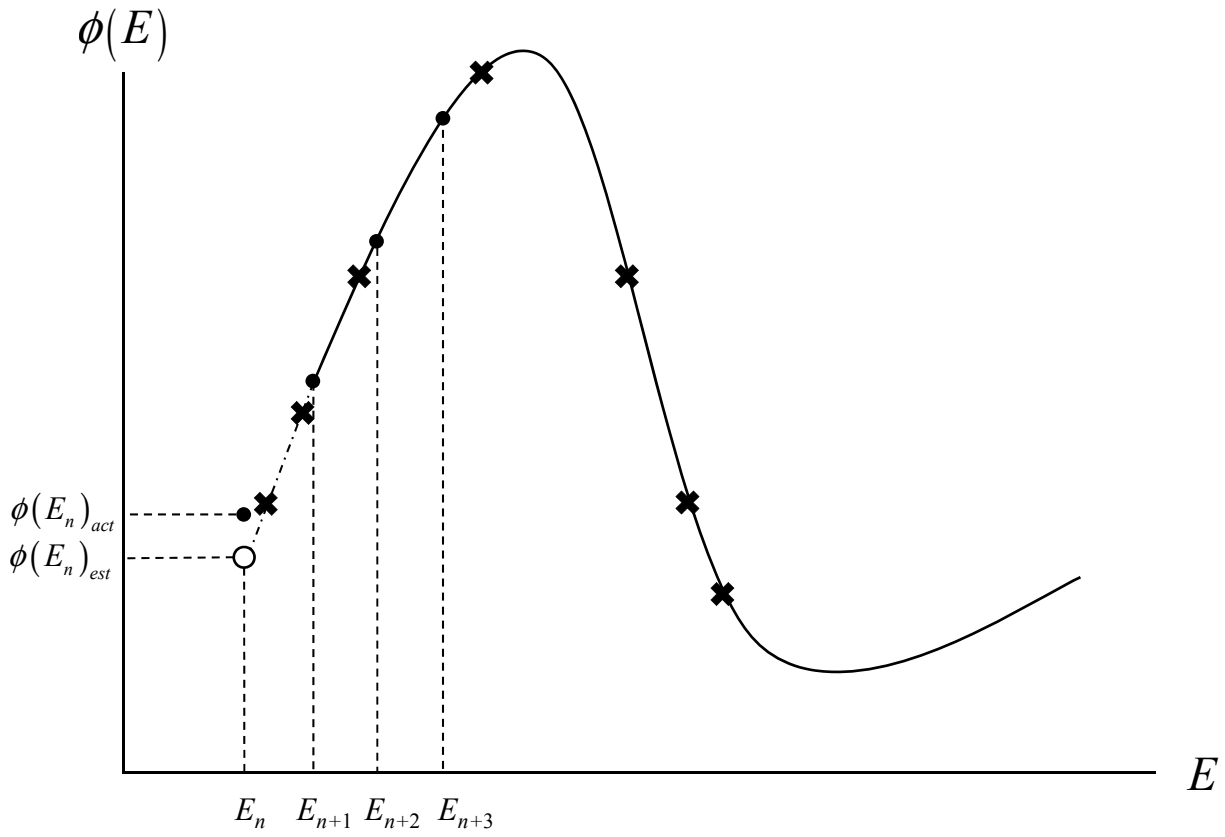

Figure 4-4. Example of flux estimation-iteration procedure used in PWFSG. The points E_{n+1}, E_{n+2}, and E_{n+3} are used to estimate the value at E_n via a quadratic extrapolation, shown above as $\phi(E_n)_{est}$. When the GKQ points (denoted by **x**) are calculated, this estimate is used for the region where the flux is not known. Upon the first iteration the flux estimate is updated with the calculated value which also updates the interpolated GKQ node points. This procedure is repeated until the value of the flux converges on the actual value, shown above as $\phi(E_n)_{act}$.

CHAPTER 5
PWFSG VALIDATION

Overview

To quantify the utility of the GKQ algorithm, the PWFSG program was executed with three example cases and the results compared to those of other solution techniques. PWFSG results were compared to the high-fidelity Monte Carlo program, MCNP5.1.51[50] and another deterministic spectrum generation program, Continuous Energy Transport Module (CENTRM).[37] CENTRM uses a hybrid of pointwise (PW) and multigroup (MG) flux solutions combined with a sub-moment expansion of the scattering source.[36,38] The homogenous infinite medium PW flux solution algorithm used by CENTRM is similar to PWFSG with the exception the scattering source term (i.e., sub-moment expansion versus GKQ integration).

The selected example problems are intended to represent a sodium fast reactor (SFR). The first example problem is an infinite medium of U-238. The second is a homogenized infinite medium with isotopic compositions representing a typical SFR pin. The third example is an infinite medium with isotopic compositions representing recycled nuclear fuel from a light water reactor (LWR) placed in a SFR.

All MCNP cases simulated 5 billion particle histories using custom weight-windows for particle population control. The weight window treatment was included to reduce MCNP stochastic error by controlling particle population in the resonance region.

The PWFSG and MCNP cases were executed on an 8-way Intel® Xeon® X5550 2.67 GHz processor that supported symmetric multi-processing and hyperthreading. This architecture allowed for up to 16 separate processes to be executed in parallel. MCNP utilized this architecture by running particle histories in parallel. PWFSG used this architecture in a more limited sense by calculating the transfer source for different isotopes on separate process threads;

however, this speedup was only realized on cases with multiple isotopes. CENTRM did not support any parallelization and was run on Intel® Core™ Duo 2.00 GHz architecture with SCALE utility scripts.

PWFSG and CENTRM only support fixed source distributions. To facilitate program-to-program comparison, every system was modeled with a fixed fission source distribution representing the energy distribution of fission neutrons from Pu-239. This spectrum is given by the Watt fission distribution where E is given in units of MeV.

$$S(E) = C \exp(-E/a) \sinh\left[(bE)^{1/2}\right] \tag{5-1}$$

For Pu-239 the parameters a and b are 0.966 and 2.842, respectively, with C as an arbitrary scaling factor. The fission neutron production in MCNP was disabled using the NONU card, with the above analytic expression specified on the MCNP SDEF card. A plot of this source is shown in Fig. 5-1.

CENTRM requires the neutron source to be given group-wise. Equation (5-1) was integrated over the 238 SCALE energy group structure and the integral of the source over each energy group was input into CENTRM as required in section F18.5 of Ref. 37.

PWFSG was developed with a source input feature similar to MCNP. The type of fixed source spectrum and any spectrum-specific parameters are specified in the input. PWFSG then uses the analytic expression for the described fixed source spectrum. For this case, the Watt spectrum with the same a and b parameters were given in the input causing PWFSG to calculate the source at a given energy via in Eq. (5-1).

All three programs used ENDF/B-VII.0 nuclear data in their calculation process. PWFSG used the native ENDF/B-VII.0 files and PENDF files produced by NJOY. ACE tables, also created by using NJOY from ENDF/B-VII.0 data files were used in MCNP. CENTRM uses the

appropriate SCALE modules to pre-process the ENDF/B-VII.0 data into the required format. In particular the CENTRM process involved the execution of the Bondarenko AMPX Interpolator (BONAMI)[23] module, to generate the shielding MG cross sections as well as Code to Read And Write Data for Discretized solution (CRAWDAD)[51] to generate the PW libraries used by CENTRM.

The same energy mesh was used in all three programs so that quantitative comparison of the different spectra was possible. PWFSG and CENTRM use a similar algorithm for determine the appropriate energy mesh, while MCNP requires the energy mesh be input prior to execution. To obtain the same mesh for all three programs, PWFSG was run first to generate an energy mesh. This mesh was input into MCNP. Any differences in the CENTRM energy mesh were adapted to the PWFSG energy mesh via linear interpolation. This adaption is possible because "a linear variation of the flux between energy points is assumed" in CENTRM as noted in Section F18.1.1 of Ref 37.

Spectrum Normalization

Each program has a different internal procedure for normalizing the flux spectrum; therefore, each output spectrum must be scaled so that program-to-program comparisons can be made. Once all three spectra where normalized appropriately, the residual errors between PWFSG and MCNP and between CENTRM and MCNP were calculated.

The MCNP spectrum is assumed to be the true spectrum due to the high-fidelity of the Monte Carlo method, the thorough verification and validation of MCNP,[52] and 5 billion particle histories tracked.

The MCNP flux values were divided by their respective energy mesh interval size and scaled by an arbitrary value to place most of the flux values between 0 and 100, as shown in Eq. (5-2). Dividing by the energy mesh interval size was necessary because MCNP flux values

are integrated over the energy mesh during tallying. This yields flux values in units of 1/cm^2-s. This division converts the integrated MCNP flux to its PW equivalent with units of 1/cm^2-eV-s.

$$\phi'_{i,MCNP} = C\frac{\phi_{i.MCNP}}{\left(E_{i,MCNP} - E_{i-1,MCNP}\right)} \tag{5-2}$$

The PWFSG and CENTRM results were then scaled and shifted to obtain the closest fit to the MCNP results. The scaling and shifting of flux energy spectrum is possible because the spectrum is simply a weighting function for the generation of group constants. This scaling and shifting will not have an impact on the resulting group constants because the weighting spectrum is normalized during the group constant generation process (See Eq. (4-7)).

The flux points from PWFSG and CENTRM were scaled and shifted, as in Eq. (5-3), using constant values of A and B so that the spectral shape was preserved.

$$\phi'_i = A\phi_i + B \tag{5-3}$$

The constants A and B were determined by minimizing the sums of the squares, S_r, of the residuals between MCNP and the respective program.

$$S_r = \sum_i \left(\phi_{i,MCNP} - \phi_{i,PWFSG/CENTRM}\right)^2 \tag{5-4}$$

This minimization was performed using a nonlinear Generalized Reduced Gradient (GRG) optimization algorithm,[53] subject to two constraints. First, the flux must remain positive over the region of comparison. Second, the mean of the residuals must be zero.

Error Calculation

The standard deviation of the residuals gives a measure of the variation of a program's results about the MCNP data for the cases studied. For comparison between CENTRM and PWFSG results, a coefficients of determination (r^2) were calculated as in Eq. (5-5).[54]

$$r^2 = \frac{S_t - S_r}{S_t} \tag{5-5}$$

$$S_t = \sum_i \left(\phi_{i,MCNP} - \bar{\phi}_{MCNP} \right)^2 \tag{5-6}$$

The S_t parameter is a measure of the total variation in the measured data. The purpose of the regression model is to then explain this variation with a functional dependence (e.g., a linear function). In this application of regression analysis, the MCNP results take the role of the experimental data, with the model taken as the results from PWFSG or CENTRM.

An r^2 value of 100% would indicate that a PWFSG or CENTRM model exactly matches the MCNP data and explains all of the variation observed in MCNP. The r^2 value is normalized by S_t allowing for comparison between the different cases.

An improvement factor, F, was calculated via Eq. (5-7).

$$F = \frac{\left(1 - r^2\right)_{CENTRM}}{\left(1 - r^2\right)_{PWFSG}} \tag{5-7}$$

This improvement factor quantifies the improvement of the PWFSG match to the MCNP results compared to CENTRM.

U-238 Infinite Medium Case

Model Description

The first example case is an infinite medium of U-238. The use of a single isotope in this case is intended to give a straightforward comparison of PWFSG to CENTRM and MCNP. Only one isotope influences the cross section and energy transfer behavior in the system, which allows for more direct inference on what is affecting the flux spectra calculated by the three programs.

The infinite medium of U-238 is modeled at a temperature of 900 K with temperature-appropriate cross sections. A number density of 1.0 was input into all the programs.

For a single isotope in an infinite medium, the number density only scales the final spectrum and does not affect its shape.

Results

The execution times required for the U-238 infinite medium case by the three programs are summarized in Table 5-1. CENTRM and PWFSG executed in just a few minutes while MCNP required almost two days. The normalized spectra are given in Fig. 5-2. Zoomed views of the resonance regions of the spectra are given in Fig. 5-3.

A plot of the MCNP relative error from this simulation is shown in Fig. 5-4. The comparison of the flux spectra was truncated to between 1 keV and 10 MeV. This energy range includes the majority of the flux peak, as shown in Fig. 5-2, and had MCNP relative error below 1%.

There is generally good agreement among the three programs. A plot of the PWFSG and CENTRM residuals (i.e., absolute error) compared to MCNP is shown in Fig. 5-5. The standard deviation of the residuals as well as the r^2 values are shown in Table 5-2. Both programs have r^2 values very close to 100% indicating good agreement with MCNP. The improvement factor for this case was 6.4, indicating that PWFSG provides a significant improvement over CENTRM. The main region of discrepancy between the programs is in the unresolved resonance region (20 keV to 149 keV), where resonances exist but are unable to be measured experimentally.

An upper PW cutoff of 25 keV was input into CENTRM to include the resolved resonance range of U-238. Above this point, CENTRM relies on the BONAMI module of SCALE to generate the self-shielded MG cross sections. The errors observed in CENTRM in this region are likely from the simplified Bondarenko approach in BONAMI.

To test the contribution of the Bondarenko approach to the CENTRM results, the PW boundary was moved to the upper comparison boundary of 10 MeV. The new results are shown

in Fig. 5-6. The standard deviation of the residuals increased from 0.8240 to 4.20, the r^2 value decreased from 99.65% to 90.86%, and the improvement factor increased to 166.3. There was also some non-physical variation in the CENTRM spectrum at higher energies, which may be caused by a numerical issue.

The agreement between CENTRM and MCNP for the CENTRM PW case was likely decreased due to the kinematic assumptions in CENTRM. From page F18.1.3 of the CENTRM manual it is noted that:

> Within the epithermal PW range, the slowing-down source due to elastic and discrete-level inelastic reactions is computed using the PW flux and the rigorous scatter kernel based upon the neutron kinematic relations for s-wave scattering. Continuum inelastic scatter is approximated by an analytical evaporation spectrum, assumed isotropic in the laboratory system.[37]

The assumptions of isotropic scattering in the center-of-mass coordinate system for elastic and discrete-level inelastic scatter (i.e., s-wave based scatter) and isotropic scattering in the laboratory system for continuum inelastic scatter may cause large errors at higher energies. Scattering dominates in general for U-238 at high energies as shown in Fig. 5-7. Above 1 MeV, elastic and inelastic scattering cross sections contribute comparably to the total cross section. Above 2-3 MeV, almost half of the inelastic contribution is from continuum inelastic. At these energies, the scattering can show strong angular dependence as shown in Fig. 5-8. These dependences are not well-represented with assumed isotropy.

PWFSG has excellent agreement with MCNP throughout the comparison energy range with an r^2 value of 99.95%. An examination of Fig. 5-5 reveals that, as with CENTRM, the main discrepancy is in the unresolved resonance energy range. PWFSG currently has no method for including unresolved resonance contributions, where MCNP uses a probability table method.

The infinite medium U-238 case was executed again in MCNP with the unresolved resonance probability table method disabled. The spectra from this result are shown in Fig. 5-9

and summarized in Table 5-3. The difference at the unresolved energies is reduced; however the r^2 statistic and the standard deviation are changed only slightly. The improvement factor decreased slightly to a value of 5.4.

For comparison of the differences between these two cases it is helpful to calculate the z statistic for the residuals. The z statistic for a given residual is the value of the residual minus the mean of the residuals and normalized by the standard deviation of the residuals as in Eq. (5-8). Due to the spectrum normalization the mean of the residuals, $\bar{\varepsilon}$, is zero for this analysis.

$$z_i = \frac{\varepsilon_i - \bar{\varepsilon}}{\sigma_\varepsilon} \tag{5-8}$$

A plot of the z values versus energy for the unresolved and no-unresolved cases is given in Fig. 5-10. A histogram of the z statistic values is given in Fig. 5-11. Even though the descriptive statistics do not show a distinct improvement for the no-unresolved case, it is clear from the histogram that the variation about the MCNP results is more evenly distributed for the case without unresolved resonances. The case with the unresolved resonances included has a stronger bias towards lower values that skews the histogram. Despite the lack of improvement in the r^2 statistic, the case without unresolved resonances seems to exhibit less bias and a more random distribution of the residuals and is thus considered a better match to the MCNP data.

Based on the results for the U-238 case as well as subsequent studies, it is concluded that both PWFSG and CENTRM provide good agreement with MCNP results, yielding r^2 values over 99% in their nominal usage. In this case, the main source of CENTRM error is the scattering kinematics assumptions in the PW region. The main source of error for PWFSG is due to lack of unresolved resonance treatment. Other PWFSG error is likely due to statistical variation in the MCNP results and numerical error in PWFSG.

SFR Fuel Cell Case

Model Description

The second example case is an SFR fuel cell in a hexagonal lattice as shown in Fig. 5-12. This example provides a more realistic scenario to test the effects of multiple isotopes with different resonance energies and energy transfer behavior.

The entire fuel cell was modeled at a temperature of 900 K, because CENTRM cannot model materials in the same zone at different temperatures. PWFSG and MCNP do not share this limitation, but were also modeled at 900 K for consistency.

The fuel in the modeled SFR pin was a metallic alloy of uranium and zirconium with 10 wt% zirconium (U-10Zr), with the uranium 15% enriched in U-235. The cladding was modeled as a simplified version of HT9, a common choice for SFR cladding due to its corrosion and swelling resistant properties.[55] The composition, based on Table 1 of Ref. 55, was simplified as 12 wt% chromium, 1 wt% molybdenum, and 87 wt% iron. The coolant was modeled as liquid sodium with a density of 0.874 g/cm^3.

The theoretical densities of the metal alloys were determined using Eq. (5-9) for a metal alloy with constituent elemental densities of ρ_i and weight fractions w_i.

$$\frac{1}{\rho} = \frac{1}{\sum_i \frac{w_i}{\rho_i}} \tag{5-9}$$

The metal fuel alloy is assumed to be fabricated with this theoretical density with a gap between the fuel and cladding. Upon reaching operational temperatures, the fuel expands until making contact with the inner surface of the cladding. This expansion lowers the fuel density. The fuel density used in the number density calculations was adjusted to be 75% of the theoretical calculated from Eq. (5-9).[56] While this adjustment does not change the overall number of the

fuel atoms (i.e., density is lowered but area fraction increases proportionally to compensate), it does serve to remove the fuel-cladding gap. This condition is more characteristic of an actual SFR fuel pin at operational temperatures and also provides a simpler model.

The fuel cell geometry and materials of Fig. 5-12 were homogenized into an infinite medium. The area fractions resulting from the geometry were used to scale the number densities for the fuel, cladding and coolant. The final number densities of the isotopes in the SFR fuel cell are given in Table 5-4.

Results

The execution times required for the SFR fuel cell case are summarized with the other cases in Table 5-1. The CENTRM time included approximately 11 minutes of calculation time for CENTRM itself and the remainder in library pre-processing by BONAMI, CRAWDAD, and other SCALE utility modules. Similar to the U-238 infinite medium case, PWFSG and CENTRM required just over 10 minutes, while MCNP required almost a week of processing time. The normalized spectra for the SFR fuel cell are shown in Fig. 5-13 with a plot of the resonance region of the spectra in Fig. 5-14.

A plot of the MCNP relative error for the SFR cell is shown in Fig. 5-15. For this case the comparison of the flux spectra was performed between 400 eV and 10 MeV. As with the U-238 infinite medium case, this truncation was based on selecting the region with MCNP relative error below 1% while including the majority of the flux peak.

The comparison statistics for the SFR cell case are given in Table 5-5. The agreement between MCNP and PWFSG decreased slightly from Case 1 but the r^2 statistic indicates a good fit with a value of 98.41%. The CENTRM results show more of a discrepancy for the SFR cell with an r^2 of 87.54%. The improvement factor is 7.8, which indicates a greater benefit of PWFSG over CENTRM when compared to the U-238 case.

A plot of the CENTRM and PWFSG residuals compared to MCNP is shown in Fig. 5-16. The issues identified in the U-238 case again contribute to error in the SFR cell case. For this case, the CENTRM PW cutoff was set to 10 MeV to capture the resonance region of sodium and the structural materials. This PW cutoff caused the inclusion of a significant amount of high mass, anisotropic scattering isotopes in the PW solution between 100 keV to 10 MeV range. This inclusion caused an over-prediction by CENTRM of the flux in this range and an under-prediction in the flux values below 100 keV.

Figure 5-16 suggests the error in PWFSG again derives from the lack of an unresolved resonance treatment. The flux is under-estimated in the unresolved resonance region of the uranium isotopes between 10 keV to 200 keV. This causes the neutron balance to be over-estimated, particularly in the lower energy ranges. Without an unresolved resonance treatment, PWFSG is redistributing the neutrons that would be lost in the unresolved region to the lower resonance energies.

Despite the error from the lack of unresolved resonance treatment, PWFSG still provides excellent agreement with MCNP. This example case demonstrates that PWFSG is able to effectively model a multi-isotope problem derived from a realistic SFR application.

UNF Fuel Cell Case

Model Description

The final example case is a fuel cell with LWR used nuclear fuel (UNF). This example is to test programs' abilities to simulate multiple, similar resonant materials in a mixture. Such a condition violates many of the assumptions in traditional group constant generation methods such as the Bondarenko method and the Subgroup method. The PW solution methods in PWFSG and CENTRM do not share these assumptions; MCNP relies on direct sampling of the

cross sections. Therefore, these programs should be able to accurately model the overlapping resonances.

The same area fractions and density calculations from the SFR cell were applied to the UNF cell. The difference between the two models is in the composition of the fuel alloy. The fuel is assumed to be an alloy of 70 wt% depleted uranium, 20 wt% transuranics (TRU), and 10 wt% zirconium (U-20TRU-10Zr).

The detailed TRU composition was determined from the fuel depletion simulation program, ORIGEN-S.[57] A pressurized water reactor (PWR) fuel composition accumulated an exposure to 41,200 MWD/MTHM over three cycles. This fuel exposure was based on previous studies[58] to determine fuel product compositions for advanced SFR designs.

The UNF fuel cell model was simplified by discarding isotopes in concentrations less than 0.0001%. The final fuel number densities were determined using the alloy weight fractions and the isotopic composition of depleted uranium with 0.2 wt% enrichment, the transuranic composition from ORIGEN-S, and the isotopic composition of zirconium.

The cladding and coolant number densities for the UNF cell remained unchanged from the SFR cell model. The final number densities used in the UNF cell model are given in Table 5-6.

Results

The execution times required for the UNF fuel cell case by the three programs are summarized along with the other cases in Table 5-1. As with the other cases, the majority of the time needed by CENTRM was for the spectrum calculation (18.5 minutes) with the remainder in library pre-processing. CENTRM and PWFSG both required less than 20 minutes to execute, while MCNP required almost 10 days.

The normalized spectra for the UNF fuel cell are shown in Fig. 5-17. The spectra are similar to the SFR cell spectra as the total system cross section is still dominated by Na-23 and

U-238. The SFR and UNF cell spectra from MCNP are shown for comparison in Fig. 5-18. The inclusion of the transuranic isotopes shifts the neutron spectra to slightly lower energies and lessens the peaks and valleys in the resonances.

The MCNP relative error for the UNF cell is shown in Fig. 5-19. As with the SFR cell, the program comparison was performed between 400 eV and 10 MeV with the UNF fuel cell comparison statistics given in Table 5-7. The agreement for both PWFSG and CENTRM is approximately the same as in the SFR cell case, with the r^2 values decreasing slightly. The improvement factor is slightly less than the SFR cell case with a value of 7.4. The residual plot of Fig. 5-20 confirms that the same error trends are present as in the SFR cell case.

The UNF cell case reveals that the inclusion of isotopes with overlapping resonances does not cause significant additional error in PWFSG or CENTRM. The PW treatment along with a rigorous scattering treatment avoids many of the deficiencies of traditional approaches when a high-fidelity neutron energy spectrum is desired.

Table 5-1. Required execution times of the three programs for the three example cases

Case	PWFSG Execution Time (minutes)	CENTRM Execution Time (minutes)	MCNP Execution Time (hours)
U-238 Infinite Medium	3.5	<1.0	47
SFR Fuel Cell	12.0	12.4	154
UNF Fuel Cell	17.7	19.3	227

Table 5-2. Error statistics for U-238 infinite medium case

Program	Standard Deviation of Residuals	r^2	$1-r^2$
PWFSG	0.3257	99.95%	0.0550%
CENTRM	0.8240	99.65%	0.3518%

Table 5-3. Error Statistics for U-238 infinite medium case with unresolved resonance treatment disabled in MCNP

Program	Standard Deviation of Residuals	r^2	$1-r^2$
PWFSG	0.3347	99.94%	0.0596%
CENTRM	0.7621	99.69%	0.3087%

Table 5-4. Homogenized number densities used in the SFR cell model

Isotope	Number Density (atoms/b-cm)
U-235	1.8858619×10^{-3}
U-238	1.0551567×10^{-2}
Zr-90	1.8518384×10^{-3}
Zr-91	4.0384114×10^{-4}
Zr-92	6.1727947×10^{-4}
Zr-94	6.2555785×10^{-4}
Zr-96	1.0078032×10^{-4}
Fe-54	7.5240415×10^{-4}
Fe-56	1.1811136×10^{-2}
Fe-57	2.7277064×10^{-4}
Fe-58	3.6300765×10^{-5}
Cr-50	8.2857689×10^{-5}
Cr-52	1.5978281×10^{-3}
Cr-53	1.8118088×10^{-4}
Cr-54	4.5099755×10^{-5}
Mo-92	1.2782226×10^{-5}
Mo-94	7.9673577×10^{-6}
Mo-95	1.3712469×10^{-5}
Mo-96	1.4367084×10^{-5}
Mo-97	8.2257585×10^{-6}
Mo-98	2.0784037×10^{-5}
Mo-100	8.2946654×10^{-6}
Na-23	8.4013761×10^{-3}

Table 5-5. Error statistics for SFR fuel cell case

Program	Standard Deviation of Residuals	r^2	$1-r^2$
PWFSG	2.9460	98.41%	1.59%
CENTRM	8.2412	87.54%	12.46%

Table 5-6. Homogenized number densities used in the UNF cell model

Isotope	Number Density (atoms/b-cm)
U-235	1.9614993×10^{-5}
U-238	9.6642491×10^{-3}
Am-241	1.3566604×10^{-4}
Am-243	3.4663778×10^{-5}
Cm-244	8.2528486×10^{-6}
Cm-245	4.6175738×10^{-7}
Np-237	1.5733084×10^{-4}
Pu-238	5.5200518×10^{-5}
Pu-239	1.3077054×10^{-3}
Pu-240	6.5959724×10^{-4}
Pu-241	2.3354193×10^{-4}
Pu-242	1.5570373×10^{-4}
Zr-90	1.8573215×10^{-3}
Zr-91	4.0503688×10^{-4}
Zr-92	6.1910718×10^{-4}
Zr-94	6.2741007×10^{-4}
Zr-96	1.0107872×10^{-4}
Fe-54	7.5240415×10^{-4}
Fe-56	1.1811136×10^{-2}
Fe-57	2.7277064×10^{-4}
Fe-58	3.6300765×10^{-5}
Cr-50	8.2857689×10^{-5}
Cr-52	1.5978281×10^{-3}
Cr-53	1.8118088×10^{-4}
Cr-54	4.5099755×10^{-5}
Mo-92	1.2782226×10^{-5}
Mo-94	7.9673577×10^{-6}
Mo-95	1.3712469×10^{-5}
Mo-96	1.4367084×10^{-5}
Mo-97	8.2257585×10^{-6}
Mo-98	2.0784037×10^{-5}
Mo-100	8.2946654×10^{-6}
Na-23	8.4013761×10^{-3}

Table 5-7. Error statistics for UNF fuel cell case

Program	Standard Deviation of Residuals	r^2	$1-r^2$
PWFSG	2.9204	98.24%	1.76%
CENTRM	7.9724	87.07%	12.93%

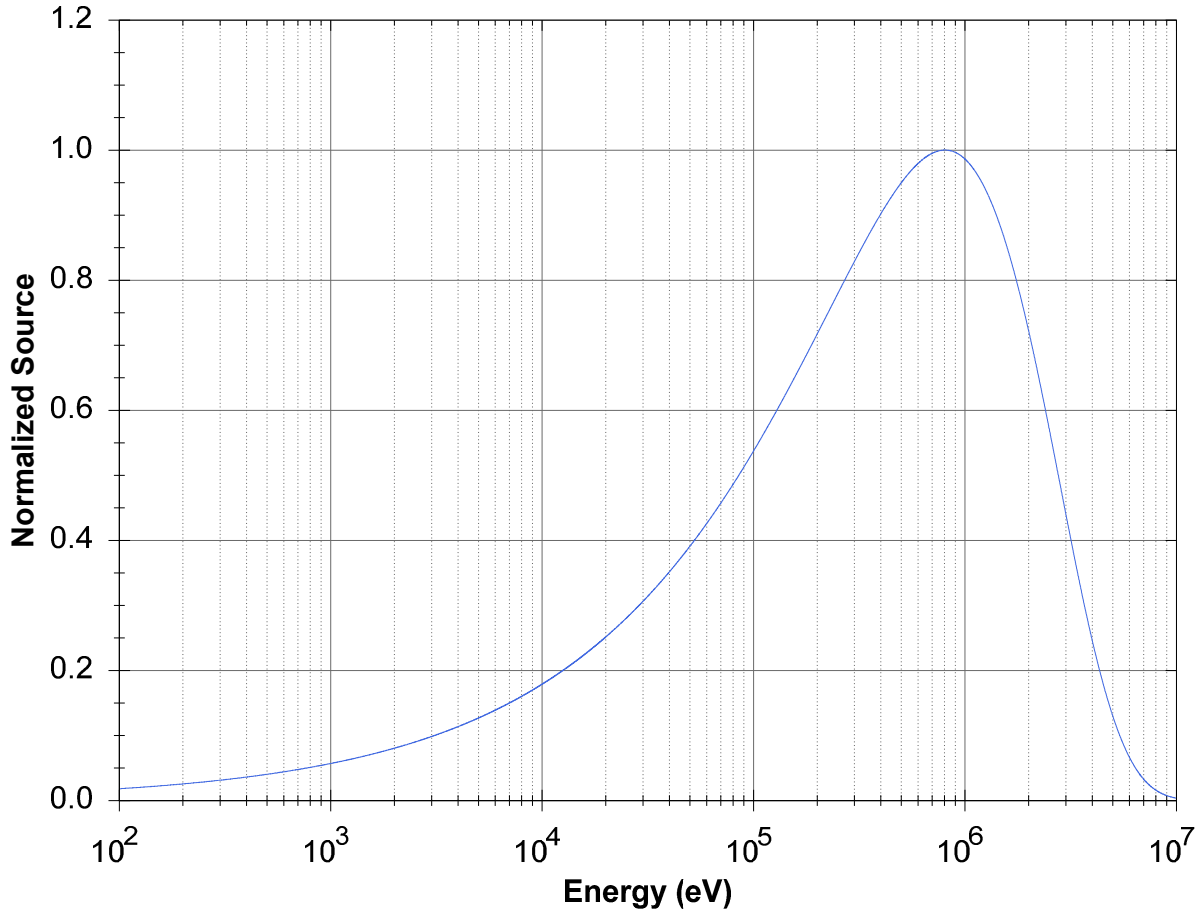

Figure 5-1. Source distribution used for example cases. The source distribution is generated from a Watt fission spectrum with fitting parameters intended to match the fission neutron distribution from Pu-239.

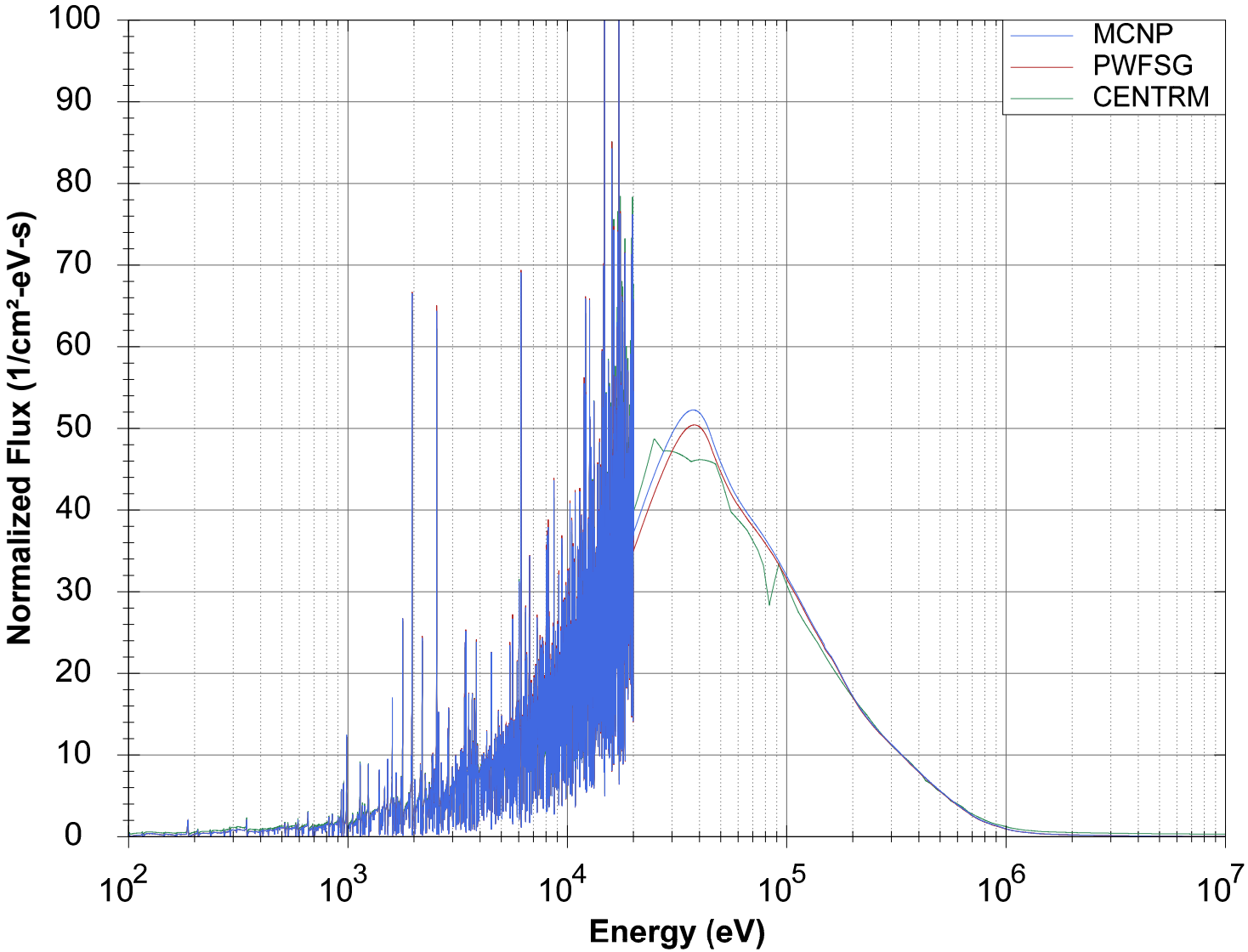

Figure 5-2. Neutron energy spectra generated by MCNP, PWFSG, and CENTRM for the U-238 infinite medium case

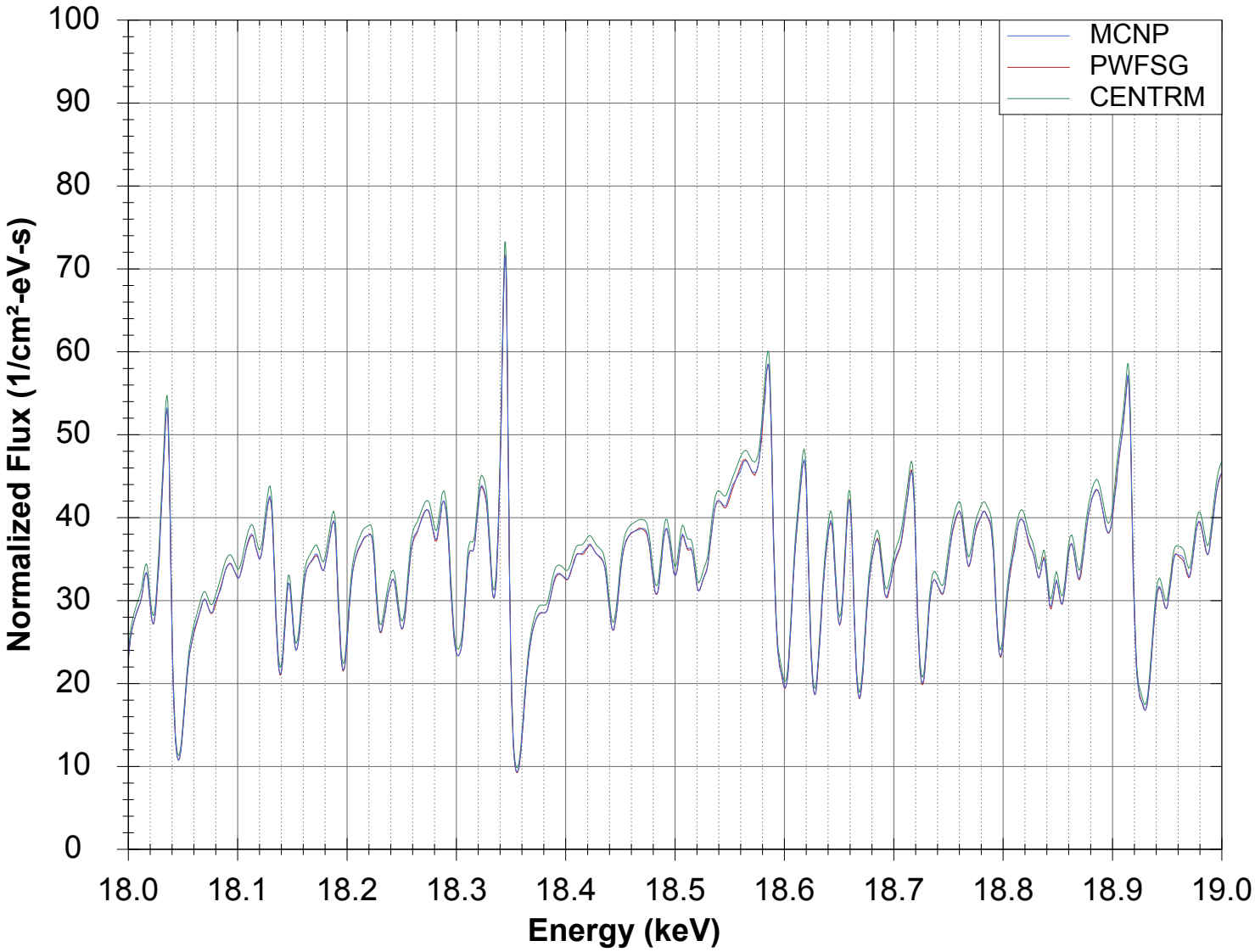

Figure 5-3. Neutron energy spectrum for the U-238 infinite medium case in the resonance region between 18 and 19 keV

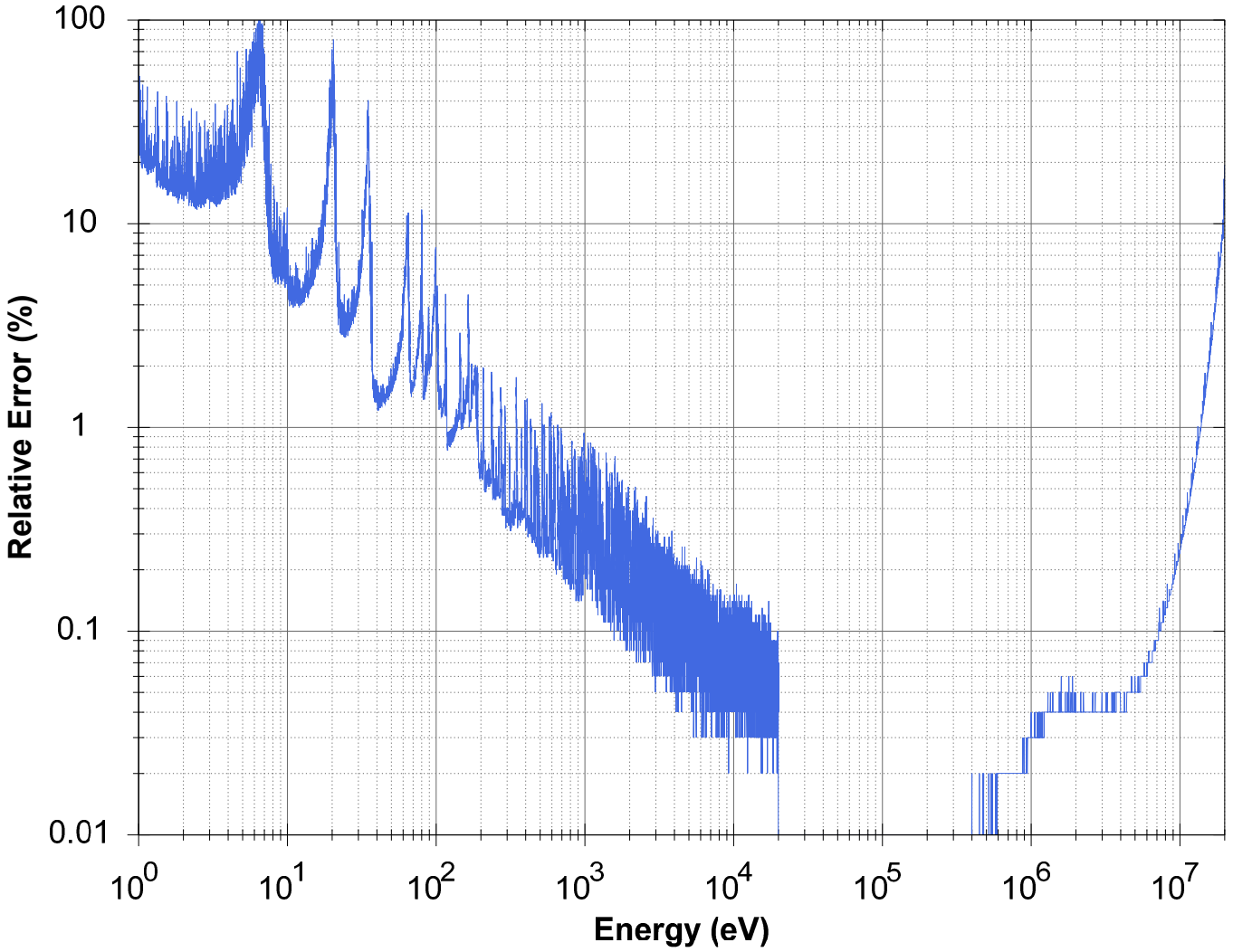

Figure 5-4. Statistical relative error from MCNP U-238 infinite medium case. MCNP output truncates results below 0.01% resulting in a "flat" value of 0.01 between 20 keV and 300 keV above.

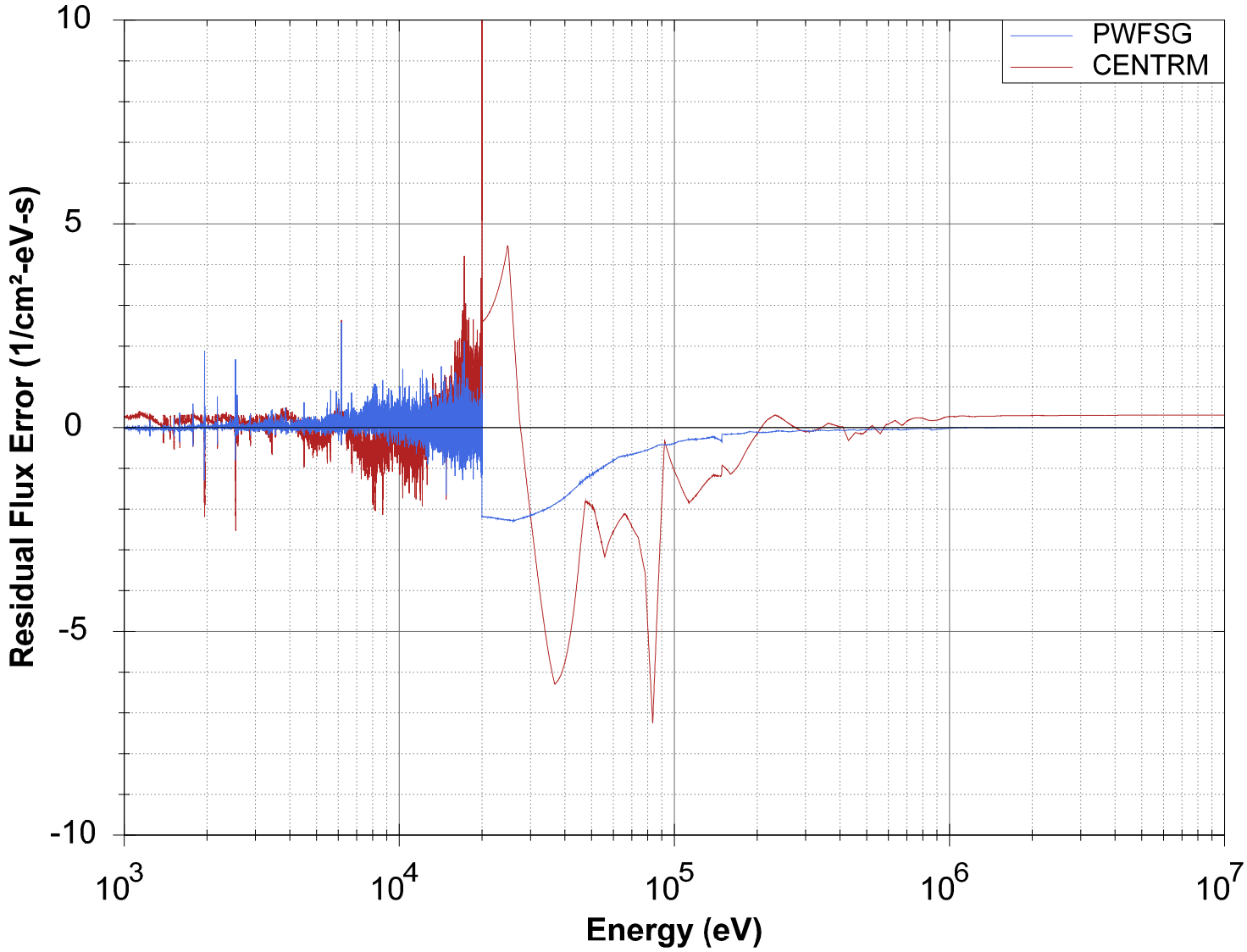

Figure 5-5. Residual flux error from difference in PWFSG or CENTRM and MCNP results for U-238 infinite medium case

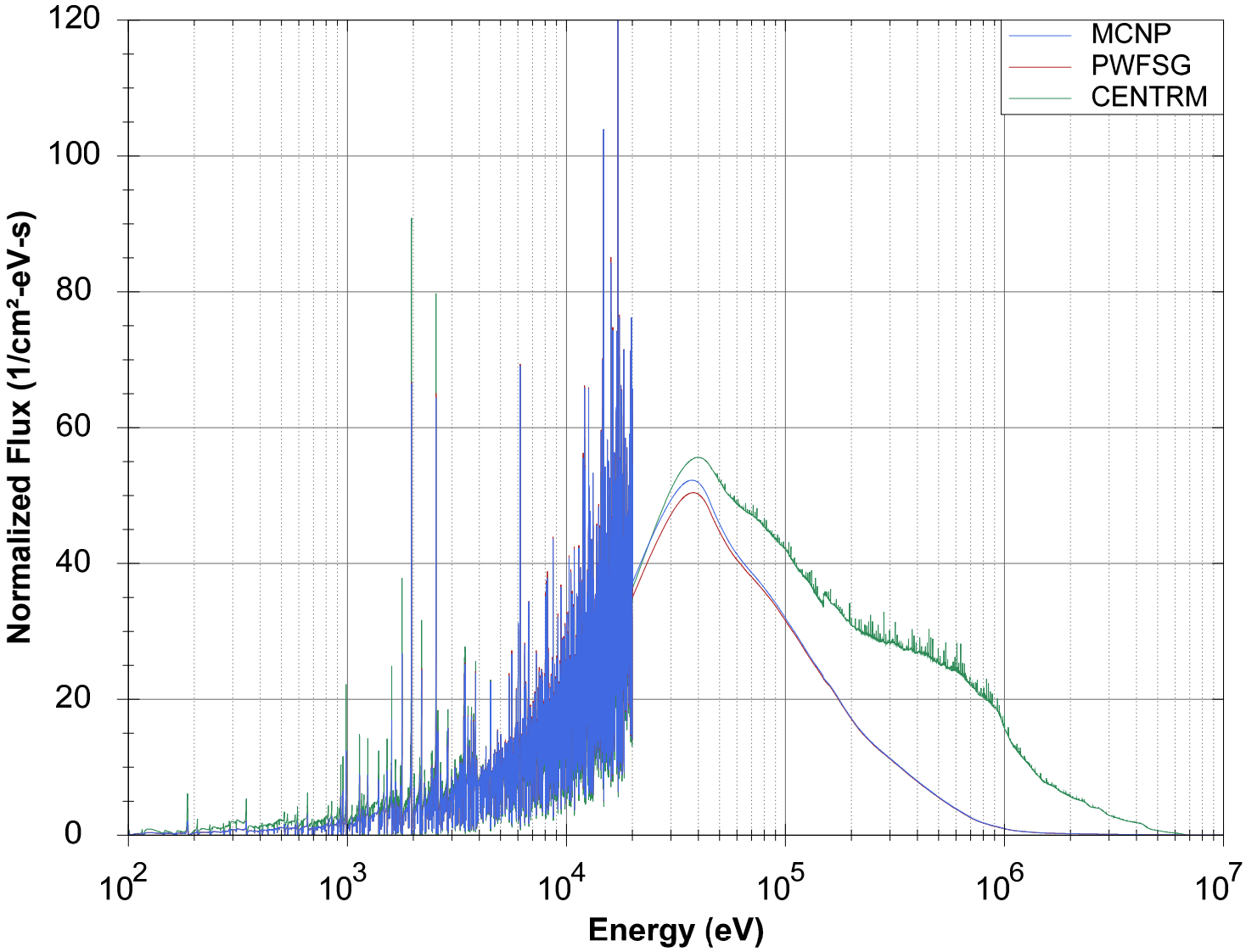

Figure 5-6. Neutron energy spectra for the U-238 infinite medium case with CENTRM extending PW treatment to 10 MeV

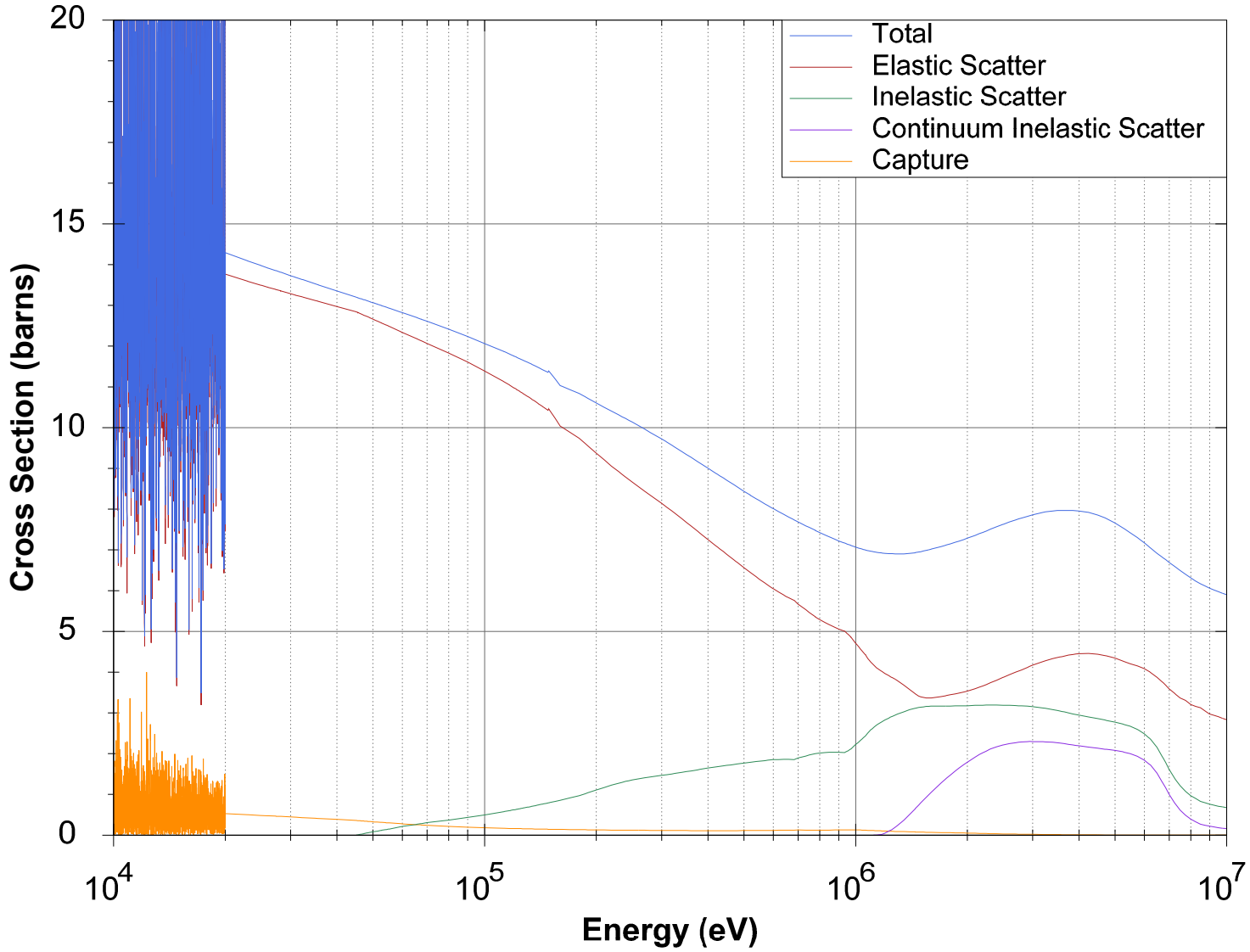

Figure 5-7. Various cross sections for U-238 between 10 keV and 10 MeV

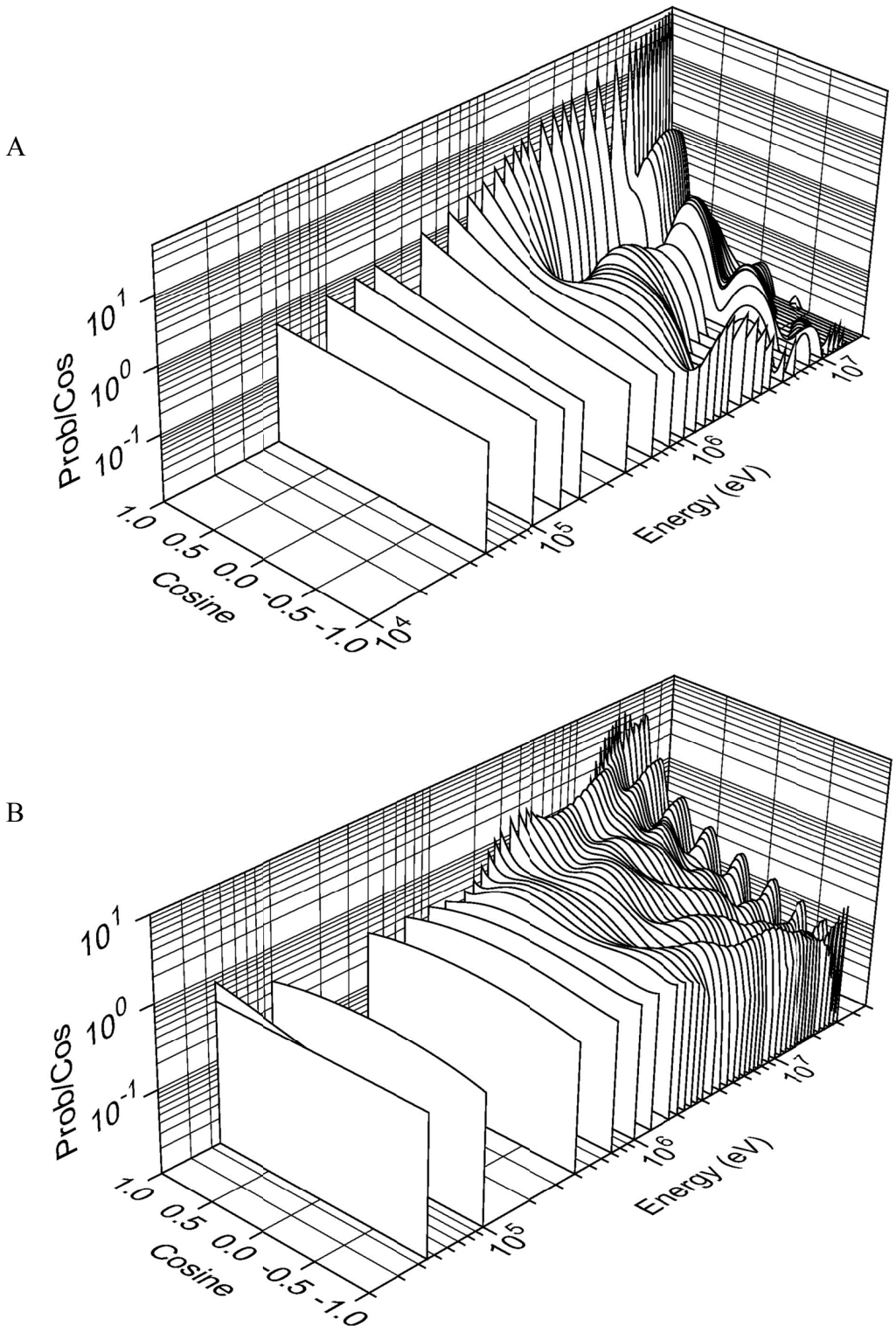

Figure 5-8. Angular scattering distribution versus energy for U-238. A) For elastic scattering. B) For first discrete-level inelastic scattering. Distributions are presented in in center-of-mass coordinate system.

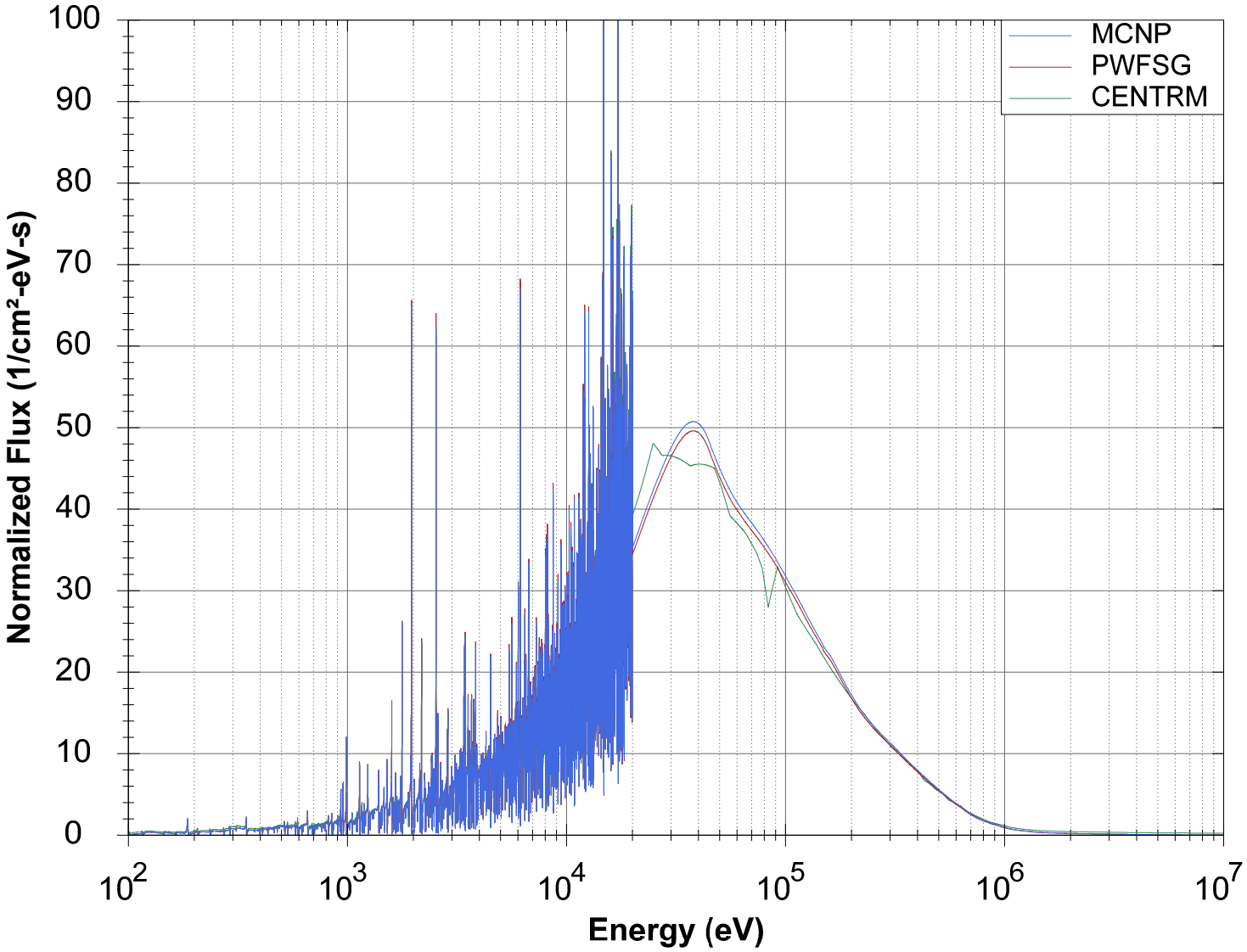

Figure 5-9. Neutron energy spectra for the U-238 case with unresolved resonance treatment disabled in MCNP

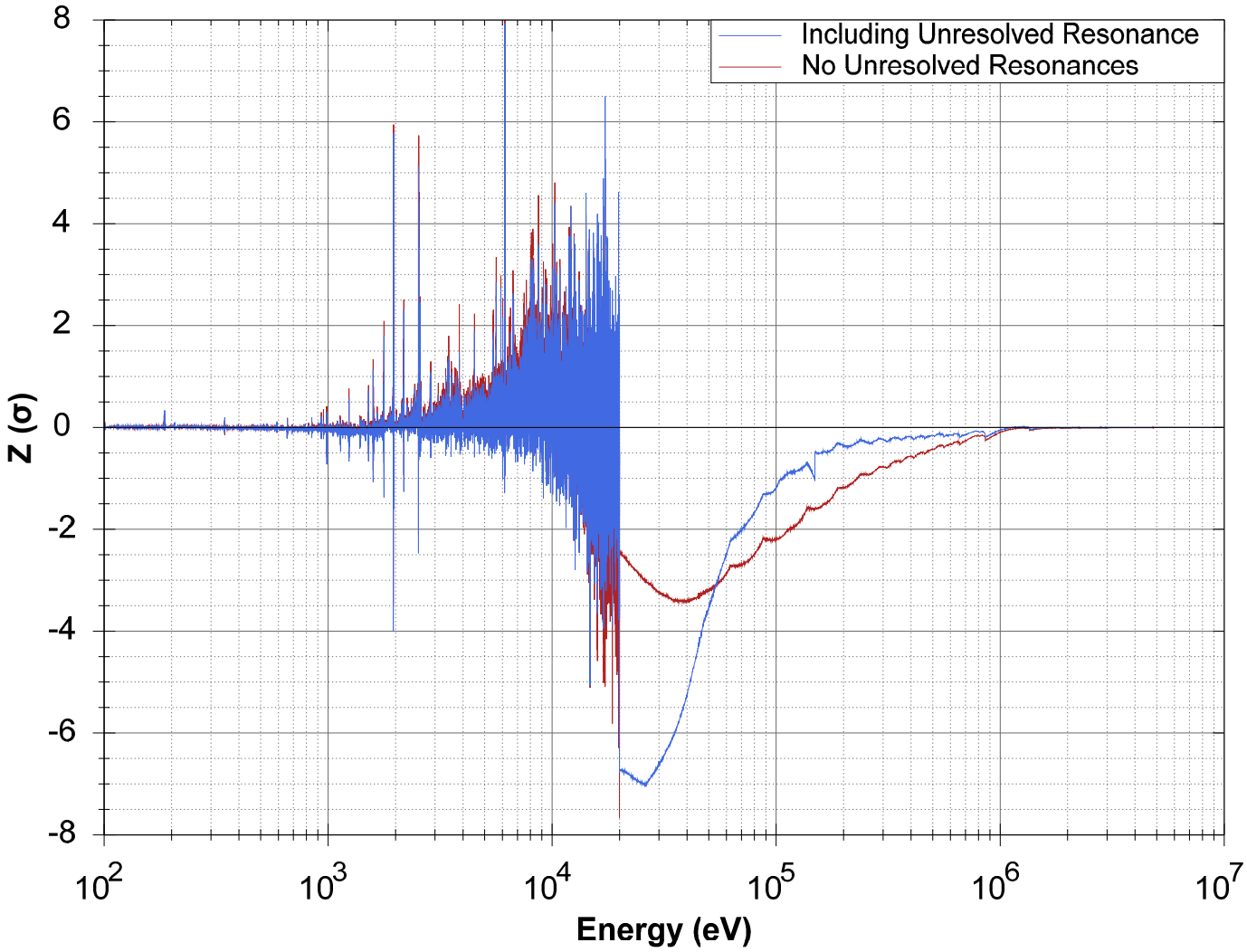

Figure 5-10. Standardized residuals (*z* statistics) from PWFSG generated by comparison to MCNP with and without unresolved resonance treatment

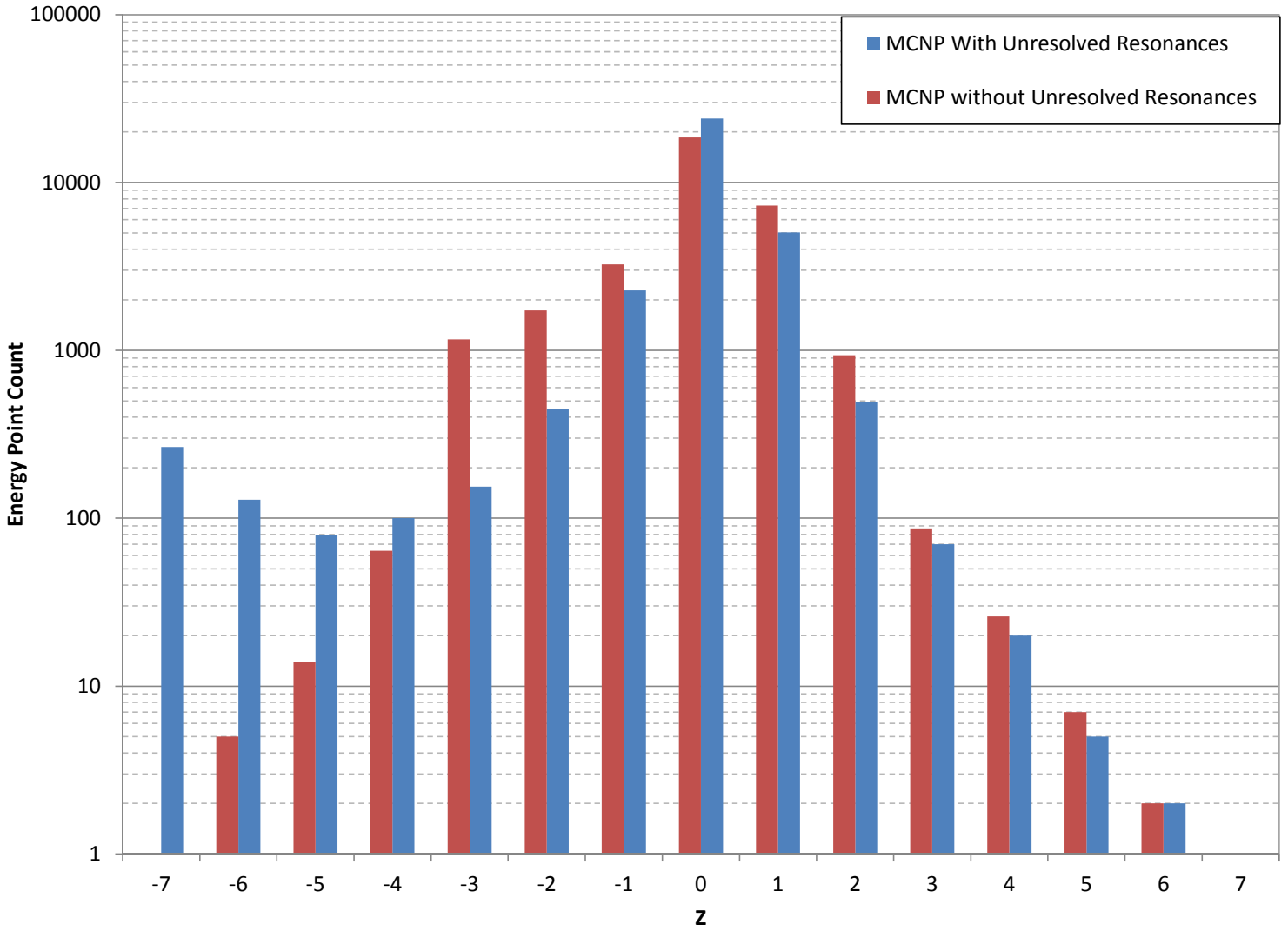

Figure 5-11. Histogram of standardized residuals from PWFSG compared to MCNP with and without unresolved resonance treatment

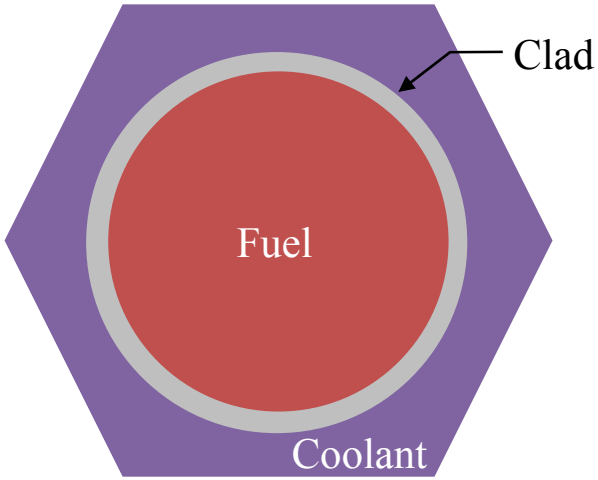

Figure 5-12. Geometry used for SFR and UNF cell model

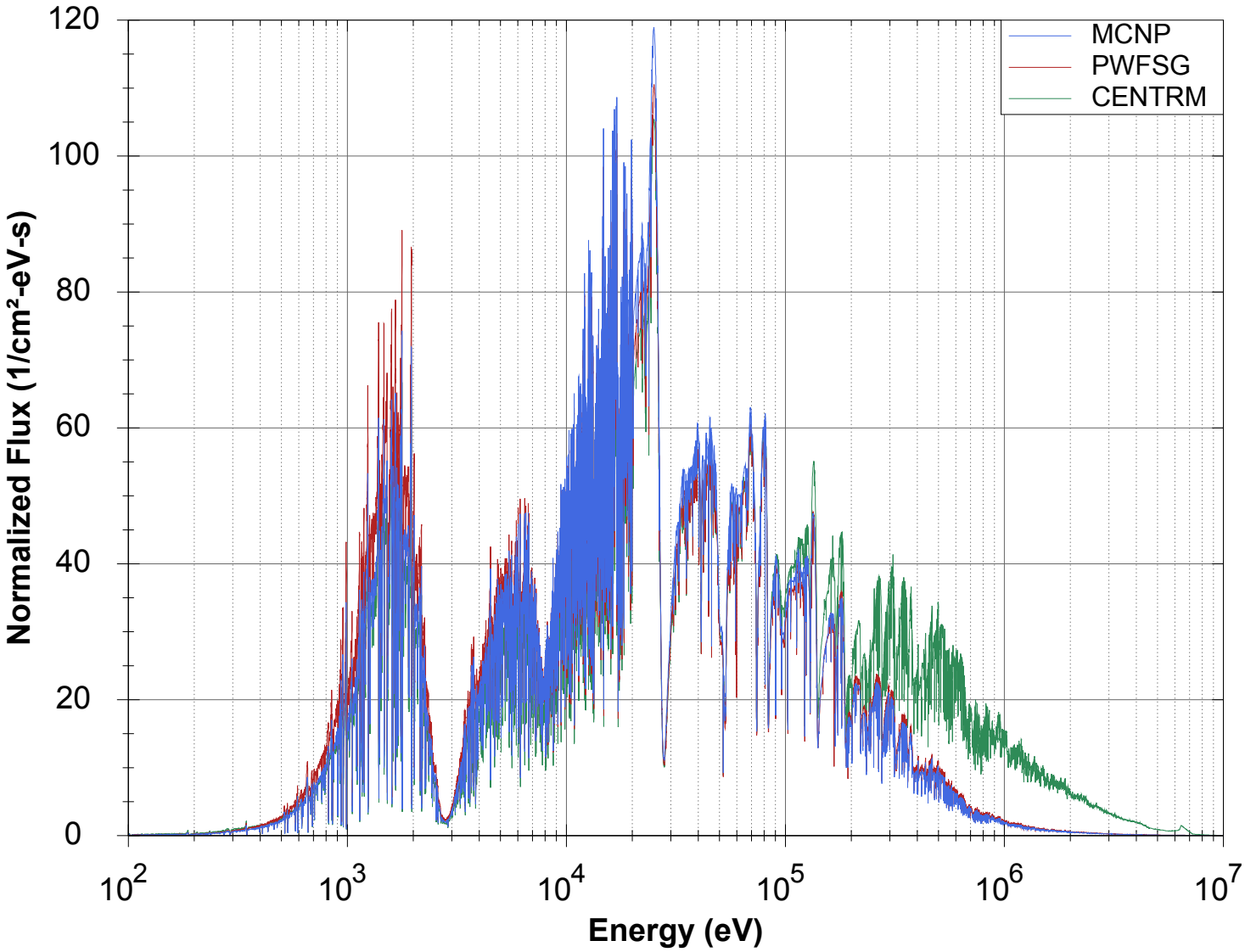

Figure 5-13. Neutron energy spectra generated by MCNP, PWFSG, and CENTRM for the SFR fuel cell case

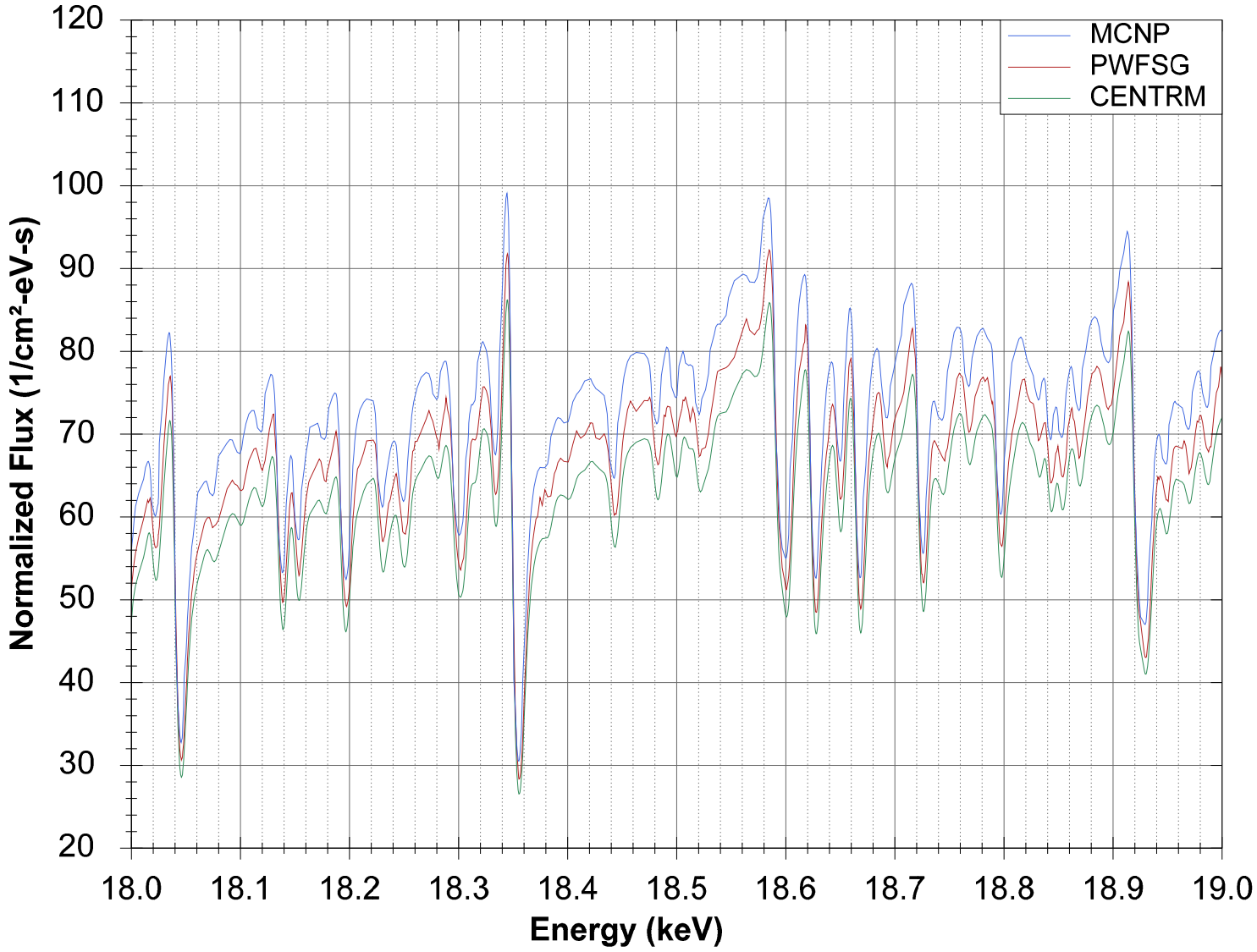

Figure 5-14. Neutron energy spectra for the SFR fuel cell case in the resonance region between 18 and 19 keV

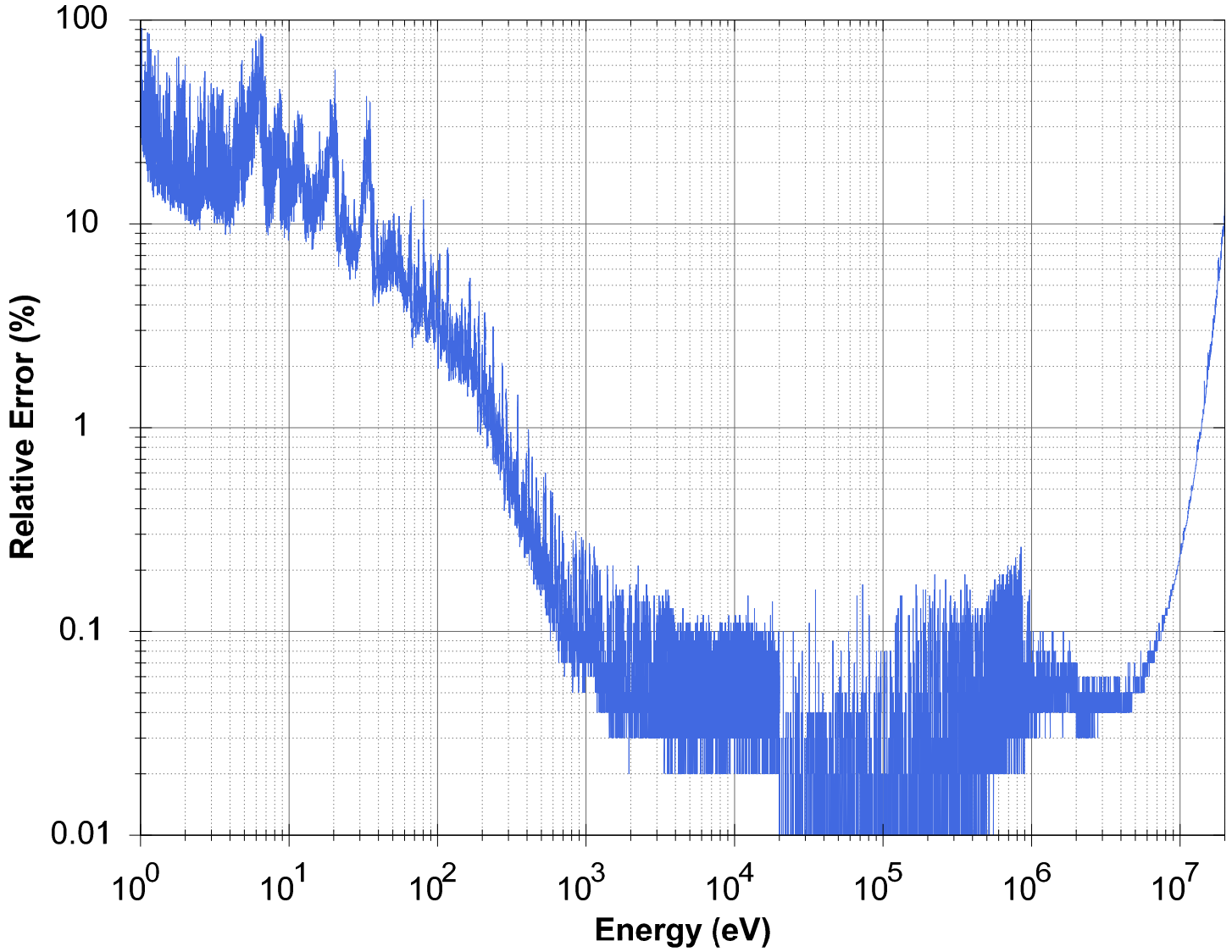

Figure 5-15. Statistical relative error from MCNP SFR fuel cell case

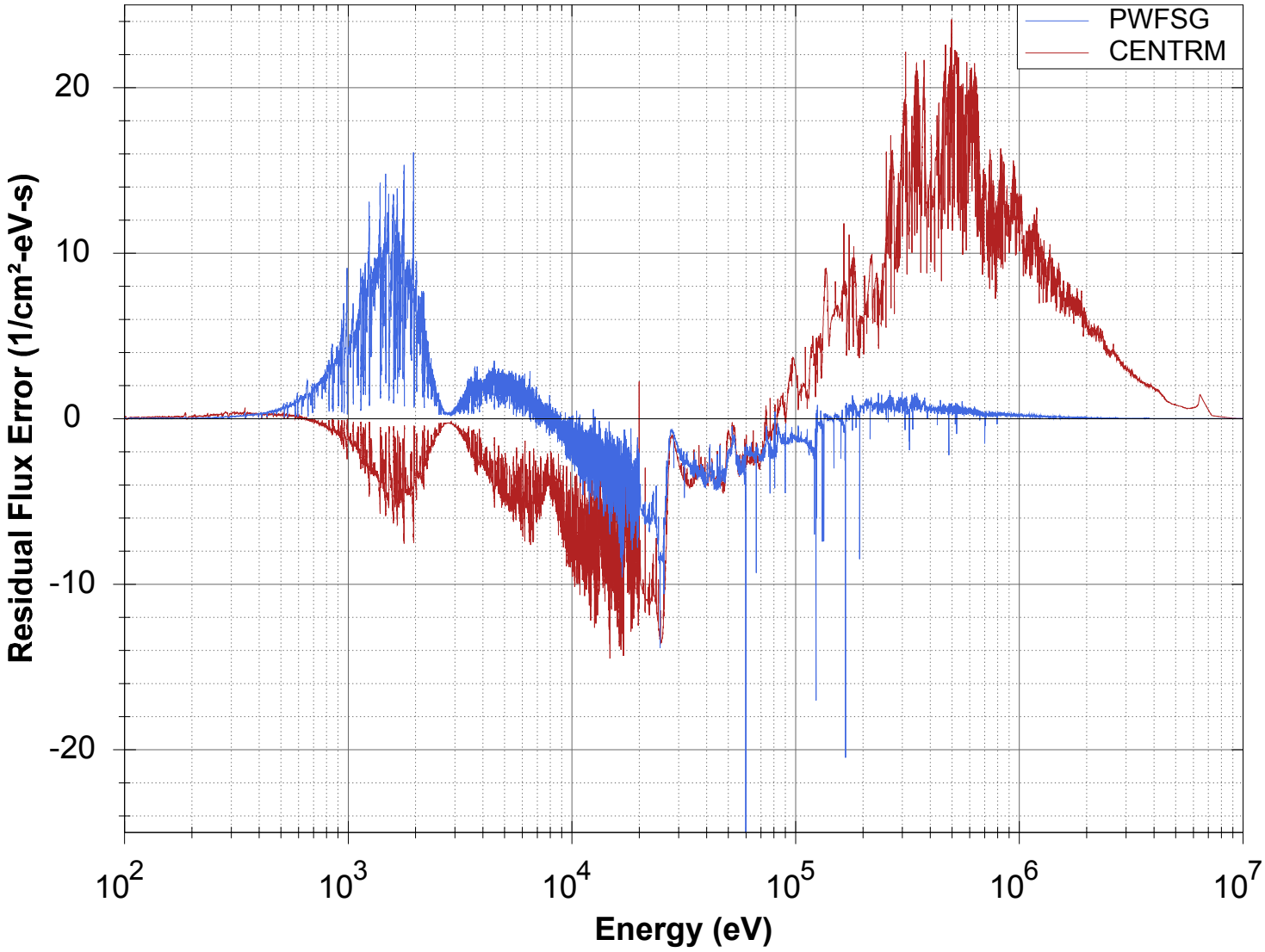

Figure 5-16. Residual flux error from difference in PWFSG or CENTRM and MCNP results for SFR fuel cell case

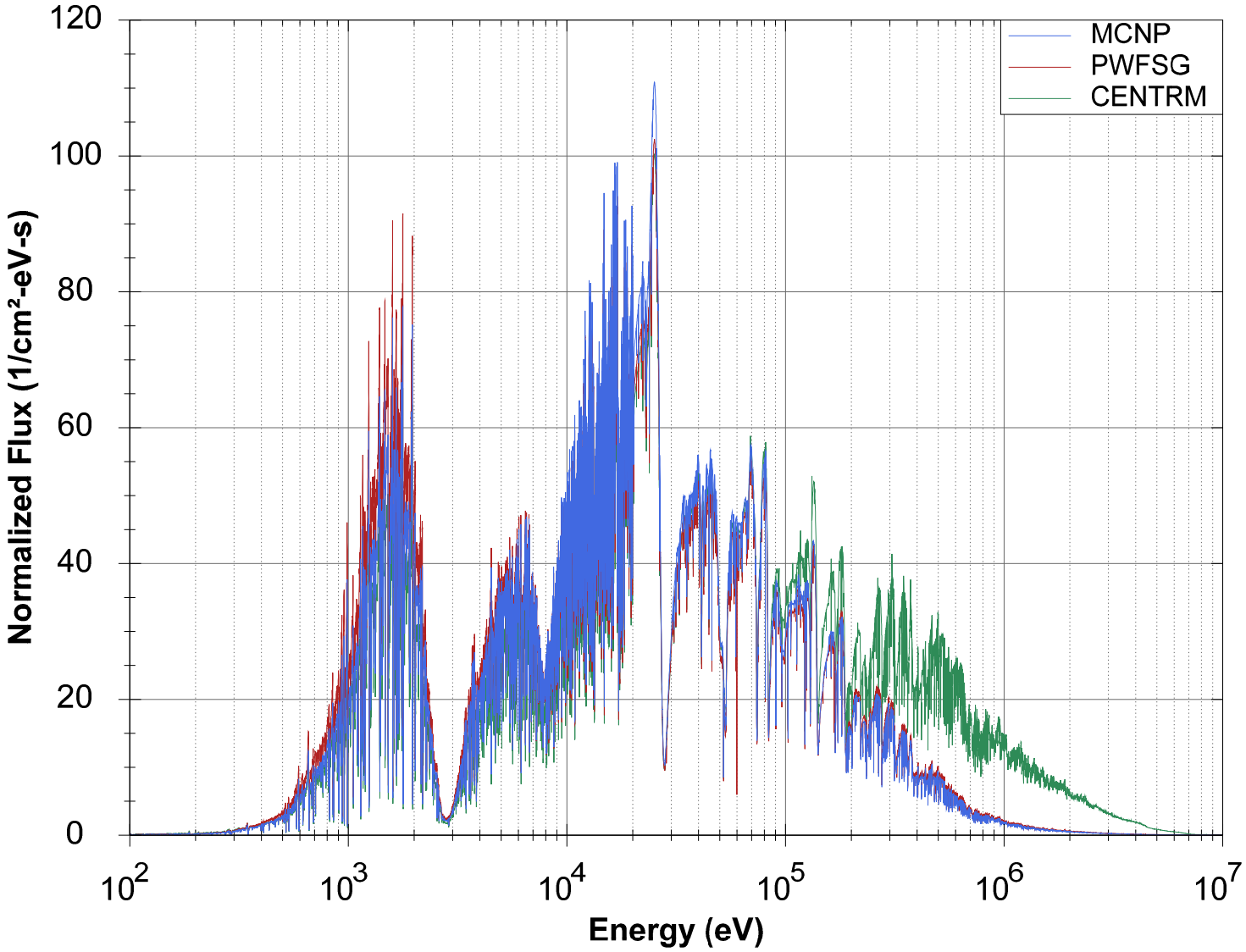

Figure 5-17. Neutron energy spectra generated by MCNP, PWFSG, and CENTRM for the UNF fuel cell case

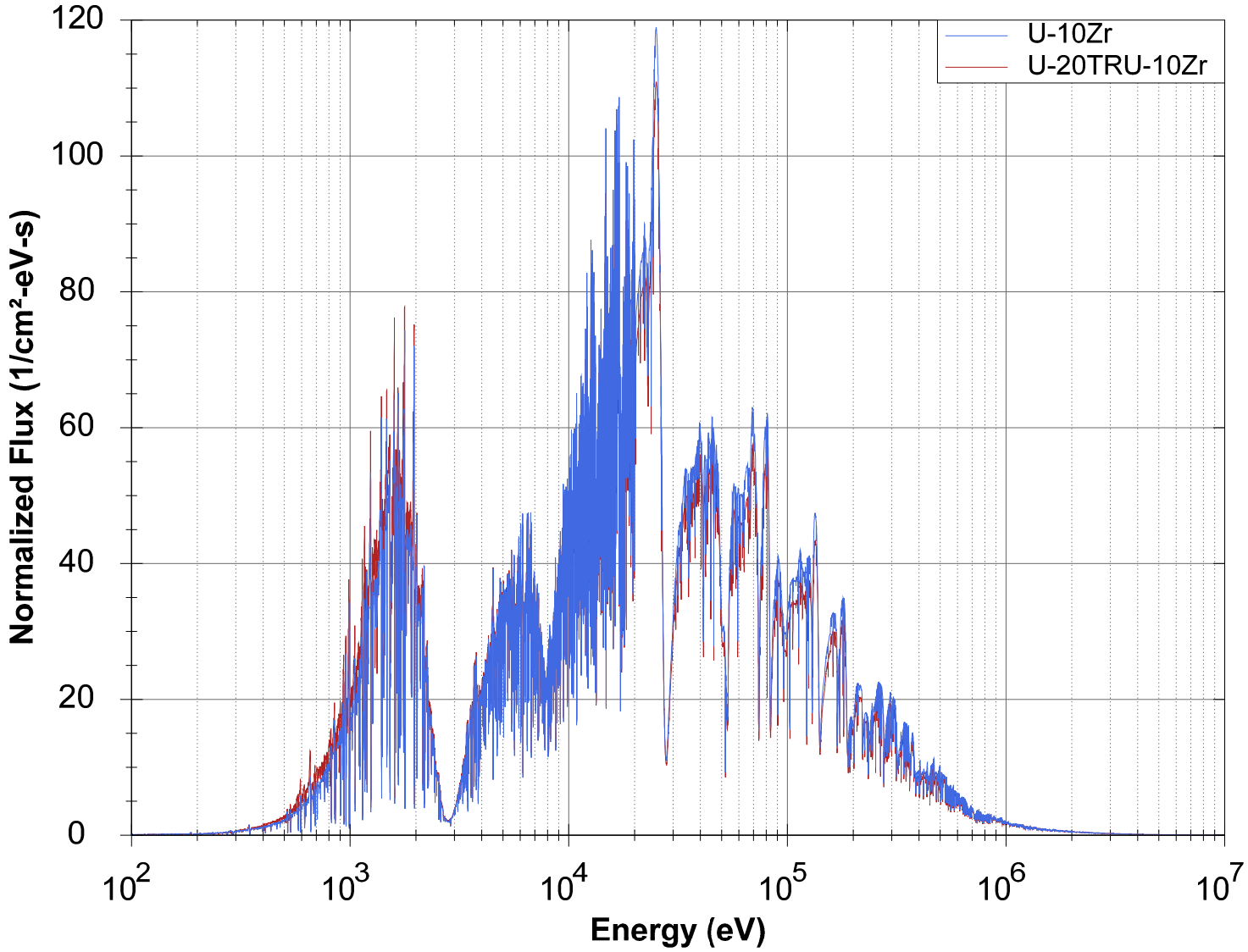

Figure 5-18. MCNP spectra for SFR fuel cell with U-10Zr fuel and UNF fuel cell with U-20TRU-10Zr fuel

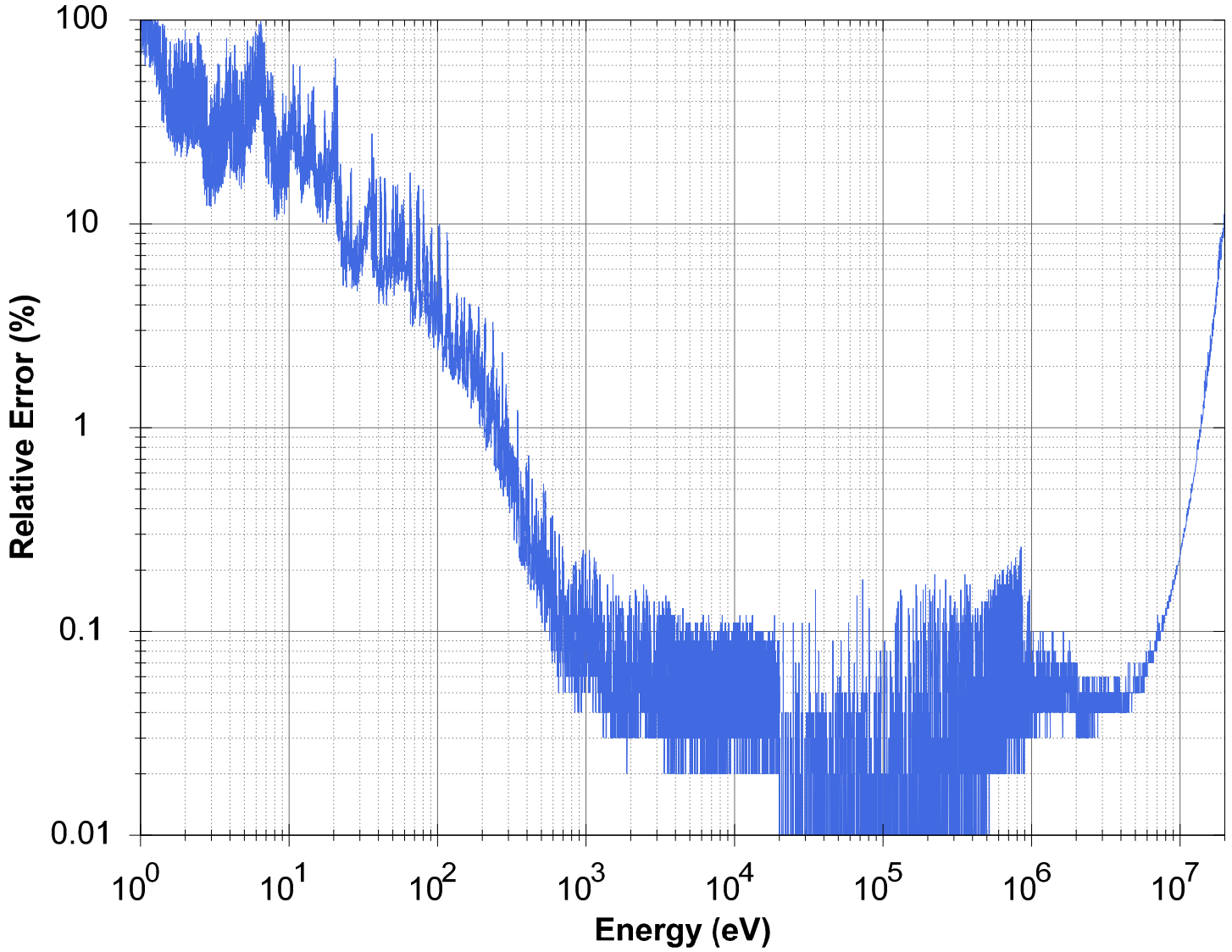

Figure 5-19. Statistical relative error from MCNP for the UNF fuel cell case

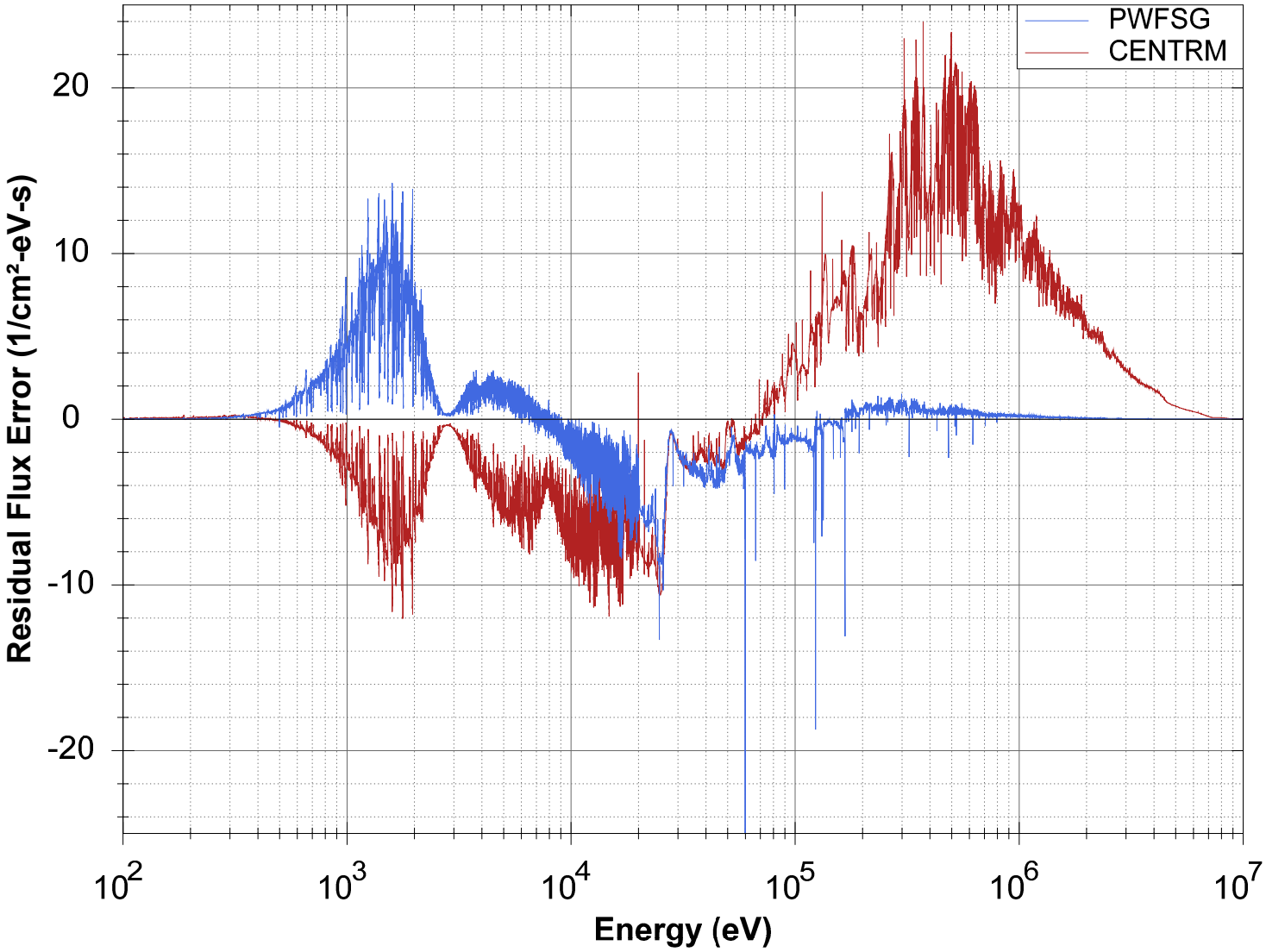

Figure 5-20. Residual flux error from difference in PWFSG or CENTRM and MCNP results for UNF fuel cell case

CHAPTER 6
CONCLUSIONS AND RECOMMENDATIONS FOR FUTURE WORK

Conclusions

The example cases included in Chapter 5 demonstrate that the pointwise (PW) Gauss-Kronrod Quadrature (GKQ) algorithm provides a robust treatment of the transfer source without a noticeable increase in the computational cost. The PWFSG results have excellent agreement with the high-fidelity Monte Carlo results, with computation time comparable to CENTRM. PWFSG reduces the residual error a factor of 6 as compared to CENTRM. The improvement factors, which are a measure of the residual error decrease in PWFSG compared to CENTRM, are summarized in Table 6-1.

Part of the computational efficiency in PWFSG is due to the scaling performance with increasing isotopes, due to parallelizing the transfer source calculation. This scaling would not be present on single-core architecture or in a model with only one isotope.

The main cause of the error in CENTRM is the kinematic assumptions in the PW solution region. These assumptions may be acceptable for LWR applications where the resonance region lies at lower energies (e.g., below 100 keV). CENTRM would then rely on the traditional Bondarenko approach (i.e., BONAMI module) at higher energies (e.g., above 100 keV). However, for SFR applications where the PW region could extend into the MeV range, the kinematic assumptions are invalid and cause significant error. The U-238 infinite medium case demonstrates that both CENTRM and PWFSG offer good agreement with MCNP when the CENTRM PW treatment was limited to below 25 keV.

The SFR and UNF fuel cell cases demonstrate that CENTRM significantly over-predicts the flux above 100 keV. Therefore, the GKQ algorithm in PWFSG offers added robustness to the transfer source term calculation.

Future Work

The greatest discrepancy in the PWFSG results is from the lack of an unresolved resonance treatment. The effect of these unresolved resonances is small compared to the CENTRM error, but still causes under-prediction of the flux in the unresolved resonance range. The addition of an unresolved resonance treatment to PWFSG would be an important next step in improving and demonstrating the GKQ transfer source approach. A possible method for implementing this is a stochastic approach that randomly adjusts the cross section in the unresolved resonance region based on probability tables as implemented in MCNP.[59]

The majority of the processing time required by PWFSG is for cross section and transfer probability interpolation. The development of a more efficient library lookup and interpolation scheme could make the GKQ algorithm appealing for production use.

The GKQ algorithm within PWFSG controls error by interval sizing rather than increasing the order of the node-weight set. Early implementations of PWFSG found the interval-halving approach to be more efficient and robust than increasing the order of the GKQ set; the (G_7,K_{15}) Gauss-Kronrod node-weight set was chosen to balance accuracy and computational cost. It is possible that a hybrid approach of interval sizing and quadrature order may improve the performance of PWFSG. A parametric study would be beneficial to quantifying the merits of both approaches.

Additional features could be added to PWFSG such as:

- Internal resonance reconstruction and temperature Doppler-broadening
- Thermal scattering treatment
- Eigenvalue calculation (i.e., fission source) capability

Such features may be necessary for extension to other common reactor applications, particularly LWR analysis. These considerations have implementations in programs such as NJOY and CENTRM; integration into PWFSG would be straightforward.

Finally, the GKQ algorithm in PWFSG provided only infinite medium spatial treatment to focus the comparison of the GKQ algorithm on the energy spectra effects, which are of primary importance in fast reactor applications. CENTRM provides methods to couple the PW solution with one-dimensional transport calculations. Extension of the PWFSG program to include spatial effects would extend the applicability of this PW algorithm to applications where spatial variation within a unit cell is important.

Table 6-1. Summary of improvement factors for test cases

Case	Improvement Factor, F
U-238 Infinite Medium	6.4
SFR Fuel Cell	7.8
UNF Fuel Cell	7.4

APPENDIX A
MCNP INPUT DATA

U-238 Infinite Medium

```
Infinite Medium of U238 with Pu-239 Fission Source
1  1   0.01   -1
99 0          1

c 10000 cm sphere
1 so  10000

nps 5e9
c Uranium-238 at 900 K
m1    92238.72c     1.0000
sdef  erg=d1
sp1   -3  0.966 2.842  $ Watt fission spectrum of Pu-239
wwp:n  5  2  4  0  0
#       wwe:n
       1.00E-06
       1.00E-05
       1.00E-04
       1.00E-03
       1.00E-02
       4.00E-02
       1.00E-01
       2.00E-01
       4.00E-01
       1.50E+00
       2.00E+00
       3.00E+00
       4.00E+00
       5.00E+00
       1.00E+01
       2.00E+01
wwn1:n    3.56E-04   0.0
wwn2:n    1.14E-03   0.0
wwn3:n    3.61E-03   0.0
wwn4:n    1.21E-02   0.0
wwn5:n    3.93E-02   0.0
wwn6:n    7.40E-02   0.0
wwn7:n    1.46E-01   0.0
wwn8:n    2.08E-01   0.0
wwn9:n    2.70E-01   0.0
wwn10:n   3.21E-01   0.0
wwn11:n   2.68E-01   0.0
wwn12:n   1.95E-01   0.0
wwn13:n   1.14E-01   0.0
wwn14:n   6.17E-02   0.0
wwn15:n   1.44E-02   0.0
wwn16:n   1.90E-04   0.0
nonu
print
prdmp 0 0 0 3
rand gen=2
```

```
f4:n  1
e4      1.00085430009E-07
        1.00256508946E-07
        1.00427880384E-07
        1.00599544322E-07
                …
```

Energy mesh truncated due to size. Mesh includes 43,283 points between 0.1 eV and 20 MeV.

SFR Fuel Cell

```
Infinite medium of homogenized SFR Fuel Cell at 900 K
1  1   0.01   -1
99 0          1

c 10000 cm sphere
1 so  10000

nps 5e9
c Homogenized fuel cell at 900 K
m1      92235.72c    1.8858619E-03
        92238.72c    1.0551567E-02
        40090.72c    1.8518384E-03
        40091.72c    4.0384114E-04
        40092.72c    6.1727947E-04
        40094.72c    6.2555785E-04
        40096.72c    1.0078032E-04
        26054.72c    7.5240415E-04
        26056.72c    1.1811136E-02
        26057.72c    2.7277064E-04
        26058.72c    3.6300765E-05
        24050.72c    8.2857689E-05
        24052.72c    1.5978281E-03
        24053.72c    1.8118088E-04
        24054.72c    4.5099755E-05
        42092.72c    1.2782226E-05
        42094.72c    7.9673577E-06
        42095.72c    1.3712469E-05
        42096.72c    1.4367084E-05
        42097.72c    8.2257585E-06
        42098.72c    2.0784037E-05
        42100.72c    8.2946654E-06
        11023.72c    8.4013761E-03
sdef  erg=d1
sp1   -3  0.966 2.842  $ Watt fission spectrum of Pu-239
wwp:n  5  2  4  0  0
#         wwe:n
        1.00E-06
        1.00E-05
        1.00E-04
        1.00E-03
        1.00E-02
        4.00E-02
        1.00E-01
        2.00E-01
        4.00E-01
        1.50E+00
        2.00E+00
        3.00E+00
        4.00E+00
        5.00E+00
        1.00E+01
        2.00E+01
wwn1:n    3.56E-04   0.0
wwn2:n    1.14E-03   0.0
```

```
wwn3:n    3.61E-03   0.0
wwn4:n    1.21E-02   0.0
wwn5:n    3.93E-02   0.0
wwn6:n    7.40E-02   0.0
wwn7:n    1.46E-01   0.0
wwn8:n    2.08E-01   0.0
wwn9:n    2.70E-01   0.0
wwn10:n   3.21E-01   0.0
wwn11:n   2.68E-01   0.0
wwn12:n   1.95E-01   0.0
wwn13:n   1.14E-01   0.0
wwn14:n   6.17E-02   0.0
wwn15:n   1.44E-02   0.0
wwn16:n   1.90E-04   0.0
nonu
print
prdmp 3j 3
rand gen=2
f4:n  1
e4      1.00085430009E-07
        1.00256508946E-07
        1.00427880384E-07
        1.00599544322E-07
        …
```

Energy mesh truncated due to size. Mesh includes 49,114 points between 0.1 eV and 20 MeV.

UNF Fuel Cell

```
Infinite medium of homogenized SFR Fuel Cell with 20% TRU
1  1   0.01   -1
99 0          1

c 10000 cm sphere
1 so  10000

nps 5e9
c Homogenized fuel cell at 900 K
m1      92235.72c    1.9614993E-05
        92238.72c    9.6642491E-03
        95241.72c    1.3566604E-04
        95243.72c    3.4663778E-05
        96244.72c    8.2528486E-06
        96245.72c    4.6175738E-07
        93237.72c    1.5733084E-04
        94238.72c    5.5200518E-05
        94239.72c    1.3077054E-03
        94240.72c    6.5959724E-04
        94241.72c    2.3354193E-04
        94242.72c    1.5570373E-04
        40090.72c    1.8573215E-03
        40091.72c    4.0503688E-04
        40092.72c    6.1910718E-04
        40094.72c    6.2741007E-04
        40096.72c    1.0107872E-04
        26054.72c    7.5240415E-04
        26056.72c    1.1811136E-02
        26057.72c    2.7277064E-04
        26058.72c    3.6300765E-05
        24050.72c    8.2857689E-05
        24052.72c    1.5978281E-03
        24053.72c    1.8118088E-04
        24054.72c    4.5099755E-05
        42092.72c    1.2782226E-05
        42094.72c    7.9673577E-06
        42095.72c    1.3712469E-05
        42096.72c    1.4367084E-05
        42097.72c    8.2257585E-06
        42098.72c    2.0784037E-05
        42100.72c    8.2946654E-06
        11023.72c    8.4013761E-03
sdef  erg=d1
sp1   -3  0.966 2.842  $ Watt fission spectrum of Pu-239
wwp:n  5  2  4  0  0
#       wwe:n
        1.00E-06
        1.00E-05
        1.00E-04
        1.00E-03
        1.00E-02
        4.00E-02
        1.00E-01
        2.00E-01
```

```
        4.00E-01
        1.50E+00
        2.00E+00
        3.00E+00
        4.00E+00
        5.00E+00
        1.00E+01
        2.00E+01
wwn1:n    3.56E-04   0.0
wwn2:n    1.14E-03   0.0
wwn3:n    3.61E-03   0.0
wwn4:n    1.21E-02   0.0
wwn5:n    3.93E-02   0.0
wwn6:n    7.40E-02   0.0
wwn7:n    1.46E-01   0.0
wwn8:n    2.08E-01   0.0
wwn9:n    2.70E-01   0.0
wwn10:n   3.21E-01   0.0
wwn11:n   2.68E-01   0.0
wwn12:n   1.95E-01   0.0
wwn13:n   1.14E-01   0.0
wwn14:n   6.17E-02   0.0
wwn15:n   1.44E-02   0.0
wwn16:n   1.90E-04   0.0
nonu
print
prdmp 3j 3
rand gen=2
f4:n  1
e4      1.0008296558356E-07
        1.0024910302666E-07
        1.0041551646903E-07
        1.0058220591232E-07
        …
```

Energy mesh truncated due to size. Mesh includes 49,481 points between 0.1 eV and 20 MeV.

APPENDIX B
PWFSG INPUT DATA

U-238 Infinite Medium

```
<?xml version="1.0" encoding="utf-8"?>
<pwfsg>
  <isotopes>
    <isotope name="U-238" matId="9237" atomDensity="1.000">
      <endfFile path="n-092_U_238.endf"></endfFile>
      <pendfFile path="n-092_U_238.pendf"></pendfFile>
    </isotope>
  </isotopes>
  <source type="Watt">
    <parameters a="0.966" b="2.842"></parameters>
  </source>
  <options>
    <thinningTolerance>0.001</thinningTolerance>
    <collisionRateTolerance>0.5</collisionRateTolerance>
    <fluxErrorTolerance>0.001</fluxErrorTolerance>
    <maxFractionalEnergyChange>0.1</maxFractionalEnergyChange>
  </options>
</pwfsg>
```

SFR Fuel Cell

```
<?xml version="1.0" encoding="utf-8"?>
<pwfsg>
  <isotopes>
    <isotope name="U-235" matId="9228" atomDensity="1.8858619E-03">
      <endfFile path="n-092_U_235.endf"></endfFile>
      <pendfFile path="n-092_U_235.pendf"></pendfFile>
    </isotope>
    <isotope name="U-238" matId="9237" atomDensity="1.0551567E-02">
      <endfFile path="n-092_U_238.endf"></endfFile>
      <pendfFile path="n-092_U_238.pendf"></pendfFile>
    </isotope>
    <isotope name="Zr-90" matId="4025" atomDensity="1.8518384E-03">
      <endfFile path="n-040_Zr_090.endf"></endfFile>
      <pendfFile path="n-040_Zr_090.pendf"></pendfFile>
    </isotope>
    <isotope name="Zr-91" matId="4028" atomDensity="4.0384114E-04">
      <endfFile path="n-040_Zr_091.endf"></endfFile>
      <pendfFile path="n-040_Zr_091.pendf"></pendfFile>
    </isotope>
    <isotope name="Zr-92" matId="4031" atomDensity="6.1727947E-04">
      <endfFile path="n-040_Zr_092.endf"></endfFile>
      <pendfFile path="n-040_Zr_092.pendf"></pendfFile>
    </isotope>
    <isotope name="Zr-94" matId="4037" atomDensity="6.2555785E-04">
      <endfFile path="n-040_Zr_094.endf"></endfFile>
      <pendfFile path="n-040_Zr_094.pendf"></pendfFile>
    </isotope>
    <isotope name="Zr-96" matId="4043" atomDensity="1.0078032E-04">
      <endfFile path="n-040_Zr_096.endf"></endfFile>
      <pendfFile path="n-040_Zr_096.pendf"></pendfFile>
    </isotope>
    <isotope name="Fe-54" matId="2625" atomDensity="7.5240415E-04">
      <endfFile path="n-026_Fe_054.endf"></endfFile>
      <pendfFile path="n-026_Fe_054.pendf"></pendfFile>
    </isotope>
    <isotope name="Fe-56" matId="2631" atomDensity="1.1811136E-02">
      <endfFile path="n-026_Fe_056.endf"></endfFile>
      <pendfFile path="n-026_Fe_056.pendf"></pendfFile>
    </isotope>
    <isotope name="Fe-57" matId="2634" atomDensity="2.7277064E-04">
      <endfFile path="n-026_Fe_057.endf"></endfFile>
      <pendfFile path="n-026_Fe_057.pendf"></pendfFile>
    </isotope>
    <isotope name="Fe-58" matId="2637" atomDensity="3.6300765E-05">
      <endfFile path="n-026_Fe_058.endf"></endfFile>
      <pendfFile path="n-026_Fe_058.pendf"></pendfFile>
    </isotope>
    <isotope name="Cr-50" matId="2425" atomDensity="8.2857689E-05">
      <endfFile path="n-024_Cr_050.endf"></endfFile>
      <pendfFile path="n-024_Cr_050.pendf"></pendfFile>
    </isotope>
    <isotope name="Cr-52" matId="2431" atomDensity="1.5978281E-03">
      <endfFile path="n-024_Cr_052.endf"></endfFile>
      <pendfFile path="n-024_Cr_052.pendf"></pendfFile>
```

```
    </isotope>
    <isotope name="Cr-53" matId="2434" atomDensity="1.8118088E-04">
      <endfFile path="n-024_Cr_053.endf"></endfFile>
      <pendfFile path="n-024_Cr_053.pendf"></pendfFile>
    </isotope>
    <isotope name="Cr-54" matId="2437" atomDensity="4.5099755E-05">
      <endfFile path="n-024_Cr_054.endf"></endfFile>
      <pendfFile path="n-024_Cr_054.pendf"></pendfFile>
    </isotope>
    <isotope name="Mo-92" matId="4225" atomDensity="1.2782226E-05">
      <endfFile path="n-042_Mo_092.endf"></endfFile>
      <pendfFile path="n-042_Mo_092.pendf"></pendfFile>
    </isotope>
    <isotope name="Mo-94" matId="4231" atomDensity="7.9673577E-06">
      <endfFile path="n-042_Mo_094.endf"></endfFile>
      <pendfFile path="n-042_Mo_094.pendf"></pendfFile>
    </isotope>
    <isotope name="Mo-95" matId="4234" atomDensity="1.3712469E-05">
      <endfFile path="n-042_Mo_095.endf"></endfFile>
      <pendfFile path="n-042_Mo_095.pendf"></pendfFile>
    </isotope>
    <isotope name="Mo-96" matId="4237" atomDensity="1.4367084E-05">
      <endfFile path="n-042_Mo_096.endf"></endfFile>
      <pendfFile path="n-042_Mo_096.pendf"></pendfFile>
    </isotope>
    <isotope name="Mo-97" matId="4240" atomDensity="8.2257585E-06">
      <endfFile path="n-042_Mo_097.endf"></endfFile>
      <pendfFile path="n-042_Mo_097.pendf"></pendfFile>
    </isotope>
    <isotope name="Mo-98" matId="4243" atomDensity="2.0784037E-05">
      <endfFile path="n-042_Mo_098.endf"></endfFile>
      <pendfFile path="n-042_Mo_098.pendf"></pendfFile>
    </isotope>
    <isotope name="Mo-100" matId="4249" atomDensity="8.2946654E-06">
      <endfFile path="n-042_Mo_100.endf"></endfFile>
      <pendfFile path="n-042_Mo_100.pendf"></pendfFile>
    </isotope>
    <isotope name="Na-23" matId="1125" atomDensity="8.4013761E-03">
      <endfFile path="n-011_Na_023.endf"></endfFile>
      <pendfFile path="n-011_Na_023.pendf"></pendfFile>
    </isotope>
  </isotopes>
  <source type="Watt">
    <parameters a="0.966" b="2.842"></parameters>
  </source>
  <options>
    <thinningTolerance>0.001</thinningTolerance>
    <collisionRateTolerance>0.5</collisionRateTolerance>
    <fluxErrorTolerance>0.001</fluxErrorTolerance>
    <maxFractionalEnergyChange>0.1</maxFractionalEnergyChange>
  </options>
</pwfsg>
```

UNF Fuel Cell

```
<?xml version="1.0" encoding="utf-8"?>
<pwfsg>
  <isotopes>
    <isotope name="U-235" matId="9228" atomDensity="1.9614993E-05">
      <endfFile path="n-092_U_235.endf"></endfFile>
      <pendfFile path="n-092_U_235.pendf"></pendfFile>
    </isotope>
    <isotope name="U-238" matId="9237" atomDensity="9.6642491E-03">
      <endfFile path="n-092_U_238.endf"></endfFile>
      <pendfFile path="n-092_U_238.pendf"></pendfFile>
    </isotope>
    <isotope name="Am-241" matId="9543" atomDensity="1.3566604E-04">
      <endfFile path="n-095_Am_241.endf"></endfFile>
      <pendfFile path="n-095_Am_241.pendf"></pendfFile>
    </isotope>
    <isotope name="Am-243" matId="9549" atomDensity="3.4663778E-05">
      <endfFile path="n-095_Am_243.endf"></endfFile>
      <pendfFile path="n-095_Am_243.pendf"></pendfFile>
    </isotope>
    <isotope name="Cm-244" matId="9637" atomDensity="8.2528486E-06">
      <endfFile path="n-096_Cm_244.endf"></endfFile>
      <pendfFile path="n-096_Cm_244.pendf"></pendfFile>
    </isotope>
    <isotope name="Cm-245" matId="9640" atomDensity="4.6175738E-07">
      <endfFile path="n-096_Cm_245.endf"></endfFile>
      <pendfFile path="n-096_Cm_245.pendf"></pendfFile>
    </isotope>
    <isotope name="Np-237" matId="9346" atomDensity="1.5733084E-04">
      <endfFile path="n-093_Np_237.endf"></endfFile>
      <pendfFile path="n-093_Np_237.pendf"></pendfFile>
    </isotope>
    <isotope name="Pu-238" matId="9434" atomDensity="5.5200518E-05">
      <endfFile path="n-094_Pu_238.endf"></endfFile>
      <pendfFile path="n-094_Pu_238.pendf"></pendfFile>
    </isotope>
    <isotope name="Pu-239" matId="9437" atomDensity="1.3077054E-03">
      <endfFile path="n-094_Pu_239.endf"></endfFile>
      <pendfFile path="n-094_Pu_239.pendf"></pendfFile>
    </isotope>
    <isotope name="Pu-240" matId="9440" atomDensity="6.5959724E-04">
      <endfFile path="n-094_Pu_240.endf"></endfFile>
      <pendfFile path="n-094_Pu_240.pendf"></pendfFile>
    </isotope>
    <isotope name="Pu-241" matId="9443" atomDensity="2.3354193E-04">
      <endfFile path="n-094_Pu_241.endf"></endfFile>
      <pendfFile path="n-094_Pu_241.pendf"></pendfFile>
    </isotope>
    <isotope name="Pu-242" matId="9446" atomDensity="1.5570373E-04">
      <endfFile path="n-094_Pu_242.endf"></endfFile>
      <pendfFile path="n-094_Pu_242.pendf"></pendfFile>
    </isotope>
    <isotope name="Zr-90" matId="4025" atomDensity="1.8573215E-03">
      <endfFile path="n-040_Zr_090.endf"></endfFile>
      <pendfFile path="n-040_Zr_090.pendf"></pendfFile>
```

```
</isotope>
<isotope name="Zr-91" matId="4028" atomDensity="4.0503688E-04">
  <endfFile path="n-040_Zr_091.endf"></endfFile>
  <pendfFile path="n-040_Zr_091.pendf"></pendfFile>
</isotope>
<isotope name="Zr-92" matId="4031" atomDensity="6.1910718E-04">
  <endfFile path="n-040_Zr_092.endf"></endfFile>
  <pendfFile path="n-040_Zr_092.pendf"></pendfFile>
</isotope>
<isotope name="Zr-94" matId="4037" atomDensity="6.2741007E-04">
  <endfFile path="n-040_Zr_094.endf"></endfFile>
  <pendfFile path="n-040_Zr_094.pendf"></pendfFile>
</isotope>
<isotope name="Zr-96" matId="4043" atomDensity="1.0107872E-04">
  <endfFile path="n-040_Zr_096.endf"></endfFile>
  <pendfFile path="n-040_Zr_096.pendf"></pendfFile>
</isotope>
<isotope name="Fe-54" matId="2625" atomDensity="7.5240415E-04">
  <endfFile path="n-026_Fe_054.endf"></endfFile>
  <pendfFile path="n-026_Fe_054.pendf"></pendfFile>
</isotope>
<isotope name="Fe-56" matId="2631" atomDensity="1.1811136E-02">
  <endfFile path="n-026_Fe_056.endf"></endfFile>
  <pendfFile path="n-026_Fe_056.pendf"></pendfFile>
</isotope>
<isotope name="Fe-57" matId="2634" atomDensity="2.7277064E-04">
  <endfFile path="n-026_Fe_057.endf"></endfFile>
  <pendfFile path="n-026_Fe_057.pendf"></pendfFile>
</isotope>
<isotope name="Fe-58" matId="2637" atomDensity="3.6300765E-05">
  <endfFile path="n-026_Fe_058.endf"></endfFile>
  <pendfFile path="n-026_Fe_058.pendf"></pendfFile>
</isotope>
<isotope name="Cr-50" matId="2425" atomDensity="8.2857689E-05">
  <endfFile path="n-024_Cr_050.endf"></endfFile>
  <pendfFile path="n-024_Cr_050.pendf"></pendfFile>
</isotope>
<isotope name="Cr-52" matId="2431" atomDensity="1.5978281E-03">
  <endfFile path="n-024_Cr_052.endf"></endfFile>
  <pendfFile path="n-024_Cr_052.pendf"></pendfFile>
</isotope>
<isotope name="Cr-53" matId="2434" atomDensity="1.8118088E-04">
  <endfFile path="n-024_Cr_053.endf"></endfFile>
  <pendfFile path="n-024_Cr_053.pendf"></pendfFile>
</isotope>
<isotope name="Cr-54" matId="2437" atomDensity="4.5099755E-05">
  <endfFile path="n-024_Cr_054.endf"></endfFile>
  <pendfFile path="n-024_Cr_054.pendf"></pendfFile>
</isotope>
<isotope name="Mo-92" matId="4225" atomDensity="1.2782226E-05">
  <endfFile path="n-042_Mo_092.endf"></endfFile>
  <pendfFile path="n-042_Mo_092.pendf"></pendfFile>
</isotope>
<isotope name="Mo-94" matId="4231" atomDensity="7.9673577E-06">
  <endfFile path="n-042_Mo_094.endf"></endfFile>
  <pendfFile path="n-042_Mo_094.pendf"></pendfFile>
```

```
    </isotope>
    <isotope name="Mo-95" matId="4234" atomDensity="1.3712469E-05">
      <endfFile path="n-042_Mo_095.endf"></endfFile>
      <pendfFile path="n-042_Mo_095.pendf"></pendfFile>
    </isotope>
    <isotope name="Mo-96" matId="4237" atomDensity="1.4367084E-05">
      <endfFile path="n-042_Mo_096.endf"></endfFile>
      <pendfFile path="n-042_Mo_096.pendf"></pendfFile>
    </isotope>
    <isotope name="Mo-97" matId="4240" atomDensity="8.2257585E-06">
      <endfFile path="n-042_Mo_097.endf"></endfFile>
      <pendfFile path="n-042_Mo_097.pendf"></pendfFile>
    </isotope>
    <isotope name="Mo-98" matId="4243" atomDensity="2.0784037E-05">
      <endfFile path="n-042_Mo_098.endf"></endfFile>
      <pendfFile path="n-042_Mo_098.pendf"></pendfFile>
    </isotope>
    <isotope name="Mo-100" matId="4249" atomDensity="8.2946654E-06">
      <endfFile path="n-042_Mo_100.endf"></endfFile>
      <pendfFile path="n-042_Mo_100.pendf"></pendfFile>
    </isotope>
    <isotope name="Na-23" matId="1125" atomDensity="8.4013761E-03">
      <endfFile path="n-011_Na_023.endf"></endfFile>
      <pendfFile path="n-011_Na_023.pendf"></pendfFile>
    </isotope>
  </isotopes>
  <source type="Watt">
    <parameters a="0.966" b="2.842"></parameters>
  </source>
  <options>
    <thinningTolerance>0.001</thinningTolerance>
    <collisionRateTolerance>0.5</collisionRateTolerance>
    <fluxErrorTolerance>0.001</fluxErrorTolerance>
    <maxFractionalEnergyChange>0.1</maxFractionalEnergyChange>
  </options>
</pwfsg>
```

APPENDIX C
CENTRM INPUT DATA

U-238 Infinite Medium

```
=shell
del  C:\scale6\tmpdir\ft88f001
copy C:\scale6\data\xn238v7 ft88f001
end

=ajax
0$$ 11 0
1$$ 1 T
'   Input library  / Number of isotopes to copy
2$$          88                        1   T
'   Isotope ZAID
3$$ 92238  T
end

=bonami
'   Input library  / Scratch / Scratch / Output library
0$$           11        0        18              1
'   Geometry flag /  Number of zones / Mix Table length / XS edit flag /
1$$           0               1               1             0
' Bondarenko edit flag / Dancoff factor
                  0            0    T
' Mixture numbers by isotope
3$$          1
'   Nuclide IDs
4$$       92238
'   Nuclide concentrations (atom/b-cm)
5**       1.000
'   Mixtures by zone
6$$              1
'   Temperatures by zone
8**          9.00000E+02
'    New Identifier in Mixing tables
10$$ 92238
'  Zone types (0 - fuel, 1 - mod, 2 - clad)
11$$ 0 t
end

=worker
'   Input master lib  / Input working lib  / Output lib
0$$              1                0           4
'   Scratch / Scratch / Output Temp-Interpolated lib
        18       19                          0
'   Num nuclides to read from master lib / Num to read from working lib
1$$                              1                         0
' Output print option / Flag to copy master / Flag to copy working
                -2                -1                -1
' Sequence # of master / Sequence # of working / Sequence # of output
                  1                  1                  1  T
'   IDs from master to copy
2$$                92238
```

```
'   Thermal scat. kernel temps
6**               9.00000E+02  T
end

=crawdad
'   Output CENTRM lib / Scratch / Scratch / CE-KENO lib
0$$               81        17        18            77
'   Number of PW nuclides / CENTRM Identifier header / Print flag
1$$                  1                   66666            1
' Lib format 0/1= old/new / Temp interp method / Thermal lib out flag
                     0                   0                    1
' Extra unused integer flags
e  T
' Data Blocks 2 and 3 repeated for each nuclide
'   ZAID for PW mat / ENDF version / ENDF mod / Number of temps for iso
2$$           92238              7        -1                        1
'   MTs to be included / Mod number of therm data / Data source
                  0                        -1             0
'   Lower PW energy limit (eV) / Upper PW energy limit (eV)
3**               1.00000E-04                   2.000E+07   T
'   Nuclide temps to process
4**               9.00000E+02        T
end

=centrm
CENTRM: U-238 Inf medium at 900 K
'   Punch logical / Thermal kernel / MG working lib / PW lib
0$$            7               0               4       81
' MG flux restart / MG output / PW output / MG Angular output
               0         25          15                16
' Scratch for thermal matrices / Optional PW xs print / Scratch
                         17                   18        19
' Not used / Scratch
        8         9
'   Geometry / Num Zones / Num Intervals / Left BC / Right BC
1$$        0          1               1         0          0
' Num Mixtures / Mix Table Length / Sn order / Max Pn Order
            1                1          0             64
' Source type / Inner iter max / Upscatter outer iter max
           0             20                    100
' UMG range calc type / LMG range calc type / PW range calc type
                 2                   2                   3
' MG source and XS linearization / Pn order for PW calc
                           3                   64
' PW Inelastic scat option
                     1
'   Mix XS print opt / Flux print opt / Balance Table print
2$$               0               3                   1
'  Vol source flag / Boundary source flag / Group diffusion coeff
               1                   0                   2
'  Density factors / Extra print opt / Mass scattering restriction
               0               1                         0
'  Restrictive order / correlate PW and MG flux / Not used
               64                      0          0
'   Upscatter converg / Point converge / Source normalization
3**       1.00000E-04       1.00000E-05            1.00000E+00
```

```
'  Material Buckling (1/cm) / LMG range cutoff / UMG range cutoff
              0.00000E+00        1.00000E+00        2.00000E+04
'  Thinning tolerance / Frac Lethargy gain allowance / Not used
         1.00000E-03                  1.00000E-01     0.0+00  T
' Mixture numbers
13$$ 1
'    Isotope identifiers
14$$ 92238
'    Isotope concentrations (atoms/barn -cm)
15** 1.0000  T
'    Source number by interval
30$$                      1
'   Volumetric source by interval and group
31**
9.60817162E+00
3.17979593E+01
6.59123252E+01
8.56636328E+01
2.43855982E+02
3.77567052E+03
1.28597182E+04
4.60351593E+04
1.38805606E+05
8.15300416E+04
3.79836723E+05
2.48427549E+05
7.00361135E+04
3.27183503E+05
2.70261891E+05
8.33884439E+04
3.74944768E+04
3.36258630E+04
5.85884438E+04
4.43603989E+04
9.01939217E+04
8.26073314E+04
8.36331980E+04
1.86862972E+04
2.33946264E+04
1.30216633E+04
3.85419406E+04
6.56569747E+04
6.63587719E+04
8.37785121E+03
6.47534398E+04
2.47279973E+04
2.09256714E+04
4.53887848E+04
2.61351971E+04
2.61944753E+04
1.72324738E+04
1.70284606E+04
5.77192278E+04
4.66022640E+04
4.99461055E+04
3.18813210E+04
```

1.26057183E+04
1.50973866E+04
7.29640582E+03
1.39403173E+03
3.16257286E+03
8.79634792E+02
5.44082929E+03
3.09154071E+03
7.39829777E+02
1.78832320E+03
4.78581570E+03
1.37584123E+03
1.92836547E+03
8.18316897E+02
6.21239675E+02
2.30800307E+02
2.85248739E+02
2.47910671E+02
1.66350391E+01
7.22464162E+01
3.73318571E+01
2.40880149E+01
7.17972519E+00
3.01104369E+01
1.72285861E+01
3.28882021E+00
2.14460394E+01
1.09147995E+01
1.28414744E+01
5.69800237E-01
4.99268036E+00
8.50801791E+00
5.78975626E-01
1.22854750E+00
7.58383952E-01
6.08854788E-02
3.57555982E-01
1.50727273E-01
1.33636800E+00
5.55129899E-02
7.29341847E-02
1.24595534E-01
1.37520215E-01
1.64285979E-01
1.25052132E-01
3.03432451E-02
5.95509100E-02
5.80038225E-02
6.33520693E-02
3.43022322E-02
5.35190864E-02
2.61154789E-02
7.07635424E-02
1.71328389E-02
1.69037426E-02
1.66714974E-02

1.05932305E-02
1.51276633E-02
2.06023547E-02
1.35097265E-02
1.77278940E-02
1.52402758E-02
1.49822591E-02
5.28742327E-03
1.15134061E-02
1.03232229E-02
1.52244183E-02
8.98228896E-03
8.37672169E-03
4.87860058E-03
1.44154236E-02
4.73073359E-03
1.16612495E-02
2.25959045E-02
2.15908251E-02
2.05365695E-02
1.17925057E-02
7.63261220E-03
7.44410831E-03
3.64984888E-03
1.06528502E-02
6.84752080E-03
5.98340417E-03
4.53136990E-03
4.11089618E-03
5.23049636E-03
5.93595252E-03
2.30651781E-03
8.28927848E-03
4.68833258E-03
4.94308066E-03
4.42159243E-03
6.72609125E-04
1.10504696E-03
1.08476815E-03
1.06410289E-03
1.04302821E-03
2.41462206E-03
1.53760807E-03
9.30521181E-04
2.64379700E-03
8.94803183E-04
7.37182167E-04
1.07578364E-03
2.96845515E-04
1.46573523E-04
8.74074895E-05
2.88040554E-04
2.83093703E-04
2.78056296E-04
2.72842238E-04
2.67637866E-04

2.36266798E-04
2.06301869E-04
2.27834294E-04
2.23216548E-04
2.90342781E-04
1.41968410E-04
1.85896124E-04
2.04400187E-04
1.99289297E-04
1.93998326E-04
1.88561965E-04
1.02369949E-04
1.00619824E-04
9.88582973E-05
9.70245353E-05
9.51573073E-05
4.69024254E-05
4.63891110E-05
4.59451129E-05
4.54225447E-05
1.80570699E-05
1.79600451E-05
1.78629090E-05
1.78011816E-05
1.77388567E-05
1.76407264E-05
1.75424699E-05
1.74789609E-05
1.74148298E-05
1.73155201E-05
1.72160676E-05
1.71506875E-05
1.70676326E-05
1.70011138E-05
1.68833560E-05
4.18810395E-05
4.13474874E-05
4.08069592E-05
4.02591739E-05
7.88444405E-05
7.65582839E-05
7.42017016E-05
7.17677517E-05
6.92482701E-05
3.36499964E-05
3.29835503E-05
6.39118808E-05
6.10689577E-05
5.80869496E-05
5.49431732E-05
2.62342689E-05
2.53737371E-05
2.44829653E-05
2.35585205E-05
2.25962658E-05
2.15911402E-05

```
2.05368407E-05
1.94253475E-05
1.82461874E-05
1.69852318E-05
1.56226084E-05
1.41287680E-05
5.19545583E-06
4.91426775E-06
4.61596116E-06
4.29696175E-06
3.95224224E-06
3.57432714E-06
3.15119418E-06
1.31712363E-06
3.39885712E-06
3.93899278E-07
3.32630523E-07
1.13030151E-07
9.96495113E-08
4.41874128E-08
3.99621932E-08
3.52314226E-08
1.85727491E-08
1.11786295E-08
1.24561889E-08
1.05187008E-08
1.14415023E-08
1.08834188E-09
t
'   Zone number by interval
36$$ 1
'   Mixture number by zone
39$$ 1
'   Temperature by zone
41**          9.00000E+02
t
end
```

SFR Fuel Cell

```
=shell
del  C:\scale6\tmpdir\ft88f001
copy C:\scale6\data\xn238v7 ft88f001
end

=ajax
0$$ 11 0
1$$ 1 T
'   Input library  / Number of isotopes to copy
2$$          88                        23   T
'   Isotope ZAID
3$$ 92235  92238  40090  40091  40092  40094
    40096  26054  26056  26057  26058  24050
    24052  24053  24054  42092  42094  42095
    42096  42097  42098  42100  11023    T
end

=bonami
'   Input library  / Scratch / Scratch / Output library
0$$           11        0        18              1
'   Geometry flag /  Number of zones / Mix Table length / XS edit flag /
1$$           0               1               23             1
' Bondarenko edit flag / Dancoff factor
                  1             0    T
' Mixture numbers by isotope
3$$  1 1 1 1 1 1 1 1 1 1
     1 1 1 1 1 1 1 1 1 1
     1 1 1
'   Nuclide IDs
4$$ 92235  92238  40090  40091  40092  40094
    40096  26054  26056  26057  26058  24050
    24052  24053  24054  42092  42094  42095
    42096  42097  42098  42100  11023
'   Nuclide concentrations (atom/b-cm)
5** 1.8858619E-03  1.0551567E-02  1.8518384E-03
    4.0384114E-04  6.1727947E-04  6.2555785E-04
    1.0078032E-04  7.5240415E-04  1.1811136E-02
    2.7277064E-04  3.6300765E-05  8.2857689E-05
    1.5978281E-03  1.8118088E-04  4.5099755E-05
    1.2782226E-05  7.9673577E-06  1.3712469E-05
    1.4367084E-05  8.2257585E-06  2.0784037E-05
    8.2946654E-06  8.4013761E-03
'   Mixtures by zone
6$$               1
'   Temperatures by zone
8**          9.00000E+02
'    New Identifier in Mixing tables
10$$ 92235  92238  40090  40091  40092  40094
     40096  26054  26056  26057  26058  24050
     24052  24053  24054  42092  42094  42095
     42096  42097  42098  42100  11023
'  Zone types (0 - fuel, 1 - mod, 2 - clad)
11$$ 0 t
end
```

```
=worker
'   Input master lib  / Input working lib  / Output lib
0$$              1                  0           4
'   Scratch / Scratch / Output Temp-Interpolated lib
        18       19                          0
'   Num nuclides to read from master lib / Num to read from working lib
1$$                             23                          0
' Output print option / Flag to copy master / Flag to copy working
                -2                 -1                 -1
' Sequence # of master / Sequence # of working / Sequence # of output
                  1                  1                  1  T
'   IDs from master to copy
2$$  92235  92238  40090  40091  40092  40094
     40096  26054  26056  26057  26058  24050
     24052  24053  24054  42092  42094  42095
     42096  42097  42098  42100  11023
'   Thermal scat. kernel temps
6**  9.00000E+02 9.00000E+02 9.00000E+02 9.00000E+02 9.00000E+02
     9.00000E+02 9.00000E+02 9.00000E+02 9.00000E+02 9.00000E+02
     9.00000E+02 9.00000E+02 9.00000E+02 9.00000E+02 9.00000E+02
     9.00000E+02 9.00000E+02 9.00000E+02 9.00000E+02 9.00000E+02
     9.00000E+02 9.00000E+02 9.00000E+02     T
end

=crawdad
'   Output CENTRM lib / Scratch / Scratch / CE-KENO lib
0$$              81        17        18           77
'   Number of PW nuclides / CENTRM Identifier header / Print flag
1$$                 23                  66666           1
' Lib format 0/1= old/new / Temp interp method / Thermal lib out flag
                    0                  0                  1
' Extra unused integer flags
e  T
' Data Blocks 2 and 3 repeated for each nuclide
'   ZAID for PW mat / ENDF version / ENDF mod / Number of temps for iso
2$$          92235             7        -1                          1
'   MTs to be included / Mod number of therm data / Data source
                  0                       -1            0
'   Lower PW energy limit (eV) / Upper PW energy limit (eV)
3**               1.00000E-04                  1.000E+07   T
'   Nuclide temps to process
4**               9.00000E+02        T
'   ZAID for PW mat / ENDF version / ENDF mod / Number of temps for iso
2$$          92238             7        -1                          1
'   MTs to be included / Mod number of therm data / Data source
                  0                       -1            0
'   Lower PW energy limit (eV) / Upper PW energy limit (eV)
3**               1.00000E-04                  2.000E+07   T
'   Nuclide temps to process
4**               9.00000E+02        T
'   ZAID for PW mat / ENDF version / ENDF mod / Number of temps for iso
2$$          40090             7        -1                          1
'   MTs to be included / Mod number of therm data / Data source
                  0                       -1            0
'   Lower PW energy limit (eV) / Upper PW energy limit (eV)
```

```
3**             1.00000E-04                 2.000E+07   T
'   Nuclide temps to process
4**             9.00000E+02       T
'   ZAID for PW mat / ENDF version / ENDF mod / Number of temps for iso
2$$         40091           7       -1                  1
'   MTs to be included / Mod number of therm data / Data source
                0                   -1          0
'   Lower PW energy limit (eV) / Upper PW energy limit (eV)
3**             1.00000E-04                 2.000E+07   T
'   Nuclide temps to process
4**             9.00000E+02       T
'   ZAID for PW mat / ENDF version / ENDF mod / Number of temps for iso
2$$         40092           7       -1                  1
'   MTs to be included / Mod number of therm data / Data source
                0                   -1          0
'   Lower PW energy limit (eV) / Upper PW energy limit (eV)
3**             1.00000E-04                 2.000E+07   T
'   Nuclide temps to process
4**             9.00000E+02       T
'   ZAID for PW mat / ENDF version / ENDF mod / Number of temps for iso
2$$         40094           7       -1                  1
'   MTs to be included / Mod number of therm data / Data source
                0                   -1          0
'   Lower PW energy limit (eV) / Upper PW energy limit (eV)
3**             1.00000E-04                 2.000E+07   T
'   Nuclide temps to process
4**             9.00000E+02       T
'   ZAID for PW mat / ENDF version / ENDF mod / Number of temps for iso
2$$         40096           7       -1                  1
'   MTs to be included / Mod number of therm data / Data source
                0                   -1          0
'   Lower PW energy limit (eV) / Upper PW energy limit (eV)
3**             1.00000E-04                 2.000E+07   T
'   Nuclide temps to process
4**             9.00000E+02       T
'   ZAID for PW mat / ENDF version / ENDF mod / Number of temps for iso
2$$         26054           7       -1                  1
'   MTs to be included / Mod number of therm data / Data source
                0                   -1          0
'   Lower PW energy limit (eV) / Upper PW energy limit (eV)
3**             1.00000E-04                 2.000E+07   T
'   Nuclide temps to process
4**             9.00000E+02       T
'   ZAID for PW mat / ENDF version / ENDF mod / Number of temps for iso
2$$         26056           7       -1                  1
'   MTs to be included / Mod number of therm data / Data source
                0                   -1          0
'   Lower PW energy limit (eV) / Upper PW energy limit (eV)
3**             1.00000E-04                 2.000E+07   T
'   Nuclide temps to process
4**             9.00000E+02       T
'   ZAID for PW mat / ENDF version / ENDF mod / Number of temps for iso
2$$         26057           7       -1                  1
'   MTs to be included / Mod number of therm data / Data source
                0                   -1          0
'   Lower PW energy limit (eV) / Upper PW energy limit (eV)
```

```
3**             1.00000E-04                 2.000E+07   T
'   Nuclide temps to process
4**             9.00000E+02       T
'   ZAID for PW mat / ENDF version / ENDF mod / Number of temps for iso
2$$         26058           7       -1                  1
'   MTs to be included / Mod number of therm data / Data source
                0                   -1          0
'   Lower PW energy limit (eV) / Upper PW energy limit (eV)
3**             1.00000E-04                 2.000E+07   T
'   Nuclide temps to process
4**             9.00000E+02       T
'   ZAID for PW mat / ENDF version / ENDF mod / Number of temps for iso
2$$         24050           7       -1                  1
'   MTs to be included / Mod number of therm data / Data source
                0                   -1          0
'   Lower PW energy limit (eV) / Upper PW energy limit (eV)
3**             1.00000E-04                 2.000E+07   T
'   Nuclide temps to process
4**             9.00000E+02       T
'   ZAID for PW mat / ENDF version / ENDF mod / Number of temps for iso
2$$         24052           7       -1                  1
'   MTs to be included / Mod number of therm data / Data source
                0                   -1          0
'   Lower PW energy limit (eV) / Upper PW energy limit (eV)
3**             1.00000E-04                 2.000E+07   T
'   Nuclide temps to process
4**             9.00000E+02       T
'   ZAID for PW mat / ENDF version / ENDF mod / Number of temps for iso
2$$         24053           7       -1                  1
'   MTs to be included / Mod number of therm data / Data source
                0                   -1          0
'   Lower PW energy limit (eV) / Upper PW energy limit (eV)
3**             1.00000E-04                 2.000E+07   T
'   Nuclide temps to process
4**             9.00000E+02       T
'   ZAID for PW mat / ENDF version / ENDF mod / Number of temps for iso
2$$         24054           7       -1                  1
'   MTs to be included / Mod number of therm data / Data source
                0                   -1          0
'   Lower PW energy limit (eV) / Upper PW energy limit (eV)
3**             1.00000E-04                 2.000E+07   T
'   Nuclide temps to process
4**             9.00000E+02       T
'   ZAID for PW mat / ENDF version / ENDF mod / Number of temps for iso
2$$         42092           7       -1                  1
'   MTs to be included / Mod number of therm data / Data source
                0                   -1          0
'   Lower PW energy limit (eV) / Upper PW energy limit (eV)
3**             1.00000E-04                 2.000E+07   T
'   Nuclide temps to process
4**             9.00000E+02       T
'   ZAID for PW mat / ENDF version / ENDF mod / Number of temps for iso
2$$         42094           7       -1                  1
'   MTs to be included / Mod number of therm data / Data source
                0                   -1          0
'   Lower PW energy limit (eV) / Upper PW energy limit (eV)
```

```
3**              1.00000E-04                 2.000E+07   T
'   Nuclide temps to process
4**             9.00000E+02       T
'   ZAID for PW mat / ENDF version / ENDF mod / Number of temps for iso
2$$         42095            7        -1                  1
'   MTs to be included / Mod number of therm data / Data source
                 0                   -1           0
'   Lower PW energy limit (eV) / Upper PW energy limit (eV)
3**              1.00000E-04                 2.000E+07   T
'   Nuclide temps to process
4**             9.00000E+02       T
'   ZAID for PW mat / ENDF version / ENDF mod / Number of temps for iso
2$$         42096            7        -1                  1
'   MTs to be included / Mod number of therm data / Data source
                 0                   -1           0
'   Lower PW energy limit (eV) / Upper PW energy limit (eV)
3**              1.00000E-04                 2.000E+07   T
'   Nuclide temps to process
4**             9.00000E+02       T
'   ZAID for PW mat / ENDF version / ENDF mod / Number of temps for iso
2$$         42097            7        -1                  1
'   MTs to be included / Mod number of therm data / Data source
                 0                   -1           0
'   Lower PW energy limit (eV) / Upper PW energy limit (eV)
3**              1.00000E-04                 2.000E+07   T
'   Nuclide temps to process
4**             9.00000E+02       T
'   ZAID for PW mat / ENDF version / ENDF mod / Number of temps for iso
2$$         42098            7        -1                  1
'   MTs to be included / Mod number of therm data / Data source
                 0                   -1           0
'   Lower PW energy limit (eV) / Upper PW energy limit (eV)
3**              1.00000E-04                 2.000E+07   T
'   Nuclide temps to process
4**             9.00000E+02       T
'   ZAID for PW mat / ENDF version / ENDF mod / Number of temps for iso
2$$         42100            7        -1                  1
'   MTs to be included / Mod number of therm data / Data source
                 0                   -1           0
'   Lower PW energy limit (eV) / Upper PW energy limit (eV)
3**              1.00000E-04                 2.000E+07   T
'   Nuclide temps to process
4**             9.00000E+02       T
'   ZAID for PW mat / ENDF version / ENDF mod / Number of temps for iso
2$$         11023            7        -1                  1
'   MTs to be included / Mod number of therm data / Data source
                 0                   -1           0
'   Lower PW energy limit (eV) / Upper PW energy limit (eV)
3**              1.00000E-04                 2.000E+07   T
'   Nuclide temps to process
4**             9.00000E+02       T
end

=centrm
CENTRM: Homogenized SFR Cell
'   Punch logical / Thermal kernel / MG working lib / PW lib
```

```
0$$            7              0              4      81
' MG flux restart / MG output / PW output / MG Angular output
               0         25         15               16
' Scratch for thermal matrices / Optional PW xs print / Scratch
                        17                 18       19
' Not used / Scratch
       8        9
'   Geometry / Num Zones / Num Intervals / Left BC / Right BC
1$$       0         1             1        0         0
' Num Mixtures / Mix Table Length / Sn order / Max Pn Order
           1              23         0            64
' Source type / Inner iter max / Upscatter outer iter max
           0             20                   100
' UMG range calc type / LMG range calc type / PW range calc type
                2                  2                  3
' MG source and XS linearization / Pn order for PW calc
                        3                  64
' PW Inelastic scat option
                     1
'   Mix XS print opt / Flux print opt / Balance Table print
2$$              0              3                  1
'  Vol source flag / Boundary source flag / Group diffusion coeff
              1                  0                  2
'  Density factors / Extra print opt / Mass scattering restriction
              0              1                      0
'  Restrictive order / correlate PW and MG flux / Not used
               64                    0         0
'   Upscatter converg / Point converge / Source normalization
3**       1.00000E-04      1.00000E-05           1.00000E+00
'  Material Buckling (1/cm) / LMG range cutoff / UMG range cutoff
             0.00000E+00        1.00000E+00        5.00000E+06
'  Thinning tolerance / Frac Lethargy gain allowance / Not used
         1.00000E-03                  1.00000E-01     0.0+00  T
' Mixture numbers
13$$ 1 1 1 1 1 1 1 1 1 1
    1 1 1 1 1 1 1 1 1 1
    1 1 1
'   Isotope identifiers
14$$ 92235  92238  40090  40091  40092  40094
    40096  26054  26056  26057  26058  24050
    24052  24053  24054  42092  42094  42095
    42096  42097  42098  42100  11023
'   Isotope concentrations (atoms/barn -cm)
15** 1.8858619E-03  1.0551567E-02  1.8518384E-03
    4.0384114E-04  6.1727947E-04  6.2555785E-04
    1.0078032E-04  7.5240415E-04  1.1811136E-02
    2.7277064E-04  3.6300765E-05  8.2857689E-05
    1.5978281E-03  1.8118088E-04  4.5099755E-05
    1.2782226E-05  7.9673577E-06  1.3712469E-05
    1.4367084E-05  8.2257585E-06  2.0784037E-05
    8.2946654E-06  8.4013761E-03  T
'   Source number by interval
30$$                     1
'   Volumetric source by interval and group
31**
9.60817162E+00
```

3.17979593E+01
6.59123252E+01
8.56636328E+01
2.43855982E+02
3.77567052E+03
1.28597182E+04
4.60351593E+04
1.38805606E+05
8.15300416E+04
3.79836723E+05
2.48427549E+05
7.00361135E+04
3.27183503E+05
2.70261891E+05
8.33884439E+04
3.74944768E+04
3.36258630E+04
5.85884438E+04
4.43603989E+04
9.01939217E+04
8.26073314E+04
8.36331980E+04
1.86862972E+04
2.33946264E+04
1.30216633E+04
3.85419406E+04
6.56569747E+04
6.63587719E+04
8.37785121E+03
6.47534398E+04
2.47279973E+04
2.09256714E+04
4.53887848E+04
2.61351971E+04
2.61944753E+04
1.72324738E+04
1.70284606E+04
5.77192278E+04
4.66022640E+04
4.99461055E+04
3.18813210E+04
1.26057183E+04
1.50973866E+04
7.29640582E+03
1.39403173E+03
3.16257286E+03
8.79634792E+02
5.44082929E+03
3.09154071E+03
7.39829777E+02
1.78832320E+03
4.78581570E+03
1.37584123E+03
1.92836547E+03
8.18316897E+02
6.21239675E+02

2.30800307E+02
2.85248739E+02
2.47910671E+02
1.66350391E+01
7.22464162E+01
3.73318571E+01
2.40880149E+01
7.17972519E+00
3.01104369E+01
1.72285861E+01
3.28882021E+00
2.14460394E+01
1.09147995E+01
1.28414744E+01
5.69800237E-01
4.99268036E+00
8.50801791E+00
5.78975626E-01
1.22854750E+00
7.58383952E-01
6.08854788E-02
3.57555982E-01
1.50727273E-01
1.33636800E+00
5.55129899E-02
7.29341847E-02
1.24595534E-01
1.37520215E-01
1.64285979E-01
1.25052132E-01
3.03432451E-02
5.95509100E-02
5.80038225E-02
6.33520693E-02
3.43022322E-02
5.35190864E-02
2.61154789E-02
7.07635424E-02
1.71328389E-02
1.69037426E-02
1.66714974E-02
1.05932305E-02
1.51276633E-02
2.06023547E-02
1.35097265E-02
1.77278940E-02
1.52402758E-02
1.49822591E-02
5.28742327E-03
1.15134061E-02
1.03232229E-02
1.52244183E-02
8.98228896E-03
8.37672169E-03
4.87860058E-03
1.44154236E-02

4.73073359E-03
1.16612495E-02
2.25959045E-02
2.15908251E-02
2.05365695E-02
1.17925057E-02
7.63261220E-03
7.44410831E-03
3.64984888E-03
1.06528502E-02
6.84752080E-03
5.98340417E-03
4.53136990E-03
4.11089618E-03
5.23049636E-03
5.93595252E-03
2.30651781E-03
8.28927848E-03
4.68833258E-03
4.94308066E-03
4.42159243E-03
6.72609125E-04
1.10504696E-03
1.08476815E-03
1.06410289E-03
1.04302821E-03
2.41462206E-03
1.53760807E-03
9.30521181E-04
2.64379700E-03
8.94803183E-04
7.37182167E-04
1.07578364E-03
2.96845515E-04
1.46573523E-04
8.74074895E-05
2.88040554E-04
2.83093703E-04
2.78056296E-04
2.72842238E-04
2.67637866E-04
2.36266798E-04
2.06301869E-04
2.27834294E-04
2.23216548E-04
2.90342781E-04
1.41968410E-04
1.85896124E-04
2.04400187E-04
1.99289297E-04
1.93998326E-04
1.88561965E-04
1.02369949E-04
1.00619824E-04
9.88582973E-05
9.70245353E-05

9.51573073E-05
4.69024254E-05
4.63891110E-05
4.59451129E-05
4.54225447E-05
1.80570699E-05
1.79600451E-05
1.78629090E-05
1.78011816E-05
1.77388567E-05
1.76407264E-05
1.75424699E-05
1.74789609E-05
1.74148298E-05
1.73155201E-05
1.72160676E-05
1.71506875E-05
1.70676326E-05
1.70011138E-05
1.68833560E-05
4.18810395E-05
4.13474874E-05
4.08069592E-05
4.02591739E-05
7.88444405E-05
7.65582839E-05
7.42017016E-05
7.17677517E-05
6.92482701E-05
3.36499964E-05
3.29835503E-05
6.39118808E-05
6.10689577E-05
5.80869496E-05
5.49431732E-05
2.62342689E-05
2.53737371E-05
2.44829653E-05
2.35585205E-05
2.25962658E-05
2.15911402E-05
2.05368407E-05
1.94253475E-05
1.82461874E-05
1.69852318E-05
1.56226084E-05
1.41287680E-05
5.19545583E-06
4.91426775E-06
4.61596116E-06
4.29696175E-06
3.95224224E-06
3.57432714E-06
3.15119418E-06
1.31712363E-06
3.39885712E-06

```
3.93899278E-07
3.32630523E-07
1.13030151E-07
9.96495113E-08
4.41874128E-08
3.99621932E-08
3.52314226E-08
1.85727491E-08
1.11786295E-08
1.24561889E-08
1.05187008E-08
1.14415023E-08
1.08834188E-09
t
'   Zone number by interval
36$$ 1
'   Mixture number by zone
39$$ 1
'   Temperature by zone
41**          9.00000E+02
t
end
```

UNF Fuel Cell

```
=shell
del  C:\scale6\tmpdir\ft88f001
copy C:\scale6\data\xn238v7 ft88f001
end

=ajax
0$$ 11 0
1$$ 1 T
'   Input library  / Number of isotopes to copy
2$$          88                        33   T
'   Isotope ZAID
3$$ 92235  92238  95241  95243  96244  96245
    93237  94238  94239  94240  94241  94242
    40090  40091  40092  40094  40096  26054
    26056  26057  26058  24050  24052  24053
    24054  42092  42094  42095  42096  42097
    42098  42100  11023  T
end

=bonami
'   Input library  / Scratch / Scratch / Output library
0$$          11        0        18              1
'   Geometry flag /  Number of zones / Mix Table length / XS edit flag /
1$$           0              1              33            1
' Bondarenko edit flag / Dancoff factor
                 1            0    T
' Mixture numbers by isotope
3$$  1 1 1 1 1 1 1 1 1 1
     1 1 1 1 1 1 1 1 1 1
     1 1 1 1 1 1 1 1 1 1
     1 1 1
'   Nuclide IDs
4$$ 92235  92238  95241  95243  96244  96245
    93237  94238  94239  94240  94241  94242
    40090  40091  40092  40094  40096  26054
    26056  26057  26058  24050  24052  24053
    24054  42092  42094  42095  42096  42097
    42098  42100  11023
'   Nuclide concentrations (atom/b-cm)
5** 1.9614993E-05 9.6642491E-03 1.3566604E-04
    3.4663778E-05 8.2528486E-06 4.6175738E-07
    1.5733084E-04 5.5200518E-05 1.3077054E-03
    6.5959724E-04 2.3354193E-04 1.5570373E-04
    1.8573215E-03 4.0503688E-04 6.1910718E-04
    6.2741007E-04 1.0107872E-04 7.5240415E-04
    1.1811136E-02 2.7277064E-04 3.6300765E-05
    8.2857689E-05 1.5978281E-03 1.8118088E-04
    4.5099755E-05 1.2782226E-05 7.9673577E-06
    1.3712469E-05 1.4367084E-05 8.2257585E-06
    2.0784037E-05 8.2946654E-06 8.4013761E-03
'   Mixtures by zone
6$$              1
'   Temperatures by zone
8**          9.00000E+02
```

```
'    New Identifier in Mixing tables
10$$ 92235  92238  95241  95243  96244  96245
     93237  94238  94239  94240  94241  94242
     40090  40091  40092  40094  40096  26054
     26056  26057  26058  24050  24052  24053
     24054  42092  42094  42095  42096  42097
     42098  42100  11023
'  Zone types (0 - fuel, 1 - mod, 2 - clad)
11$$ 0 t
end

=worker
'   Input master lib  / Input working lib  / Output lib
0$$              1                  0           4
'   Scratch / Scratch / Output Temp-Interpolated lib
        18       19                          0
'   Num nuclides to read from master lib / Num to read from working lib
1$$                              33                          0
' Output print option / Flag to copy master / Flag to copy working
                -2                 -1                  -1
' Sequence # of master / Sequence # of working / Sequence # of output
                  1                   1                   1  T
'   IDs from master to copy
2$$ 92235  92238  95241  95243  96244  96245
    93237  94238  94239  94240  94241  94242
    40090  40091  40092  40094  40096  26054
    26056  26057  26058  24050  24052  24053
    24054  42092  42094  42095  42096  42097
    42098  42100  11023
'   Thermal scat. kernel temps
6**  9.00000E+02 9.00000E+02 9.00000E+02 9.00000E+02 9.00000E+02
     9.00000E+02 9.00000E+02 9.00000E+02 9.00000E+02 9.00000E+02
     9.00000E+02 9.00000E+02 9.00000E+02 9.00000E+02 9.00000E+02
     9.00000E+02 9.00000E+02 9.00000E+02 9.00000E+02 9.00000E+02
     9.00000E+02 9.00000E+02 9.00000E+02 9.00000E+02 9.00000E+02
     9.00000E+02 9.00000E+02 9.00000E+02 9.00000E+02 9.00000E+02
     9.00000E+02 9.00000E+02 9.00000E+02     T
end

=crawdad
'   Output CENTRM lib / Scratch / Scratch / CE-KENO lib
0$$              81        17        18           77
'   Number of PW nuclides / CENTRM Identifier header / Print flag
1$$                  33                   66666           1
' Lib format 0/1= old/new / Temp interp method / Thermal lib out flag
                     0                  0                   1
' Extra unused integer flags
e  T
' Data Blocks 2 and 3 repeated for each nuclide
'   ZAID for PW mat / ENDF version / ENDF mod / Number of temps for iso
2$$          92235             7        -1                    1
'   MTs to be included / Mod number of therm data / Data source
                  0                    -1           0
'   Lower PW energy limit (eV) / Upper PW energy limit (eV)
3**              1.00000E-04                  1.000E+07   T
'   Nuclide temps to process
```

```
4**            9.00000E+02       T
'   ZAID for PW mat / ENDF version / ENDF mod / Number of temps for iso
2$$          92238            7        -1                    1
'   MTs to be included / Mod number of therm data / Data source
                 0                    -1           0
'   Lower PW energy limit (eV) / Upper PW energy limit (eV)
3**             1.00000E-04                1.000E+07   T
'   Nuclide temps to process
4**            9.00000E+02       T
'   ZAID for PW mat / ENDF version / ENDF mod / Number of temps for iso
2$$          95241            7        -1                    1
'   MTs to be included / Mod number of therm data / Data source
                 0                    -1           0
'   Lower PW energy limit (eV) / Upper PW energy limit (eV)
3**             1.00000E-04                1.000E+07   T
'   Nuclide temps to process
4**            9.00000E+02       T
'   ZAID for PW mat / ENDF version / ENDF mod / Number of temps for iso
2$$          95243            7        -1                    1
'   MTs to be included / Mod number of therm data / Data source
                 0                    -1           0
'   Lower PW energy limit (eV) / Upper PW energy limit (eV)
3**             1.00000E-04                1.000E+07   T
'   Nuclide temps to process
4**            9.00000E+02       T
'   ZAID for PW mat / ENDF version / ENDF mod / Number of temps for iso
2$$          96244            7        -1                    1
'   MTs to be included / Mod number of therm data / Data source
                 0                    -1           0
'   Lower PW energy limit (eV) / Upper PW energy limit (eV)
3**             1.00000E-04                1.000E+07   T
'   Nuclide temps to process
4**            9.00000E+02       T
'   ZAID for PW mat / ENDF version / ENDF mod / Number of temps for iso
2$$          96245            7        -1                    1
'   MTs to be included / Mod number of therm data / Data source
                 0                    -1           0
'   Lower PW energy limit (eV) / Upper PW energy limit (eV)
3**             1.00000E-04                1.000E+07   T
'   Nuclide temps to process
4**            9.00000E+02       T
'   ZAID for PW mat / ENDF version / ENDF mod / Number of temps for iso
2$$          93237            7        -1                    1
'   MTs to be included / Mod number of therm data / Data source
                 0                    -1           0
'   Lower PW energy limit (eV) / Upper PW energy limit (eV)
3**             1.00000E-04                1.000E+07   T
'   Nuclide temps to process
4**            9.00000E+02       T
'   ZAID for PW mat / ENDF version / ENDF mod / Number of temps for iso
2$$          94238            7        -1                    1
'   MTs to be included / Mod number of therm data / Data source
                 0                    -1           0
'   Lower PW energy limit (eV) / Upper PW energy limit (eV)
3**             1.00000E-04                1.000E+07   T
'   Nuclide temps to process
```

```
4**             9.00000E+02       T
'   ZAID for PW mat / ENDF version / ENDF mod / Number of temps for iso
2$$          94239            7        -1                    1
'   MTs to be included / Mod number of therm data / Data source
                  0                    -1           0
'   Lower PW energy limit (eV) / Upper PW energy limit (eV)
3**              1.00000E-04                 1.000E+07   T
'   Nuclide temps to process
4**             9.00000E+02       T
'   ZAID for PW mat / ENDF version / ENDF mod / Number of temps for iso
2$$          94240            7        -1                    1
'   MTs to be included / Mod number of therm data / Data source
                  0                    -1           0
'   Lower PW energy limit (eV) / Upper PW energy limit (eV)
3**              1.00000E-04                 1.000E+07   T
'   Nuclide temps to process
4**             9.00000E+02       T
'   ZAID for PW mat / ENDF version / ENDF mod / Number of temps for iso
2$$          94241            7        -1                    1
'   MTs to be included / Mod number of therm data / Data source
                  0                    -1           0
'   Lower PW energy limit (eV) / Upper PW energy limit (eV)
3**              1.00000E-04                 1.000E+07   T
'   Nuclide temps to process
4**             9.00000E+02       T
'   ZAID for PW mat / ENDF version / ENDF mod / Number of temps for iso
2$$          94242            7        -1                    1
'   MTs to be included / Mod number of therm data / Data source
                  0                    -1           0
'   Lower PW energy limit (eV) / Upper PW energy limit (eV)
3**              1.00000E-04                 1.000E+07   T
'   Nuclide temps to process
4**             9.00000E+02       T
'   ZAID for PW mat / ENDF version / ENDF mod / Number of temps for iso
2$$          40090            7        -1                    1
'   MTs to be included / Mod number of therm data / Data source
                  0                    -1           0
'   Lower PW energy limit (eV) / Upper PW energy limit (eV)
3**              1.00000E-04                 1.000E+07   T
'   Nuclide temps to process
4**             9.00000E+02       T
'   ZAID for PW mat / ENDF version / ENDF mod / Number of temps for iso
2$$          40091            7        -1                    1
'   MTs to be included / Mod number of therm data / Data source
                  0                    -1           0
'   Lower PW energy limit (eV) / Upper PW energy limit (eV)
3**              1.00000E-04                 1.000E+07   T
'   Nuclide temps to process
4**             9.00000E+02       T
'   ZAID for PW mat / ENDF version / ENDF mod / Number of temps for iso
2$$          40092            7        -1                    1
'   MTs to be included / Mod number of therm data / Data source
                  0                    -1           0
'   Lower PW energy limit (eV) / Upper PW energy limit (eV)
3**              1.00000E-04                 1.000E+07   T
'   Nuclide temps to process
```

```
4**            9.00000E+02       T
'   ZAID for PW mat / ENDF version / ENDF mod / Number of temps for iso
2$$          40094            7        -1                    1
'   MTs to be included / Mod number of therm data / Data source
                 0                    -1           0
'   Lower PW energy limit (eV) / Upper PW energy limit (eV)
3**             1.00000E-04                1.000E+07   T
'   Nuclide temps to process
4**            9.00000E+02       T
'   ZAID for PW mat / ENDF version / ENDF mod / Number of temps for iso
2$$          40096            7        -1                    1
'   MTs to be included / Mod number of therm data / Data source
                 0                    -1           0
'   Lower PW energy limit (eV) / Upper PW energy limit (eV)
3**             1.00000E-04                1.000E+07   T
'   Nuclide temps to process
4**            9.00000E+02       T
'   ZAID for PW mat / ENDF version / ENDF mod / Number of temps for iso
2$$          26054            7        -1                    1
'   MTs to be included / Mod number of therm data / Data source
                 0                    -1           0
'   Lower PW energy limit (eV) / Upper PW energy limit (eV)
3**             1.00000E-04                1.000E+07   T
'   Nuclide temps to process
4**            9.00000E+02       T
'   ZAID for PW mat / ENDF version / ENDF mod / Number of temps for iso
2$$          26056            7        -1                    1
'   MTs to be included / Mod number of therm data / Data source
                 0                    -1           0
'   Lower PW energy limit (eV) / Upper PW energy limit (eV)
3**             1.00000E-04                1.000E+07   T
'   Nuclide temps to process
4**            9.00000E+02       T
'   ZAID for PW mat / ENDF version / ENDF mod / Number of temps for iso
2$$          26057            7        -1                    1
'   MTs to be included / Mod number of therm data / Data source
                 0                    -1           0
'   Lower PW energy limit (eV) / Upper PW energy limit (eV)
3**             1.00000E-04                1.000E+07   T
'   Nuclide temps to process
4**            9.00000E+02       T
'   ZAID for PW mat / ENDF version / ENDF mod / Number of temps for iso
2$$          26058            7        -1                    1
'   MTs to be included / Mod number of therm data / Data source
                 0                    -1           0
'   Lower PW energy limit (eV) / Upper PW energy limit (eV)
3**             1.00000E-04                1.000E+07   T
'   Nuclide temps to process
4**            9.00000E+02       T
'   ZAID for PW mat / ENDF version / ENDF mod / Number of temps for iso
2$$          24050            7        -1                    1
'   MTs to be included / Mod number of therm data / Data source
                 0                    -1           0
'   Lower PW energy limit (eV) / Upper PW energy limit (eV)
3**             1.00000E-04                1.000E+07   T
'   Nuclide temps to process
```

```
4**            9.00000E+02       T
'   ZAID for PW mat / ENDF version / ENDF mod / Number of temps for iso
2$$          24052            7        -1                    1
'   MTs to be included / Mod number of therm data / Data source
                 0                    -1           0
'   Lower PW energy limit (eV) / Upper PW energy limit (eV)
3**             1.00000E-04                1.000E+07   T
'   Nuclide temps to process
4**            9.00000E+02       T
'   ZAID for PW mat / ENDF version / ENDF mod / Number of temps for iso
2$$          24053            7        -1                    1
'   MTs to be included / Mod number of therm data / Data source
                 0                    -1           0
'   Lower PW energy limit (eV) / Upper PW energy limit (eV)
3**             1.00000E-04                1.000E+07   T
'   Nuclide temps to process
4**            9.00000E+02       T
'   ZAID for PW mat / ENDF version / ENDF mod / Number of temps for iso
2$$          24054            7        -1                    1
'   MTs to be included / Mod number of therm data / Data source
                 0                    -1           0
'   Lower PW energy limit (eV) / Upper PW energy limit (eV)
3**             1.00000E-04                1.000E+07   T
'   Nuclide temps to process
4**            9.00000E+02       T
'   ZAID for PW mat / ENDF version / ENDF mod / Number of temps for iso
2$$          42092            7        -1                    1
'   MTs to be included / Mod number of therm data / Data source
                 0                    -1           0
'   Lower PW energy limit (eV) / Upper PW energy limit (eV)
3**             1.00000E-04                1.000E+07   T
'   Nuclide temps to process
4**            9.00000E+02       T
'   ZAID for PW mat / ENDF version / ENDF mod / Number of temps for iso
2$$          42094            7        -1                    1
'   MTs to be included / Mod number of therm data / Data source
                 0                    -1           0
'   Lower PW energy limit (eV) / Upper PW energy limit (eV)
3**             1.00000E-04                1.000E+07   T
'   Nuclide temps to process
4**            9.00000E+02       T
'   ZAID for PW mat / ENDF version / ENDF mod / Number of temps for iso
2$$          42095            7        -1                    1
'   MTs to be included / Mod number of therm data / Data source
                 0                    -1           0
'   Lower PW energy limit (eV) / Upper PW energy limit (eV)
3**             1.00000E-04                1.000E+07   T
'   Nuclide temps to process
4**            9.00000E+02       T
'   ZAID for PW mat / ENDF version / ENDF mod / Number of temps for iso
2$$          42096            7        -1                    1
'   MTs to be included / Mod number of therm data / Data source
                 0                    -1           0
'   Lower PW energy limit (eV) / Upper PW energy limit (eV)
3**             1.00000E-04                1.000E+07   T
'   Nuclide temps to process
```

```
4**             9.00000E+02       T
'   ZAID for PW mat / ENDF version / ENDF mod / Number of temps for iso
2$$          42097             7        -1                    1
'   MTs to be included / Mod number of therm data / Data source
                 0                    -1            0
'   Lower PW energy limit (eV) / Upper PW energy limit (eV)
3**              1.00000E-04                 1.000E+07   T
'   Nuclide temps to process
4**             9.00000E+02       T
'   ZAID for PW mat / ENDF version / ENDF mod / Number of temps for iso
2$$          42098             7        -1                    1
'   MTs to be included / Mod number of therm data / Data source
                 0                    -1            0
'   Lower PW energy limit (eV) / Upper PW energy limit (eV)
3**              1.00000E-04                 1.000E+07   T
'   Nuclide temps to process
4**             9.00000E+02       T
'   ZAID for PW mat / ENDF version / ENDF mod / Number of temps for iso
2$$          42100             7        -1                    1
'   MTs to be included / Mod number of therm data / Data source
                 0                    -1            0
'   Lower PW energy limit (eV) / Upper PW energy limit (eV)
3**              1.00000E-04                 1.000E+07   T
'   Nuclide temps to process
4**             9.00000E+02       T
'   ZAID for PW mat / ENDF version / ENDF mod / Number of temps for iso
2$$          11023             7        -1                    1
'   MTs to be included / Mod number of therm data / Data source
                 0                    -1            0
'   Lower PW energy limit (eV) / Upper PW energy limit (eV)
3**              1.00000E-04                 1.000E+07   T
'   Nuclide temps to process
4**             9.00000E+02       T
end

=centrm
CENTRM: Homogenized Unf Cell
'   Punch logical / Thermal kernel / MG working lib / PW lib
0$$            7              0              4      81
' MG flux restart / MG output / PW output / MG Angular output
              0         25          15               16
' Scratch for thermal matrices / Optional PW xs print / Scratch
                        17                  18        19
' Not used / Scratch
        8        9
'   Geometry / Num Zones / Num Intervals / Left BC / Right BC
1$$       0          1              1         0         0
' Num Mixtures / Mix Table Length / Sn order / Max Pn Order
            1               33          0            64
' Source type / Inner iter max / Upscatter outer iter max
           0            20                   100
' UMG range calc type / LMG range calc type / PW range calc type
                 2                  2                  3
' MG source and XS linearization / Pn order for PW calc
                         3                  64
' PW Inelastic scat option
```

```
                    1
'   Mix XS print opt / Flux print opt / Balance Table print
2$$                 0               3                   1
'  Vol source flag / Boundary source flag / Group diffusion coeff
                    1               0                   2
'  Density factors / Extra print opt / Mass scattering restriction
                    0               1                   0
'  Restrictive order / correlate PW and MG flux / Not used
                   64                       0         0
'   Upscatter converg / Point converge / Source normalization
3**       1.00000E-04      1.00000E-05           1.00000E+00
'  Material Buckling (1/cm) / LMG range cutoff / UMG range cutoff
                0.00000E+00       1.00000E+00       1.00000E+07
'  Thinning tolerance / Frac Lethargy gain allowance / Not used
           1.00000E-03                  1.00000E-01     0.0+00  T
' Mixture numbers
13$$ 1 1 1 1 1 1 1 1 1 1
     1 1 1 1 1 1 1 1 1 1
     1 1 1 1 1 1 1 1 1 1
     1 1 1
'    Isotope identifiers
14$$ 92235  92238  95241  95243  96244  96245
     93237  94238  94239  94240  94241  94242
     40090  40091  40092  40094  40096  26054
     26056  26057  26058  24050  24052  24053
     24054  42092  42094  42095  42096  42097
     42098  42100  11023
'    Isotope concentrations (atoms/barn -cm)
15** 1.9614993E-05 9.6642491E-03 1.3566604E-04
     3.4663778E-05 8.2528486E-06 4.6175738E-07
     1.5733084E-04 5.5200518E-05 1.3077054E-03
     6.5959724E-04 2.3354193E-04 1.5570373E-04
     1.8573215E-03 4.0503688E-04 6.1910718E-04
     6.2741007E-04 1.0107872E-04 7.5240415E-04
     1.1811136E-02 2.7277064E-04 3.6300765E-05
     8.2857689E-05 1.5978281E-03 1.8118088E-04
     4.5099755E-05 1.2782226E-05 7.9673577E-06
     1.3712469E-05 1.4367084E-05 8.2257585E-06
     2.0784037E-05 8.2946654E-06 8.4013761E-03  T
'    Source number by interval
30$$                        1
'   Volumetric source by interval and group
31**
9.60817162E+00
3.17979593E+01
6.59123252E+01
8.56636328E+01
2.43855982E+02
3.77567052E+03
1.28597182E+04
4.60351593E+04
1.38805606E+05
8.15300416E+04
3.79836723E+05
2.48427549E+05
7.00361135E+04
```

3.27183503E+05
2.70261891E+05
8.33884439E+04
3.74944768E+04
3.36258630E+04
5.85884438E+04
4.43603989E+04
9.01939217E+04
8.26073314E+04
8.36331980E+04
1.86862972E+04
2.33946264E+04
1.30216633E+04
3.85419406E+04
6.56569747E+04
6.63587719E+04
8.37785121E+03
6.47534398E+04
2.47279973E+04
2.09256714E+04
4.53887848E+04
2.61351971E+04
2.61944753E+04
1.72324738E+04
1.70284606E+04
5.77192278E+04
4.66022640E+04
4.99461055E+04
3.18813210E+04
1.26057183E+04
1.50973866E+04
7.29640582E+03
1.39403173E+03
3.16257286E+03
8.79634792E+02
5.44082929E+03
3.09154071E+03
7.39829777E+02
1.78832320E+03
4.78581570E+03
1.37584123E+03
1.92836547E+03
8.18316897E+02
6.21239675E+02
2.30800307E+02
2.85248739E+02
2.47910671E+02
1.66350391E+01
7.22464162E+01
3.73318571E+01
2.40880149E+01
7.17972519E+00
3.01104369E+01
1.72285861E+01
3.28882021E+00
2.14460394E+01

1.09147995E+01
1.28414744E+01
5.69800237E-01
4.99268036E+00
8.50801791E+00
5.78975626E-01
1.22854750E+00
7.58383952E-01
6.08854788E-02
3.57555982E-01
1.50727273E-01
1.33636800E+00
5.55129899E-02
7.29341847E-02
1.24595534E-01
1.37520215E-01
1.64285979E-01
1.25052132E-01
3.03432451E-02
5.95509100E-02
5.80038225E-02
6.33520693E-02
3.43022322E-02
5.35190864E-02
2.61154789E-02
7.07635424E-02
1.71328389E-02
1.69037426E-02
1.66714974E-02
1.05932305E-02
1.51276633E-02
2.06023547E-02
1.35097265E-02
1.77278940E-02
1.52402758E-02
1.49822591E-02
5.28742327E-03
1.15134061E-02
1.03232229E-02
1.52244183E-02
8.98228896E-03
8.37672169E-03
4.87860058E-03
1.44154236E-02
4.73073359E-03
1.16612495E-02
2.25959045E-02
2.15908251E-02
2.05365695E-02
1.17925057E-02
7.63261220E-03
7.44410831E-03
3.64984888E-03
1.06528502E-02
6.84752080E-03
5.98340417E-03

4.53136990E-03
4.11089618E-03
5.23049636E-03
5.93595252E-03
2.30651781E-03
8.28927848E-03
4.68833258E-03
4.94308066E-03
4.42159243E-03
6.72609125E-04
1.10504696E-03
1.08476815E-03
1.06410289E-03
1.04302821E-03
2.41462206E-03
1.53760807E-03
9.30521181E-04
2.64379700E-03
8.94803183E-04
7.37182167E-04
1.07578364E-03
2.96845515E-04
1.46573523E-04
8.74074895E-05
2.88040554E-04
2.83093703E-04
2.78056296E-04
2.72842238E-04
2.67637866E-04
2.36266798E-04
2.06301869E-04
2.27834294E-04
2.23216548E-04
2.90342781E-04
1.41968410E-04
1.85896124E-04
2.04400187E-04
1.99289297E-04
1.93998326E-04
1.88561965E-04
1.02369949E-04
1.00619824E-04
9.88582973E-05
9.70245353E-05
9.51573073E-05
4.69024254E-05
4.63891110E-05
4.59451129E-05
4.54225447E-05
1.80570699E-05
1.79600451E-05
1.78629090E-05
1.78011816E-05
1.77388567E-05
1.76407264E-05
1.75424699E-05

1.74789609E-05
1.74148298E-05
1.73155201E-05
1.72160676E-05
1.71506875E-05
1.70676326E-05
1.70011138E-05
1.68833560E-05
4.18810395E-05
4.13474874E-05
4.08069592E-05
4.02591739E-05
7.88444405E-05
7.65582839E-05
7.42017016E-05
7.17677517E-05
6.92482701E-05
3.36499964E-05
3.29835503E-05
6.39118808E-05
6.10689577E-05
5.80869496E-05
5.49431732E-05
2.62342689E-05
2.53737371E-05
2.44829653E-05
2.35585205E-05
2.25962658E-05
2.15911402E-05
2.05368407E-05
1.94253475E-05
1.82461874E-05
1.69852318E-05
1.56226084E-05
1.41287680E-05
5.19545583E-06
4.91426775E-06
4.61596116E-06
4.29696175E-06
3.95224224E-06
3.57432714E-06
3.15119418E-06
1.31712363E-06
3.39885712E-06
3.93899278E-07
3.32630523E-07
1.13030151E-07
9.96495113E-08
4.41874128E-08
3.99621932E-08
3.52314226E-08
1.85727491E-08
1.11786295E-08
1.24561889E-08
1.05187008E-08
1.14415023E-08

```
1.08834188E-09
t
'   Zone number by interval
36$$ 1
'   Mixture number by zone
39$$ 1
'   Temperature by zone
41**          9.00000E+02
t
end
```

LIST OF REFERENCES

1. D. KNOTT and E. WEHLAGE, “Description of the LANCER02 Lattice Physics Code for Single-Assembly and Multibundle Analysis, *Nucl. Sci. Eng.*, **155**, 331 (2007).

2. D. KNOTT et al., “CASMO-4 Methodology Manual,” STUDSVIK/SOA-95/02, Studsvik of America.

3. M. E. DUNN, N. M. GREENE, and L. M. PETRIE, "Status of ORNL Cross-Section Processing and Library Generation Capabilities," *Proc. Int. Workshop on Nuclear Data Needs for Generation IV Systems*, Antwerp, Belgium, April 5-7 (2005).

4. Z. ZHONG, T. J. DOWNAR, Y. XU, M. L. WILLIAMS, and M. D. DEHART, “Continuous-Energy Multidimensional S_N Transport for Problem-Dependent Resonance Self-Shielding Calculations,” *Nucl. Sci. Eng.*, **154,** 190 (2006).

5. J. J. DUDERSTADT and L. J. HAMILTON, *Nuclear Reactor Analysis*, John Wiley and Sons (1976), pp. 105-110.

6. E. E. LEWIS and W. F. MILLER, JR., *Computational Methods of Neutron Transport*, American Nuclear Society, La Grange Park, IL (1993), pp. 1-20.

7. D. E. CULLEN, “Nuclear Cross Section Preparation,” in Y. RONEN, ed., *CRC Handbook of Nuclear Reactor Calculations,* Vol. I, CRC Press, Boca Raton, FL (1986).

8. M. B. CHADWICK et al., “ENDF/B-VII.0: Next Generation Evaluated Nuclear Data Library for Nuclear Science and Technology,” *Nucl. Data Sheets,* **107**, *12,* 2931 (2006).

9. A. SANTAMARINA, et al., “The JEFF-3.1.1 Nuclear Data Library,” JEFF Report 22, OECD/NEA Report 6807 (2009).

10. K. SHIBATA et al., "JENDL-4.0: A New Library for Nuclear Science and Engineering" (to be submitted to *J. Nucl. Sci. Technol.*).

11. M. HERMAN and A. TRKOV, ENDF-6 Formats Manual, ENDF-102, Brookhaven National Laboratory, Upton, NY (2009).

12. J. J. DUDERSTADT and L. J. HAMILTON, *Nuclear Reactor Analysis*, John Wiley and Sons (1976), pp. 39-45.

13. R. D. LAWRENCE, “The DIF3D Nodal Neutronics Option for Two- and Three-Dimensional Diffusion-Theory Calculations in Hexagonal Geometry,” ANL-83-1, Argonne National Laboratory (1976).

14. M. TAMITANI, T. IWAMOTO, and B. R. MOORE, “Development of Kinetics Model for BWR Core Simulator AETNA,” *J. Nucl. Sci. Technol.,* **40**, *4*, 201 (2003).

15. G. GRANDI, L. BELBLIDIA, and C. JÖNSSON, "BWR Stability Analyses with SIMULATE-3K Benchmark against Measured Plant Data," Article in press with *Prog. Nucl. Energy* (2010).

16. J. H. FERZIGER and P. F. ZWEIFEL, *The Theory of Neutron Slowing Down in Nuclear Reactors*, MIT Press, Cambridge, MA (1966).

17. J. J. DUDERSTADT and L. J. HAMILTON, *Nuclear Reactor Analysis*, John Wiley and Sons (1976), pp. 315-332.

18. E. P. WIGNER et al., "Review of the Measurements of the Resonance Absorption of Neutrons by Uranium in Bulk," *J. Appl. Phys., **2***, 257 (1955).

19. I. CARLVIK, "The Dancoff Correction in Square and Hexagonal Lattices," Part of Carlvik's PhD Thesis, AE-257, Chamlers University, Göteborg, Sweden (1966).

20. L. W. NORDHEIM, "A New Calculation of Resonance Integrals," *Nucl. Sci. Eng.*, **12,** 457 (1962).

21. I. I. BONDARENKO, *Group Constants for Nuclear Reactor Calculations*, Consultants Bureau, New York (1964).

22. R. E. MACFARLANE and D. W. MUIR, "The NJOY Nuclear Data Processing System Version 91," LA-12740-M, Los Alamos National Laboratory (1994).

23. N. M. GREENE, "BONAMI: Resonance Self-Shielding by the Bondarenko Method," Vol. II, Sect. F1, ORNL/TM-2005/39/V6, Oak Ridge National Laboratory (2009).

24. "SCALE: A Modular Code System for Performing Standardized Computer Analyses of Licensing Evaluation," Vols. I-III, ORNL/TM-2005/39/V6, Oak Ridge National Laboratory (2009).

25. D.T. INGERSOLL et al., "Production and Testing of the VITAMIN-B6 Fine Group and the BUGLE-93 Broad Group Neutron/Photon Cross-Section Libraries Derived from ENDF/B-VI Nuclear Data," NUREG/CR-6214 (ORNL-6975), Oak Ridge National Laboratory (1995).

26. J. E. WHITE, D. T. INGERSOLL, C. O. SLATER, and R. W. ROUSSIN, "BUGLE-96: A Revised Multigroup Cross Section Library for LWR Applications Based on ENDF/B-VI Release 3," *Proc. Topl. Mtg. Radiation Protection and Shielding*, North Falmouth, Massachusetts, April 21-25, 1996, American Nuclear Society (1996).

27. R. SANCHEZ, J. MONDOT, Z. STANCOVSKI, A. COSSIC, and I. ZMIJAREVIC, "APOLLO II: A User-Oriented, Portable, Modular Code for Multi-Group Transport Assembly Calculations," *Nucl. Sci. Eng.*, **100**, 352 (1988).

28. F. D. GIUST, R. J. J. STAMM'LER, and A. A. FERRI, "HELIOS 1.7 User Guide and Manual," Studsvik Scandpower (2001).

29. L. B. LEVITT, "The Probability Table Method for Treating Unresolved Neutron Resonances in Monte Carlo Calculations," *Nucl. Sci. Eng.*, **49**, 450 (1972).

30. M. N. NIKOLAEV, "Comments on the Probability Table Method," *Nucl. Sci. Eng.*, **61**, 286 (1976).

31. D. E. CULLEN, "Application of the Probability Table Method to Multigroup Calculations of Neutron Transport," *Nucl. Sci. Eng.*, **55,** 387 (1974).

32. A. HÉRBERT, "The Ribon Extended Self-Shielding Model," *Nucl. Sci. Eng.*, **151,** 1 (2005).

33. A. HÉRBERT and M. COSTE, "Computing Moment-Based Probability Tables for Self-Shielding Calculations in Lattice Codes," *Nucl. Sci. Eng.*, **142,** 245 (2002).

34. A. HÉRBERT, "A Review of Legacy and Advanced Self-Shielding Models for Lattice Calculations," *Nucl. Sci. Eng.,* **155,** 310 (2007).

35. H. HENRYSON, B. J. TOPPEL, and C. G. STENBERG, *MC^2: A Code to Calculate Fast Neutron Spectra and Multigroup Cross Sections*, ANL-8144, Argonne National Laboratory, Argonne, IL (1976).

36. M. L. WILLIAMS and M. ASGARI, "Computation of Continuous-Energy Neutron Spectra with Discrete Ordinates Transport Theory," *Nucl. Sci. Eng.*, **121,** 172 (1995).

37. M. L. WILLIAMS, M. ASGARI, and D. F. HOLLENBACH, "CENTRM: A One-Dimensional Neutron Transport Code for Computing Point-wise Energy Spectra," Vol. II, Sect. F18, ORNL/TM-2005/39/V6, Oak Ridge National Laboratory (2009).

38. M. L. WILLIAMS, "Submoment Expansion of Neutron-Scattering Sources," *Nucl. Sci. Eng.*, **134,** 218 (2000).

39. W. M. STACY, *Nuclear Reactor Physics*, 1st Ed, WILEY-VCH Verlag GmbH & Co., (2004), pp. 379-384.

40. C. KALBACH and F. M. MANN, "Phenomenology of continuous angular distributions. I. Systematics and parameterization," *Phys. Rev.*, **C 23,** 112 (1981).

41. C. KALBACH**,** "Systematics of Continuum Angular Distributions: Extensions to higher Energies," *Phys. Rev.,* **C 37,** 2350 (1988).

42. S. C. CHAPRA and R. P. CANALE, *Numerical Methods for Engineers*, 5th Ed., McGraw-Hill (2006), pp. 620-627.

43. E.W. WEISSTEIN, "Fundamental Theorem of Gaussian Quadrature." MathWorld--A Wolfram Web Resource, http://mathworld.wolfram.com/FundamentalTheoremofGaussianQuadrature.html Accessed Sept 2010.

44. G.E. SJODEN, *Foundations in Applied Nuclear Engineering Analysis*, World Scientific (2009). pp. 57-58.

45. S. C. CHAPRA and R. P. CANALE, *Numerical Methods for Engineers*, 5th Ed., McGraw-Hill (2006), pp. 586-605.

46. F. B. HILDEBRAND, *Introduction to Numerical Analysis* 1st Ed. McGraw-Hill (1956), pp. 323-325.

47. A. S. KRONROD, *Nodes and Weights of Quadrature Formulas, Sixteen-place Tables*, Consultants Bureau (1965), Authorized translation from Russian.

48. D. KAHANER, C. MOLER, and S. NASH, *Numerical Methods and Software*, Prentice-Hall (1989), pp. 153-157.

49. S. SAHNI, *Data Structures, Algorithms, and Applications in Java*, 1st Ed., McGraw-Hill (2000), pp. 128-129.

50. J. E. SWEEZY et al., *MCNP- A General Monte Carlo N-Particle Transport Code, Version 5*, Los Alamos National Laboratory Report, LA-UR-03-1987, Los Alamos National Laboratory, Los Alamos, NM (2005).

51. L.M. PETRIE, M. L. WILLIAMS, and D. F. HOLLENBACH, "Miscellaneous Scale Utility Modules," Vol. III, Sect. M17, ORNL/TM-2005/39/V6, Oak Ridge National Laboratory (2009).

52. R. D. MOSTELLER, "Validation Suites for MCNP," LA-UR-02-0878, Los Alamos National Laboratory, *Proc. ANS Radiation Protection and Shielding Topical Mtg.*, Santa Fe, NM, April 14-17 (2002).

53. L. S. LASDON, A. D. WAREN, A. JAIN, and M. RATNER, "Design and Testing of a Generalized Reduced Gradient Code for Nonlinear Programming," *ACM Trans. on Mathematical Software*, **4,** 34 (1978).

54. S. C. CHAPRA and R. P. CANALE, *Numerical Methods for Engineers*, 5th Ed, McGraw-Hill (2006), pp. 424-471.

55. D. S. GELLES, "Development of Martensitic Steels for High Neutron Damage Applications", *J. Nucl. Mater.,* **239**, 99 (1996).

56. D. C. CRAWFORD, D. L. PORTER, and S. L. HAYES, "Fuels for Sodium-Cooled Fast Reactors: US Perspective," *J. Nucl. Mater.,* **371**, 202 (2007).

57. I. C. GAULD, O. W. HERMANN, and R. M. WESTFALL, "ORIGEN-S: SCALE System Module to Calculated Fuel Depletion, Actinide Transmutation, Fission Product Buildup and Decay, and Associated Radiation Source Terms," Vol. II, Sect. F7, ORNL/TM-2005/39/V6, Oak Ridge National Laboratory (2009).

58. B. DOOIES, A. CALDWELL, and E. LOEWEN, "Fission Product Inventory of PRISM Reactor Discharged Fuel for Actinide Burner Core Design," *Trans. Am. Nucl. Soc.,* **100,** 562 (2008).

59. L. L. CARTER, R. C. LITTLE, J. S. HENDRICKS, and R. E. MACFARLANE, "New Probability Table Treatment in MCNP for Unresolved Resonances," *ANS Radiation Protection and Shielding Division Top. Conf.,* Nashville, TN, April 19-23 (1998).

BIOGRAPHICAL SKETCH

Brian Triplett holds a bachelor's degree in nuclear engineering and a master's degree in nuclear engineering sciences from the University of Florida. His professional experience includes internships at the Crystal River Unit 3 nuclear power plant and Los Alamos National Laboratory. He currently works at GE Hitachi Nuclear Energy on the development of advanced neutronic methods in support of the design and licensing of boiling water reactors and sodium fast reactors.